Reconstruction of tsunami characteristics from the deposits of large-scale tsunamis using a deep neural network inverse model

Rimali Mitra

Doctoral Thesis

Department of Geology and Mineralogy
Division of Earth and Planetary Sciences
Graduate School of Science
Kyoto University

June, 2021

Abstract

The 2011 Tohoku-oki tsunami and the 2004 Indian Ocean tsunami caused significant economic losses and fatalities in the coastal areas. These modern tsunamis could be traced back and linked to the ancient tsunamis, such as the 869 Jogan tsunami as a precursor for the 2011 Tohoku-oki tsunami. This study proposes that the 1D inverse model using a deep neural network (DNN) has the potential to predict the values of hydraulic conditions, such as maximum inundation distance, flow velocity and maximum flow depth, sediment concentration of different grain-size. The inverse model accepts the thickness and grain-size distribution of the tsunami deposit measured in the post-tsunami survey around Sendai Plain and other locations as input parameters, and estimates the tsunami characteristics. The DNN model incorporates the forward model, which is based on the layer-averaged equations considering non-uniform, unsteady transport of suspended sediments during turbulent mixing. The forward model produced artificial training data sets representing various depositional characteristics by iterative calculation with random flow conditions. Then the DNN was trained to find relationships between simulation results and initial conditions using the artificial data sets created by the forward model. Finally, the DNN model was applied to natural field data sets from different locations. The uncertainty of the model prediction was quantified using the jackknife method. As a result, the model successfully reconstructed the flow conditions of the 2011 Tohoku-oki tsunami from Sendai Plain and Joban Coast, 2004 Indian Ocean tsunami from Phra Thong Island, Thailand. The estimated values of maximum inundation distance, flow velocity and the maximum flow depth were close to the measured values of these modern tsunamis, verifying the effectiveness of the inverse model proposed in this study. In addition, the DNN inverse model was applied to the ancient deposit of the 869 Jogan tsunami. Despite having topographical complicacy and lesser sampling locations for ancient deposits, the DNN model predicted the flow characteristics from the deposits satisfactorily. These qualitative and quantitative estimations demonstrated that the DNN inverse model is a promising tool for evaluating tsunami hazard and mitigation strategies in future studies.

Table of Contents

1 Introduction

1.1 Tsunami deposits

Tsunamis are one of the most catastrophic natural disasters. It causes extensive casualties and economical damage along the coastal regions (Morton et al., 2007; Brill, 2012). Thus, it is necessary for disaster prevention research to understand the risks of such disastrous tsunami disasters and to link them to disaster mitigation.

Tsunamis are generated by different processes, such as earthquakes, subaerial and submarine landslides, volcanic eruptions, or rarely from meteorite impacts (Brune et al., 2010; Massel, 2012; Wünnemann and Weiss, 2015; Mutaqin et al., 2019). For example, one of the most deadliest tsunamis took place in AD 1883, Indonesia, due to volacnic activities (Krakatau tsunami) (Francis, 1985; Yokoyama, 1987; Mutaqin et al., 2019). However, majority of the largest tsunamis in the past took place due to earthquake of magnitude greater than 7.0 (Board et al., 2011). In the past 100 years, around 58 tsunamis caused more than 260,000 casualties with an average of 4,600 casualties per disaster and between the years 1998 and 2017, extensive economical damage of approximately USD 280 billion, was reported (Imamura et al., 2019a). Tsunamis are the series of waves that are characterized by an extremely long wavelength (~100s km). The wave heights offshore are not necessarily large, but the wave heights and the velocity of the tsunami decreases as the depth of the water decreases. Also, the flow properties of tsunamis are affected by various processes, such as refraction due to coastal geomorphology. The indentation of coastline, such as bays or fjords can amplify wave heights and inundations (Reicherter, 2014).

Tsunamis erode substrait of shallow water and coastal areas, transporting sediment and leaving deposits over wide areas of alluvial plains and deep water (e.g., Szczuciński et al., 2012a; Richmond et al., 2012; Arai et al., 2013). Tsunami deposits from modern and ancient tsunamis are presented in several literature (Dawson and Shi, 2000; Scheffers and Kelletat, 2003) but it is often difficult to observe in geological records (Jaffe and Gelfenbaum, 2002) due to anthropogenic disturbances. Terrestrial tsunami deposits are thin (typically 1–10 cm in thickness) but they exhibit wide spatial distribution (several kms inland) as sand layers with mud intercalations. Tsunami deposits show various sedimentary features, such as parallel lamination (Goto et al., 2012) and multiple graded sublayers (Naruse et al., 2012). The mud drapes intercalated in sandy tsunami deposits, could be several millimeters

thick and are generally formed from suspension fallout during the stationary wave (Fujiwara and Kamataki, 2007). Major identifying criteria for onshore tsunami deposits are (1) they contain materials transported from the sea, such as shell fragments, (2) they exhibit upward and landward fining and thinning trends in grain-size and bed thickness from the shoreline (Jaffe and Gelfenbaum, 2002).

Tsunami deposits show widespread diversity in terms of pattern, grain-size distribution, composition, sorting and regional settings (Shiki and Yamazaki, 2008; Dawson et al., 1988; Moore, 2000). The behaviors and the effect of tsunamis on the coastline can vary depending on the adjacent sedimentary environments, such as flat coasts (Figure 1), presence of lagoons and cliffed rocky coasts, presence of tidal inlets (Reicherter, 2014) (Figure 2a, b).

The maximum inland extent of sandy deposits of tsunami is associated with the slope and complexities of the topography. Their spatial extent is larger at flat topography (Figure 1) as the effect of gravity is more on the steeper slopes due to the lesser bottom friction and waveform (Yoshii et al., 2018). The speed of flow gradually slows down at the landward part and the coarsest sediment deposition takes place near the shoreline followed by the finest sediment deposition at the further inland (Shinozaki et al., 2020). Thus, the sedimentary records show upward fining sequence at the inland area (Röbke and Vött, 2017). The extent of deposits are also affected by runup velocities of inundation flow, which typically vary 5–8 m/s are and speeds up to 20 m/s rarely. (Nanayama and Shigeno, 2006).

Lagoonal sediment records with coarse-grained deposits such as sand sheets, scour fans and washover fans deposition in fine-grained lagoonal sediments and sequence often serve as an important evidence for past tsunami (Reicherter, 2014; May et al., 2012). McSaveney et al. (2000) reported that the 1988 Papua New Guinea tsunami divided Sissano Lagoon from the open sea with the sand deposition above 1 m on the seaward beach ridge with scour holes up to 2 m deep occurred (Gianfreda et al., 2001). The 2011 Great East Japan earthquake and tsunami caused extensive morphological change of Gamo Lagoon in the northern part of Sendai Coast, Miyagi Prefecture (Hoang et al., 2016).

Along the hard coasts, such as rocky shores, the detachment of large boulders and dislocations of the smaller blocks help to delineate the tsunami landfall (Reicherter, 2014). Boulder or boulder trains are found as deposition in the nearshore zone and farther inland (Dawson, 1994, 1999; Dawson and Shi, 2000; Scheffers and Kelletat, 2003; Scheffers, 2008) (Figure 2b). It has been found that tsunamis on the coastal barriers are fewer com-

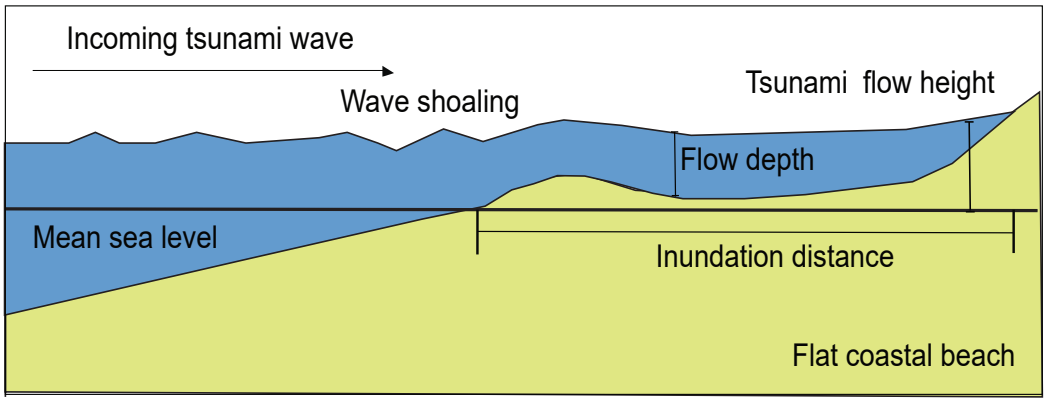

Figure 1: Schematic diagram of general tsunami parameters, modified after Reicherter (2014).

pared with the flat sandy coast (Gianfreda et al., 2001). However, at the southern coastline of Ryukyu Islands, Japan, 40 m wide, several metres high ridges were found (Ota et al., 1985) and giant blocks up to 100 m^3 has been observed up to 30 m above present sea level by a tsunami during the Holocene (Nakata and Kawana, 1995).

The diversity of tsunami deposits according to the tsunami characteristics and topography implies the possibility of using them to reconstruct the flow conditions of past tsunamis. Indeed, ancient tsunami deposits have been proved to be helpful for identifying several parameters of tsunami inundation flows, such as inundation distance, run-up height, and flow speed (Figure 1). These reconstructions help in future tsunami risk mitigation strategies along the coastal cities (Ishimura and Yamada, 2019). The tsunami deposits assessment also quantifies the recurrence intervals and the magnitude of the events, along with the flow conditions (Sugawara et al., 2012).

1.2 Historical review of tsunami deposit research

The studies and detailed investigations of tsunami deposits started in the 1950s (Shephard et al., 1950) and after the 1960's catastrophic Chilean tsunami, researchers, such as Konno (1961) and Wright and Mella (1963) discovered the presence of the event sand layers and changes in coastal topography due to hydrodynamic processes due to inland tsunami in-

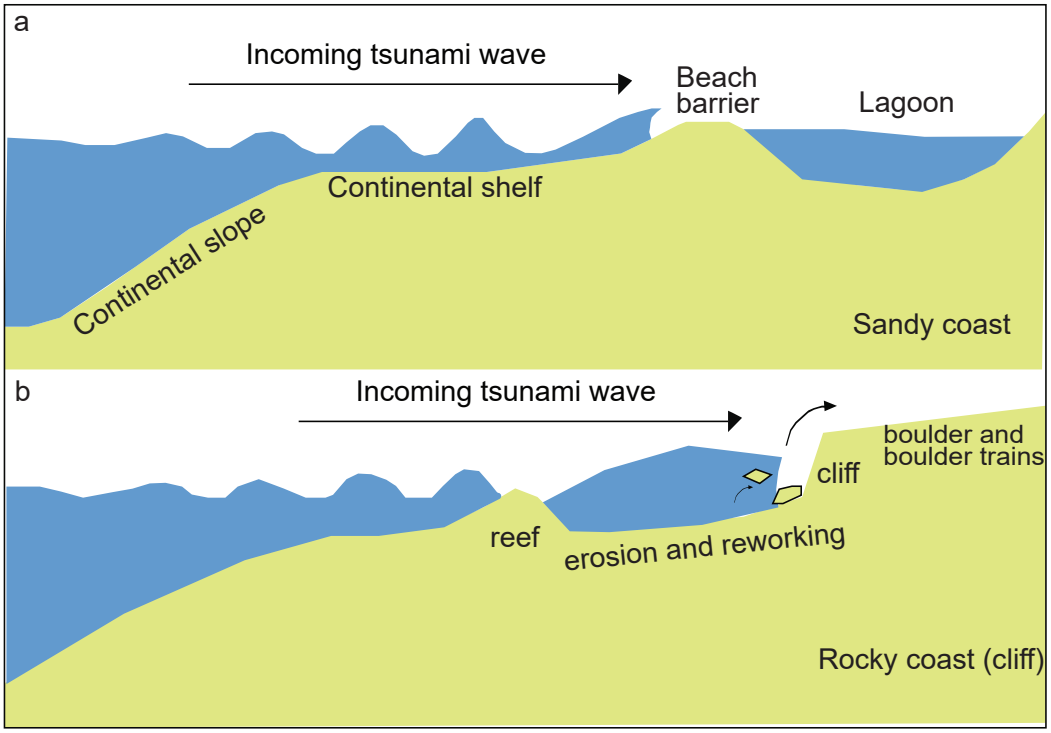

Figure 2: Schematic diagram of general tsunami parameters modified after Reicherter (2014).

undations (Shiki and Yamazaki, 2008). Post-tsunami investigations and overall scientific approach, associated tsunami research started to increase, since the 1980s (Atwater, 1987; Sugawara et al., 2008). The tsunami deposits study from a sedimentological perspective on 1983 Japan Sea earthquake tsunami was done by Minoura (1987). Dawson et al. (1988) introduced the importance of paleo-tsunami deposits study for future hazard research of tsunami deposits for disaster mitigation of tsunamis. Dawson et al. (1988) reported a massive submarine landslide on the continental slope off Storegga, western Norway, trigerred a series of tsunami waves and this event was the interpreted from sand layer deposition (dated approximately 7000 yrs B.P) along the coast of eastern Scotland. The geological records of ancient tsunamis, such as the 869 Jogan and the 1700 Cascadia tsunamis provided the major information for future coastal hazard mitigation in particular areas (Tsuji, 2021).

The importance of tsunamis or coastal flooding increased after the 2004 Indian Ocean tsunami, 2010 Chile and 2011 Tohoku-oki earthquake (Brill, 2012). The 2004 Indian Ocean tsunami off the coast of Sumatra has stimulated the study of tsunami deposits in the modern

era. This tsunami was one of the most catastrophic events around the Indian Ocean causing more than 250,000 casualities (Ramalanjaona, 2011). Several post-tsunami surveys were conducted in the affected countries, such as Thailand, Indonesia, India and Srilanka (Jankaew et al., 2008; Paris et al., 2009; Srinivasalu et al., 2007; Goto et al., 2008; Sugawara, 2021). Choowong et al. (2008a) investigated on the deposits along the Andaman Coast to delineate the flow conditions qualitatively using the sedimentary feature, such as anti-dunes and capping bedforms. Sawai et al. (2009) used diatom assemblage to interprete the sedimentological aspects. Jankaew et al. (2008) and Rubin et al. (2017) investigated on the predecessor of the 2004 Indian ocean tsunami to understand the recurrence intervals and magnitude of such large-scale tsunamis prior to the 2004 tsunami event.

Post-tsunami survey immediately after the event has been performed since 1960 (Konno, 1961). The survey of the modern tsunami deposits provided important information on the sedimentary structure for the identification of the past tsunami deposits. For example, on July 2006, Indonesian tsunami at Java island caused extensive damage and inundated around 1 km from shoreline. The pattern of sedimentary distribution recorded two individual waves at Adipala, Indonesia and the sand deposits were mostly plane-parallel laminated and rich in heavy minerals (Moore et al., 2011). At Pangandaran, Indonesia, deposits with massive and graded bedding that overlies buried soil, were observed (Maemunah et al., 2015). On February 2010, another devastating tsunami generated from a Mw 8.8 earthquake at the coast of Chile (Fritz et al., 2011). Along the central coast of Chile, large (6 to 8 meter wavelength) low-amplitude bedforms with layers of plane-parallel stratification in some deposits, were dominantly observed within the maximum inland extend of tsunami inundation (2.35 km) (Morton et al., 2010).

On, March, 2011, a great earthquake (Mw 9.0) generated one of the largest tsunamis in Japan at the Tohoku District, indicating significance of assessment of low-frequency but high-risk events that can be only inferred from pre-historical records (Abe, 1990; Watanabe, 2001; Minoura et al., 2001; Goto et al., 2012). After this event, measurements of tsunami inundations as well as video-record analysis provided a preliminary insight of the flow parameters, such as maximum inland extent of inundation (~4 km), flow inundation velocity (6.9–1.9 m/s) and flow inundation height (Hayashi and Koshimura, 2013; Mori et al., 2011a; Naruse and Abe, 2017). The post-tsunami field surveys also provided the information on spatial distribution of deposits. Several quantitative approaches (e.g., Jaffe et al., 2012;

Sugawara and Goto, 2012; Naruse and Abe, 2017) have delineated the accuracy of the numerical models. Field investigations in Sendai Plain already revealed the evidence of the 869 Jogan tsunami deposit as a separate sand layer showing features similar to those of the 2011 Tohoku-oki tsunami (Minoura et al., 2001; Sugawara et al., 2010). The 2011 Tohoku-oki tsunami increased the scope to study other pre-historic tsunamis that will be useful for further tsunami hazard mitigation around the Sendai Plain (Goto et al., 2011; Sawai et al., 2012; Sugawara, 2021).

1.3 Forward and inverse modeling of tsunamis

Tsunami hydrodynamics, sedimentation and transport models are necessary along with the field study for better understanding of quantitative analysis of tsunami characteristics, and magnitude assessment of earthquake (Jaffe and Gelfenbuam, 2007; Jaffe et al., 2016). The modeling approach involving sediment transportation started from 1960s (Eaton et al., 1961) and the model development progressed with time (Sugawara et al., 2014). Since the middle of 2000s, several researchers have introduced the inverse analysis of the tsunami deposit to reconstruct the characteristics of past tsunamis, quantitatively (e.g., Jaffe and Gelfenbuam, 2007; Soulsby et al., 2007; Tang and Weiss, 2015; Naruse and Abe, 2017) on flow conditions (steady or unsteady, uniform or non-uniform) and model parameterizations (e.g., bed roughness) and these modeling approaches include different assumptions of tsunami hydrodynamics, and bed roughness. Several inverse models were applied directly to the measured data set of tsunami deposits to estimate their flow conditions at particular regions (e.g., Jaffe et al., 2012; Naruse and Abe, 2017).

Here, I briefly introduce the forward models that predict the formation of tsunami deposits as well as the inverse models that employ the forward models to reconstruct the characteristics of past tsunamis (Li et al., 2012; Sugawara et al., 2014; Jaffe et al., 2016).

Forward model deals with a combination of sediment transport model, source model (e.g., Tsushima et al., 2012), and hydrodynamic model (Jaffe et al., 2016). In fully hydrodynamic models, conservation equations of fluid mass, momentum and transported sediment mass are considered, and the models predict erosion and deposition with spatial distribution of thickness and grain-size (Apotsos et al., 2011; Li et al., 2012; Naruse and Abe, 2017). Forward model of tsunami deposits can employ three dimensional hydrodynamic equations, such as C-HYDRO3D (Kihara and Matsuyama, 2010) or Flow3D (Hirt and Nichols, 1988).

Three-dimensional models are, however, computationally demanding, making it difficult to calculate tsunamis that inundate large areas. Therefore, most models of tsunami deposits employ the nonlinear shallow wave equations (NLSWE) with empirical formulations of sediment transport in order to reduce spatial dimensions. XBeach and TUNAMI-N2 are typical examples of the layer-averaged horizontal 2D models (Li et al., 2012; Gelfenbaum et al., 2007; Apotsos et al., 2011). Further simplification to one dimension can be applied for predicting deposition or erosion in coastal plains where the flow condition can be assumed to be uniform toward the direction perpendicular to the inundation. For example, Naruse and Abe (2017) proposed a 1D model of tsunamis that assumes quasi-steady flow condition. The hydrodynamics and sediment transport of tsunamis are always simplified with parameterization not only in 1D and 2D models but also in 3D models. Therefore, the forward model parameters are needed to be checked their appropriateness and robustness with various methods including flume experiments (Tang, 2017).

Most of the proposed forward models that employ hydrodynamic equations, require bathymetry, topography data, bottom roughness, flow velocity and water levels. These data sets may not necessarily be available for inverse analysis of ancient tsunami deposits. In contrast, the input information, such as topography or bathymetry data may not be needed in the simplified forward model such as FITTNUSS proposed by Naruse and Abe (2017), while it considers essential factors of sediment transport.

Inverse model uses the depositional features of observed tsunami deposits (some inverse models require) other measured information, such as flow depth to estimate tsunami characteristics. Inverse model can be classified to the point and 1D line models. In point models, tsunami characteristics are estimated on the basis of depositional characteristics at a single location (Moore, 2000; Smith et al., 2007; Jaffe and Gelfenbuam, 2007; Jaffe et al., 2012). 1D line models require the depositional characteristics of tsunami deposits along an 1D transect to consider their spatial variation. Examples of the 1D line model are settling column model (Soulsby et al., 2007) and FITTNUSS (Naruse and Abe, 2017).

Sugawara et al. (2015) proposed the concept of hybrid model that combines both forward and inverse model to reduce uncertainty of calculation in each model. Generally, inverse models reconstruct the flow conditions by iterating the numerical calculations with the forward model and matching the observed results with the calculated results. Since this process involves a considerable number of iterations, largely simplified forward models are

employed in the inverse models. In his concept of the hybrid model analysis, the inverse analysis is conducted for estimating the flow characteristics. Then, the forward model with higher dimensions and less simplified assumptions is used for predicting the flow dynamics of tsunamis to verify if the assumptions employed in the inverse model can be justified.

It is important to note that previous studies on inverse modeling were based on forward models using unreasonably simplified assumptions. For example, in the settling-advection model (or moving-settling tube model), it was assumed that all the sediment particles settle in the water column without any turbulent mixing, resuspension or subsequent erosion (Soulsby et al., 2007; Moore et al., 2007; Jaffe and Gelfenbuam, 2007). Tang and Weiss (2015) assumed that sediment suspension in tsunamis occurs under uniform and steady conditions and uprush stops suddenly. As a result, situations to which these inverse models are applicable are quite limited (Jaffe et al., 2016; Naruse and Abe, 2017). Moore et al. (2007) proposed a point inverse model based on advection settlings of large particles in deposit, wherein the settling velocities of the larger particles (D_{84} and D_{100}) in the deposit were used as input data, and the model estimated the average flow speed of the tsunami inundation. Moore et al. (2007) assumed that sediment grains travel without diffusion in water column and are not resuspended from bed, and thus a trajectory of a single grain is linear moving from the top of the water column at the shore and falls until it hits the bed inland. However, the movements of sediment grains do not obey such linear trajectory and they travel considerably longer distances because of the flow turbulence (Braaten et al., 1990). Under the assumption of a linear trajectory, very large flow velocity is required to explain the travel distance that was actually observed. Indeed, Sugawara (2014) indicated from the field measurements that their advection-settling assumption cannot be justified in the case of the 2011 Tohoku-oki tsunami. Smith et al. (2007) proposed another point model based on particle settlings but only the finest grain-size classes of 106–184 μm were used in this model; however, the incorporation of larger grain-size classses is essential for obtaining accurate estimation from tsunami deposits (Naruse and Abe, 2017). In contrast, Soulsby et al. (2007) proposed the 1D model that deciphered the run-up elevation and inundation distance. Although sediment dynamics and optimization of input parameters were considered, no resuspension process of sediment particles was incorporated in the model assumption, so that significant overestimation of the flow velocity also occurs similar to the method of Moore et al. (2007). Jaffe and Gelfenbuam (2007) presented a point model (TsuSed-

Mod) using the thickness and bulk grain-size distribution of suspension-graded intervals of tsunami deposits to estimate the maximum tsunami flow speed. This model assumes that sediment deposited was is in a suspension that was in equilibrium with the maximum flow speed. See Jaffe et al. (2012) for model details. It does not consider the temporal variation of deceleration of the flow. Thus, the application of TsuSedMod is limited to the study areas where only the condition of uniform and steady tsunami flow is supposed to be approached. The application of TsuSedMod involves, the spliting of tsunami deposits into two parts: the lower part deposited from run-up flow and the upper part deposited from the stagnant water. This interpretation is not always easy because both parts may be normally graded. Non-uniform sediment transport cannot be considered in this model. The estimation of flow velocity can be strongly affected by the assumptions mentioned above. Moreover, additional input information, such as flow depth was required for the model (Naruse and Abe, 2017). Choowong et al. (2008b) applied TsuSedMod to two units around Bangtao Beach, Phuket, Thailand and obtained an extremely high estimate of the 2004 Indian Ocean tsunami flow velocities (19–21 m/s), although a reason for this overestimation of flow velocity can be that they used mean grain-size instead of the entire grain-size distribution in their analysis.

To resolve issues in previous inverse models, the inverse model FITTNUSS (Naruse and Abe, 2017) was proposed, in which a forward model for calculating sediment hydrodynamics and nonuniform, unsteady suspended sediment transport processes during run-up and stagnant phases was employed. The overall computational and calculation efficiency was increased by using a transformed coordinate system of moving boundary type in the forward model. The inverse model requires the spatial variation of thickness and grain-size distribution of the tsunami deposit along 1D shoreline-normal transects. It has the ability to produce flow conditions, such as run-up flow velocity, maximum flow depth and sediment concentration. However, the model still has many limitations, such as poor performance with increasing number of training data and grain-size classes due to the optimization procedures of parameters during inversion. This model employed Limited-memory Broyden-Fletcher-Goldfarb-Shanno (LBFGS) method to optimize the flow conditions in the forward model for minimizing difference between observations and model results (Naruse and Abe, 2017). This is a quasi-Newtonian algorithm, but it requires the gradient of the objective function that can be obtained only by numerical method and tedious trial and error itera-

tions are needed for calculation. Also, it may find local minimum solutions depending on the starting values of calculation so that multiple iterations with different starting values are needed. As a result, it was difficult to deal with larger data sets, and it was impossible to use uncertainty analyses because computational statistical methods, such as the jackknife method, require iterations of an inverse analysis. Hence, a new inverse model was necessary to solve the issues of the FITTNUSS model (Naruse and Abe, 2017).

1.4 Research objectives

In this dissertation, I attempted to establish a new inversion framework of tsunamis that is a combination of the forward model of FITTNUSS and a new inverse model using deep neural network (DNN), which can be applicable to the natural grain-size distribution of large-scale modern and ancient tsunamis, such as the 2011 Tohoku-oki earthquake at Sendai Plain and Joban Coast, the 2004 Indian Ocean tsunami at Phra Thong Island and the 869 Jogan deposits. To elucidate uncertainty of results of the inverse analysis, jackknife uncertainty analysis was used to check the applicability of the model for ancient and tsunami deposits.

The objectives of the thesis are (1) establishing an inverse model using DNN and the jackknife unecrtainty analysis, (2) verification of the new method by applying to the modern tsunami deposits and (3) the application of the method to ancient tsunami deposits. For Objective (1), the method was introduced and tested with artificial data sets in chapters 2, 3 and 4. Then, to verify its applicability to the actual deposits (Objective 2), the DNN inverse model was applied to the measured tsunami deposits of the 2011 Tohoku-oki tsunami at Sendai Plain (Chapter 2). Checking further applicability, the model performance was verified by applying the same model to another large-scale, modern tsunami deposits which is the 2004 Indian Ocean tsunami in Phra Thong Island, Thailand (Chapter 3). In addition, the DNN model was applied to Odaka region, Joban Coast, Fukushima, which is a topographically complicated region where inundation of the 2011 Tohoku-oki tsunami occured in the Froude-supercritical condition (Chapter 4). In all of these three regions (Sendai Plain, Phra Thong Island and Odaka), DNN model proved its potential to estimate flow regime in the particular region. In addition to the modern examples represented in the chapters 2–4, for understanding past tsunami characteristics (Objective 3), the DNN model was applied to the ancient 869 Jogan tsunami deposits (Chapter 5). In this attempt, the applicability of the DNN model was checked, although only limited numbers of sampling points at irregular

intervals were available. This chapter provides the preliminary results of inversion of ancient tsunami characteristics with the uncertainty analysis. However, in order to improve the results for the ancient tsunami deposits, the internal algorithm of the inverse model or updatation of the forward model is required that can be done as a future work. Finally, Chapter 6 summarizes the conclusions of this thesis and proposes future works on the DNN inverse model.

2 Estimation of Tsunami Characteristics from Deposits: Inverse Modeling using a Deep-Learning Neural Network

2.1 Introduction

Tsunamis are one of the most disastrous natural hazards that occur in coastal zones. They are a threat to the overall socio-economic infrastructure of coastal-based cities (Li et al., 2012). Tsunami hazard assessment is necessary for any fast-growing coastal city. The 2004 Indian Ocean tsunami and 2011 Tohoku-oki tsunami caused devastating damage to many Asian countries, but such situations are worsened when countries lack tsunami-related preparedness for disasters that cause human causalities and extensive building damage (Imamura et al., 2019b). Ghobarah et al. (2006) reported that the debris carried by the 2004 Indian Ocean tsunami could cause major building damage. The 2004 Indian Ocean tsunami caused extensive structural and non-structural destruction of reinforced concrete buildings (Saatcioglu et al., 2005).

To mitigate tsunami disasters, a method of inverse modeling of tsunamis based on their geologic records has been developed. Tsunami deposits are defined as layers of sediment formed by hydrodynamic activities of tsunami, and research on tsunami deposits started since early 1950s (Shephard et al., 1950; Bourgeois et al., 2009).

The mode of sediment transportation and deposition by tsunamis can be understood via a detailed study of tsunami deposits (Costa et al., 2015). Also, several studies of forward modeling as well as flume experiments of tsunamis have successfully reproduced features of tsunami deposits observed in field surveys (Johnson et al., 2016; Li et al., 2012; Sugawara et al., 2012; Yoshii et al., 2018). Using this knowledge, a quantitative reconstruction of hydraulic conditions, such as flow velocity and maximum flow depth has been attempted using several inverse modeling approaches (Soulsby, 1997; Jaffe and Gelfenbuam, 2007; Jaffe et al., 2012; Tang and Weiss, 2015). However, as discussed in the Chapter 1, the over-simplified forward and inverse models are not suitable for predicting realistic situations. On the other hand, model complexity does not necessarily lead to highly accurate predictions and this is especially true when performing inverse analysis. Thus, although studies of the inverse analysis of tsunami deposits are growing rapidly, there is a pressing need for the development of a more efficient and robust method that can evaluate uncertainties of

reconstruction and can be applied to field-scale tsunami deposits.

In this study, I present a new inversion method that uses a deep neural network (DNN) (Romano et al., 2009). This inverse model incorporates the same forward model used in FITTNUSS (Naruse and Abe, 2017). In this new methodology, however, the initial conditions and model parameters of the forward model are not optimized to fit the observed characteristics of tsunami deposits. Instead, the forward model calculation was simply repeated at random initial flow conditions (e.g., maximum inundation distance, maximum flow depth, flow velocity, and sediment concentration) to produce artificial training data sets that represent depositional characteristics, such as the spatial distribution of thickness and grain-size composition. The DNN was then trained to establish a relation between the characteristics of deposits and flow conditions based on artificial data sets. The established DNN can predict the probable flow conditions from deposits instantaneously, such that it works as an inverse model based on the tsunami deposits. The performance of the model was verified using training and test data sets. Finally, this 1D model was applied to the 2011 Tohoku-oki tsunami deposits from the Sendai Plain, and a fair prediction of the flow velocity, maximum flow depth, and concentration of six grain-size classes was obtained. The data set of Sendai Plain was selected because it is one of the best preserved data sets in the history of tsunami deposits; nevertheless, further reliability checks of the model should be made with other data sets including ones collected in future studies. The precision of the model was checked using the jackknife method (appendix 8.1). The methodology and results were compared with the FITTNUSS model and the actual initial flow conditions. The comparison shows promise for the use of DNN as a tsunami hazard assessment tool.

2.2 Model Formulation

This DNN inverse model uses the forward model of FITTNUSS (Naruse and Abe, 2017) to calculate the sediment transport and deposition from the depth-averaged flow velocity, the maximum flow depth, and initial sediment concentration. The forward model can reproduce the thickness and grain-size distribution along an 1D shoreline normal transect, which is used to train the DNN inverse model. The assumption in the forward model is that the topography can be approximated as flat, so that the local topographic change is not considered in the model (Naruse and Abe, 2017).

2.2.1 Forward model

The FITTNUSS forward model is used in the present inverse model framework. The forward model is based on the layer-averaged shallow-water equations, and they are simplified in order to treat the hydraulics of tsunamis. The model calculates the spatial variation of the thickness and grain-size distribution of the tsunami deposit from input values of (1) maximum distance of horizontal run-up, (2) maximum inundation depth, (3) run-up velocity, and (4) sediment concentration of each grain-size class (Naruse and Abe, 2017). Here, I present a brief review of FITTNUSS forward model (see Naruse and Abe (2017) for details). In the FITTNUSS model, shallow layer-averaged one-dimensional equations are used, which take the following form:

$$\frac{\partial h}{\partial t} + \frac{\partial Uh}{\partial x} = 0, \tag{1}$$

$$\frac{\partial Uh}{\partial t} + \frac{\partial U^2 h}{\partial x} = ghS - \frac{1}{2}g\frac{\partial h^2}{\partial x} - u_*^2 \tag{2}$$

where t and x are considered as the time and bed-attached streamwise coordinate which is, perpendicular to the shoreline and is positive toward the landward side. Here, h refers to the tsunami inundation depth, and U is the flow velocity. The gravitational acceleration is denoted as g, S is the bed slope and u_* is the friction velocity.

The sediment conservation equation of tsunami is given as follows:

$$\frac{\partial C_i h}{\partial t} + \frac{\partial U C_i h}{\partial x} = w_{si}(F_i E_{si} - r_{0i} C_i). \tag{3}$$

In the above equation, C_i refers to the volume concentration in the suspension of the ith grain-size class. The parameters w_{si}, E_{si}, r_{0i}, and F_i represent settling velocity, sediment entrainment coefficient, ratio of near-bed to layer-averaged concentration of the ith grain-size class and volumetric fraction of the sediment particles in the bed surface active layer above the substrate respectively (Hirano, 1971). Several empirical functions are required to close equations, such as (1), (2) and (3) for evaluating friction velocity (u_*). A detailed review of equations involving parameters in closure equations, such as thickness of the active layer (L_a) (Yoshikawa and Watanabe, 2008), Shield's dimensionless shear stress (τ_{*m}), settling velocity (w_{si}) (Dietrich, 1982), sediment entrainment coefficient (E_{si}) (Van Rijn,

1984), correction of damping effects (ψ_i) (Van Rijn, 1984), are given in Naruse and Abe (2017).

For the sedimentation of tsunamis, the Exner equation of bed sediment continuity is used:

$$\frac{\partial \eta_i}{\partial t} = \frac{1}{1-\lambda_p} w_{si}(r_{0i}C_i - F_i E_{si}). \tag{4}$$

Here η_i refers to the volume per unit area (thickness) of the sediments of the ith grain-size class accounts for the porosity of the bed sediment λ_p. As a result of the sedimentation, the grain-size distribution in the active layer varies with time (Hirano, 1971), which is expressed as follows:

$$L_a \frac{\partial F_i}{\partial t} = \frac{\partial \eta_i}{\partial t} - F_i \frac{\partial \eta}{\partial t}, \tag{5}$$

Thus, the rate of total sedimentation is as follows:

$$\frac{\partial \eta}{\partial t} = \sum \frac{\partial \eta_i}{\partial t}. \tag{6}$$

Equations (4) to (6) were solved using the two step Adams-Bashforth scheme and the predictor-corrector method. Finally, the flow dynamics of tsunamis was simplified using the assumptions proposed by Soulsby et al. (2007), while considering the velocity of tsunami run-up flow as uniform and steady but that the flow depth varies with time; thus, the model is based on a quasi-steady flow assumption. The simplified equation is as follows:

$$\frac{\partial C_i}{\partial t} + U\frac{\partial C_i}{\partial x} = \frac{R_w}{H\,(Ut - x)} \left\{ w_{si}\,(F_i E_{si} - r_{0i} C_i) \right\} \tag{7}$$

where R_w and H indicate maximum inundation distance and maximum flow depth of the tsunami at the seaward (upstream) boundary of the transect, respectively.

In addition to these formulations, a transformed coordinate system (Crank, 1984) has been applied to equation (7) to increase the computational efficiency of the forward model. The implicit Euler method was used to solve the equation after applying coordinate transformation. The entire forward and inverse model were implemented using Python with the Numpy and Scipy libraries.

2.2.2 Inverse model

Although artificial neural networks have been primarily applied for learning observational data sets for constructing predictive models (Ramirez et al., 2005), in this study, they are used for learning the results of a numerical simulation to construct an inverse model. First, artificial training data sets are prepared by repetition of the forward model. Multiple flow conditions, such as maximum inundation distance, flow velocity and maximum flow depth and boundary conditions are generated randomly with a range that is possible values in natural environments. Using the generated flow conditions, the forward model calculates the grain-size and thickness distributions along 1D shore-normal transect. Thus, this procedure results in multiple combinations of flow conditions and their consequences (i.e., grain-size and thickness distribution of tsunami deposits), which are used for training and verification of the inverse model. Results of the forward model calculations (Figure 3) are given to an input layer of the NN. The nodes in the input layer receive the values of the volume per unit area of each grain-size class at grid cell used in the forward model. The feed-forward calculation through several hidden layers is then performed, in which the values at the nodes were summated with weighting coefficients that are assigned on connections to nodes in the next layer, and the computed total input data passes through the activation functions to produce the net output. The number of hidden layers was set to maximize the model performance (Smith, 2013). As a result of this feed-forward calculation, the values obtained from the output nodes provide estimates of the hydraulic conditions of tsunamis that formed the deposits. This procedure results in the training of the model followed by testing of the model performance. I validated the model performance during training using 20% of the artificial data is used to validate the model performance during training. If the model tends to overlearn, the selection of hyperparameters and the optimization method is required to be revised. After the model training with artificial data set is completed, the model is ready for application to a natural data set; however, the model performed training based on artificial data with set spacing.

Procedures for training of the inverse model Here, I describe the procedures used for generating a training data set and the preprocessing. In the present study, in the forward model, the grain-size distribution was discretized into six grain-size classes, and the number of spatial computational grids in the transformed coordinate was 50. The number of

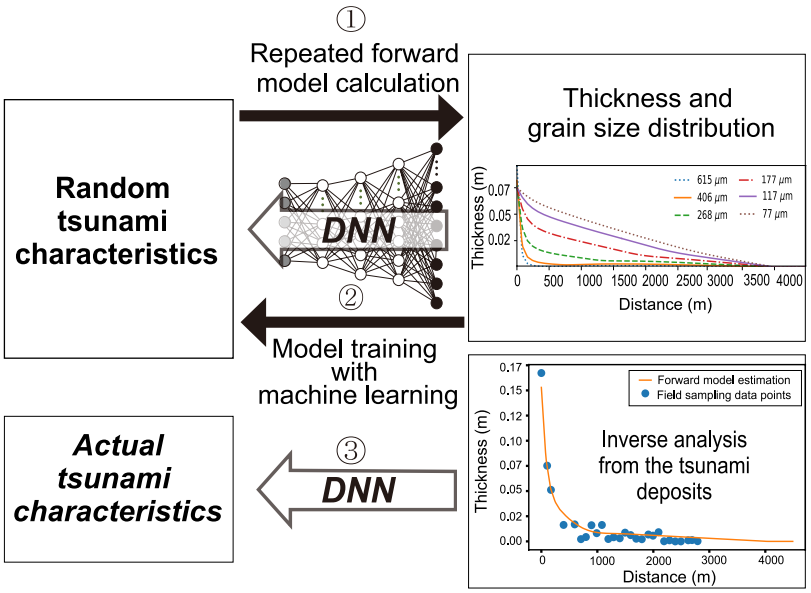

Figure 3: Workflow of the DNN inverse model.

spatial grid sizes in the fixed coordinates depends on the size of the sampling window. It is important to determine the appropriate number of training data sets produced by the forward model in order to improve the inverse model training (Jordan and Rumelhart, 1992). In this study, the number of iterations of the forward model calculation was increased incrementally, and the relation between the number of training data sets and the performance of the inverse model was investigated. The range of the inundation distances, flow velocities, maximum flow depths, and sediment concentrations used for generating the training data set is described later. The sampling window was then set to the artificial training data sets before starting the training of the DNN, and only the data in the sampling window was used for the training. This sampling window was necessary because (1) the tsunami deposit becomes too thin to measure precisely and predict computationally inland, and (2) field measurements along transects typically do not cover the entire distribution of tsunami deposits. Very thin and fine-grained tsunami deposits far inland are not easily differentiated from the background soil, and thus, the region of analysis should be limited to a relatively proximal area wherein coarser and thicker deposits are distributed. Therefore, the specific window is preferably at the proximal to middle part of the transect. As in the settings of the inverse model, the grid spacing has been maintained at a constant value of 15 m in the model. The number of grid points in the fixed coordinate varies according to the selected

interval of the sampling window. After the production of the training data set and extraction of the sampling window, the normalization of the input and teacher values was performed, which is one of the most important processes in training the neural network. As the input and teaching data have largely a different range of values from each other, the normalization of the values is required to be performed to remove the computational biases towards a specific dimension of data (Bishop, 1995). In this case, the maximum inundation distance has a larger range of values, while the values of concentration are very low. Thus, the raw values of the teaching data may predict the inundation distance preferentially, while the concentration values tend to be ignored. Therefore, both the input and teaching data in the artificial data set produced by the forward model were normalized before they were given as input to the inverse model. The input data (volume per unit area of deposits) were normalized using the following equation:

$$X_{norm} = \frac{X_{raw} - \min(X_{raw})}{\max(X_{raw}) - \min(X_{raw})} \tag{8}$$

where X_{norm} and X_{raw} are the normalized and original values of the input data respectively. $\min(X_{raw})$ and $\max(X_{raw})$ denote the minimum and maximum values of the raw input data, respectively. Similarly, the teaching data that was the original conditions used in the forward model calculation was normalized using the following equation:

$$Y_{norm} = \frac{Y_{raw} - \min(Y_{raw})}{\max(Y_{raw}) - \min(Y_{raw})} \tag{9}$$

where Y_{norm} and Y_{raw} are the normalized and original values of the teaching data respectively. $\min(Y_{raw})$ and $\max(Y_{raw})$ denote the minimum and maximum values respectively, of raw teaching data. After the training, the NN outputs the normalized values of the hydraulic conditions, such that these values were converted to values in the original scale.

Then, the training and teaching data set were given to the NN for training. The overall neural network structure consists of three parts, the input layer, hidden layers, and output layer (Figure 4). In the inverse model, the input layer of neural network structure consists of input nodes where the input values comprise the volume per unit area of each grain-size class at the spatial grids. Thus, the number of input nodes can be expressed as $M \times N$ where M and N are the total number of spatial grids and grain-size classes, respectively. In this study, the number of dense hidden layers was set as three along with the total 2500 nodes, and thus total number of layers was five (Figure 4). Here, the rectified linear activation

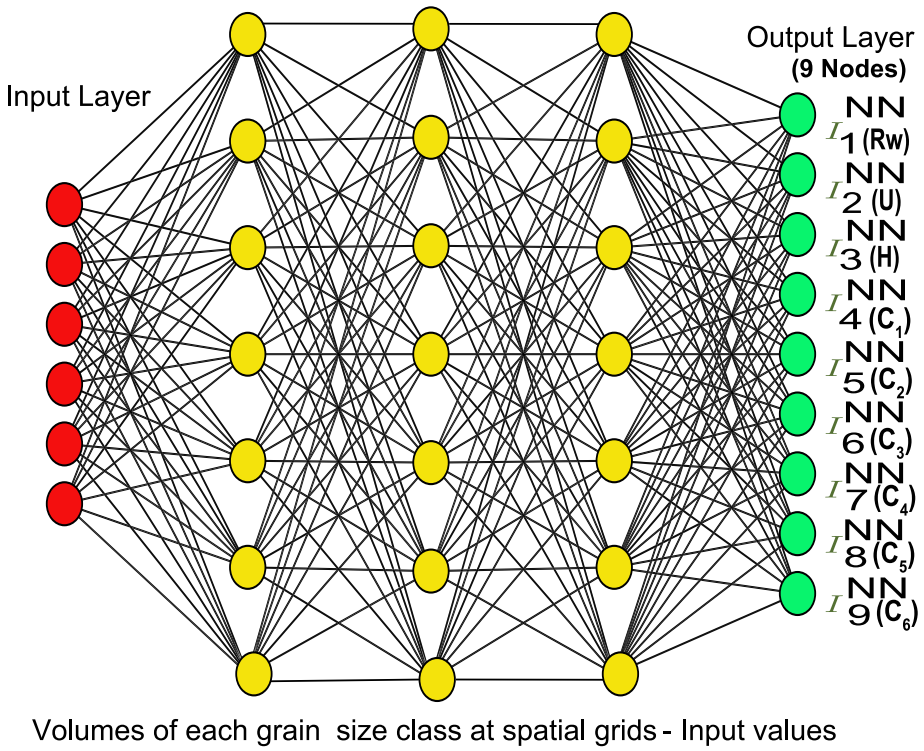

Figure 4: Neural network architecture for the inverse model. The NN structure includes one input and one output layer with three hidden layers for a total of five layers.

function (ReLU) was used as an activation function that calculates the output value from the total net weighted inputs (Ian and Yoshua, 2016). ReLU is function that is widely used for this purpose (Patterson and Gibson, 2017). The dropout has been applied to the hidden layer for regularization of the NN (Srivastava et al., 2014). The results of the feed-forward calculation of this NN during the training process were evaluated by the loss function (mean squared error), which is defined as follows:

$$J = \frac{1}{N} \sum \left(I_k^{fm} - I_k^{NN} \right)^2 \tag{10}$$

where I_k^{fm} is denoted as the teaching data that are the initial parameters used for producing in the training data and I_k^{NN} denotes the predicted parameters. This loss function quantifies

how close the NN was to an ideal inverse model. The values of this function were averaged over the entire data set (Patterson and Gibson, 2017). To minimize the loss function J, the back-propagation method with the stochastic gradient descent algorithm (SGD) was used to optimize the weight coefficients at links of the network (Patterson and Gibson, 2017). The Nesterov momentum method was used with the SGD to speed up the computation and improve convergence (Sutskever et al., 2013). Although other optimizers, such as AdaDelta, Adam, or AdaMax can provide an acceptable performance (Patterson and Gibson, 2017), this optimizer performed best for our model. This optimization process was repeated for prescribed times, and the training set was shuffled before splitting it into batch chunks that were used for the SGD optimization during each epoch.

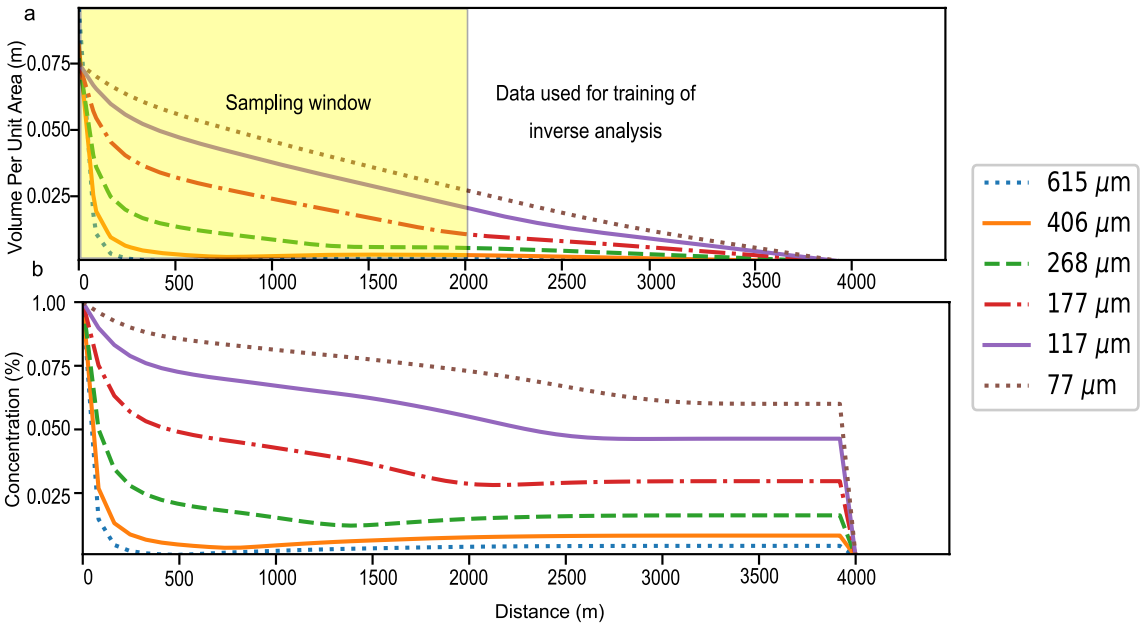

Figure 5: Example of the forward model calculation and sampling window used for the inverse analysis. (a) Spatial variation of the volume per unit area of each grain-size class of the tsunami deposit calculated using the forward model. Here volume per unit area is used for exhibiting amounts of deposition of particular grain-size class. Thickness of a tsunami deposit can be obtained by summation of volume per unit area of all grain-size classes with consideration of porosity. (b) Spatial variation of sediment concentration for each grain-size class in the run-up flow when the tsunami reached maximum inundation point.

In order to estimate how well the model was trained without overfitting, validation was performed with the validation data set that was also generated from the forward model

calculation. Among the produced data sets, 80% and 20% of the data were used for the training and validation respectively. The results of validation were used for tuning of the hyperparameters of the NN which are explained later. Finally, the performance of the model was evaluated after the hyperparameter tuning and using the test data sets, which were the data not used during the training process.

In the model, there are several hyperparameters that should be specified for the tuning of the training of the NN. The tuned hyperparameters were the learning rates, batch size and momentum used in the SGD, rates of dropout, number of hidden layers, types of activation function, and number of epochs. The hyperparameters were selected by trial and error in this study. The number of training data sets is also a hyperparameter of the inverse model, and it was tested by changing the number of repetitions of the forward model calculation. The trained model can work on a data set with a specific spatial grid in the fixed coordinate and grid spacing. In order to apply the inverse model to the natural data set in 1D vectors, the collected samples must be fit into that fixed coordinate system. A linear 1D interpolation was required as it provides values at positions between the data points, which are joined by straight line segments (Bourke, 1999). A linear 1D interpolation was applied to the natural data set in this case.

In addition to the training and validation data, 500 independent data points were kept aside for the testing of the inverse model. Therefore, after the model was trained, the model was applied to the test data sets to check its performance before applying it to the natural data sets. The good correlation between the teaching data in the test data set and the prediction of the model from the test data set shows fair ability of inverse model prediction. The residuals from the teaching data in the test data set were plotted in a histogram to determine the deviation of the prediction from the test data set from the true initial conditions.

2.3 Results of training and test of the inverse model

The hyperparameters for the training were set as follows. Among the hyperparameters (Table 1) used in the SGD algorithm, the learning rate was set as 0.02 and batch size was kept as 32 for our models (Patterson and Gibson, 2017). The use of larger or smaller learning rates did not provide improved results. Furthermore, other batch sizes were used in the training of the model, but the model was not improved. The selection of number of layers and the number nodes were tested by increasing or decreasing layers or nodes, and finally

Table 1: List of hyperparameters used for major model configuration

Hyperparameter	Settings
Optimizer	SGD
Activation function	ReLU
Learning rate	0.02
Batch size	32
Momentum	0.9 (Nestrov)
Dropout	50%
Number of epochs	2000
Number of hidden layers	3
Number of nodes	2500
Number of training data sets	4500

three hidden layers with 2500 nodes were used in the models. Another hyperparameter is the rate of dropout at each hidden layer, which was 50% in the model. Thus, during the training, 50% of the layer outputs that were randomly selected were kept inactive. This regularization process helps to reduce overfitting and increases the efficiency of the training (Srivastava et al., 2014). Finally, the number of epochs in the training process, which indicates number of times that a full data set has passed the optimization calculation (Smith and Eli, 1995), were determined depending on the rates of the progress of the training (Figure 6). This is described in the following sections.

The input parameters for the inverse model include the maximum inundation distance, flow velocity, maximum flow depth, and the sediment concentration of six grain-size classes. The range of values for the maximum inundation distance, flow velocity, maximum flow depth, and sediment concentration used for generating the training data sets were 2500 to 4500 m, 1.5 to 10 m/s, 1.5 to 12 m, and 0 to 2%, respectively. These ranges of flow conditions are also presumably applicable to other areas where large-scale tsunami inundated. These values are based on the maximum records of tsunamis in the studies of Mori and Takahashi (2012), Nakajima and Koarai (2011), Foytong et al. (2013) and Jaffe et al. (2012).

The values of the loss function of training and validation at the first epoch were 0.09 and 0.07 for the training and validation data, respectively. The value of the loss function decreased to less than 0.01 after 200 epochs. The present model was reasonably converged over 2000 epochs for both the training and validation performance. Moreover, the plot for

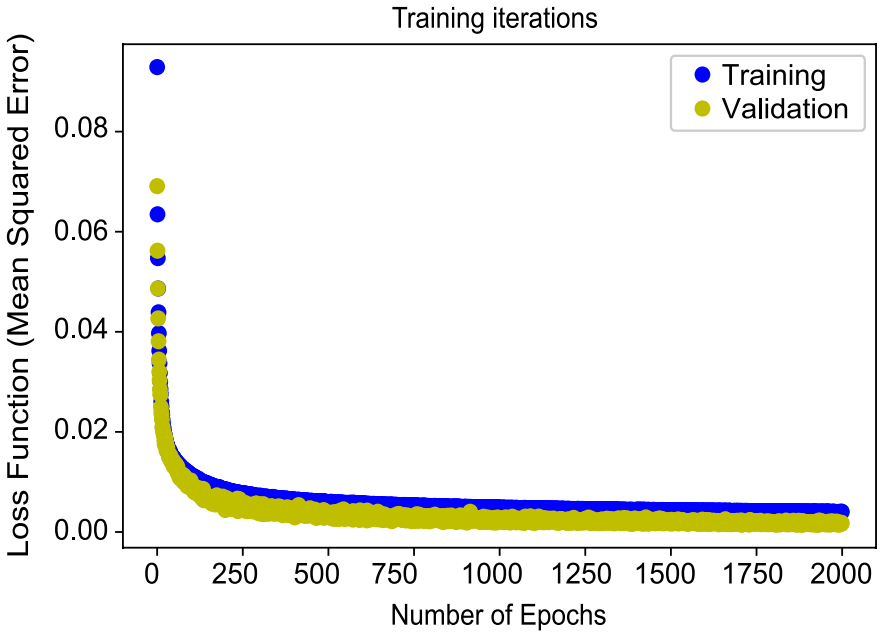

Figure 6: History of learning indicated by the variation of the loss function (mean squared error). Both the values of the loss function for the training and validation data sets decrease over 2000 epochs without any discrepancy, thus indicating that overlearning did not occur.

the loss function was smooth, and there was no anomalous oscillation. The last and lowest loss function at the final epoch was 0.0040 for the training data sets and was 0.0018 for the validation data sets. The efficiency of performance increases if the loss function reduces with the number of iteration or epochs with time. The aim is to achieve the lowest value of loss function by tuning the hyperparameters in the neural network. The sampling window was set from 0 to 2000 m in this training and the following tests (Figure 5).

For the current inverse models, the forward model was calculated repeatedly from 500 to 4500 iterations, and it provided the best result with 4500 iterations of calculations of the forward model (Figure 7). Figure 7 presents a plot of the relation between the number of training data sets and the loss function of the validation data set. The loss value of the validation data set decreases as the amount of training data increases, which creates concave-upward shape. When the number of training data in the data set was 500, the loss function was higher but decreased significantly after 1500 training data sets. The loss function reached a minimum value after 3500 training data sets and did not change much subsequently. Thus, it was suggested that the number of training data sets should be greater

than 3500. The number of training data sets thus used was 4500.

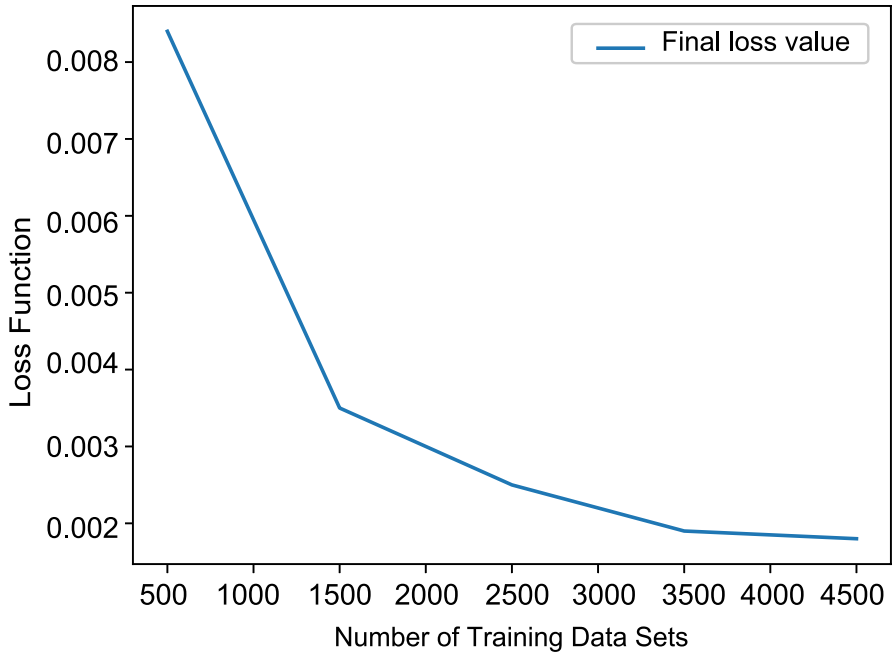

Figure 7: Relation between the loss function of the validation and number of training data sets selected for the inverse model. The results of the training improved as the number of training data sets increased, whereas it varied slightly after 4000 training data sets.

After training the model, the predictions of the inverse model estimates for test data sets were plotted against the original values used for producing the test data sets. Figure 8(a–i) shows that the nine predicted parameters from the artificial test data sets were distributed along the 1:1 line in the graph indicating that the test results were correlated with the original inputs.

Figure 9(a–i) shows histograms of the deviation of the estimated values predicted from the original values. Deviations were distributed in a relatively narrow range without large biases from the true conditions, except in the case of the maximum flow depth. Only the maximum flow depth was slightly biased. Based on the scatter diagram (Figure 9), the values of the predicted maximum flow depth were approximately 0.5 m lower than the input values.

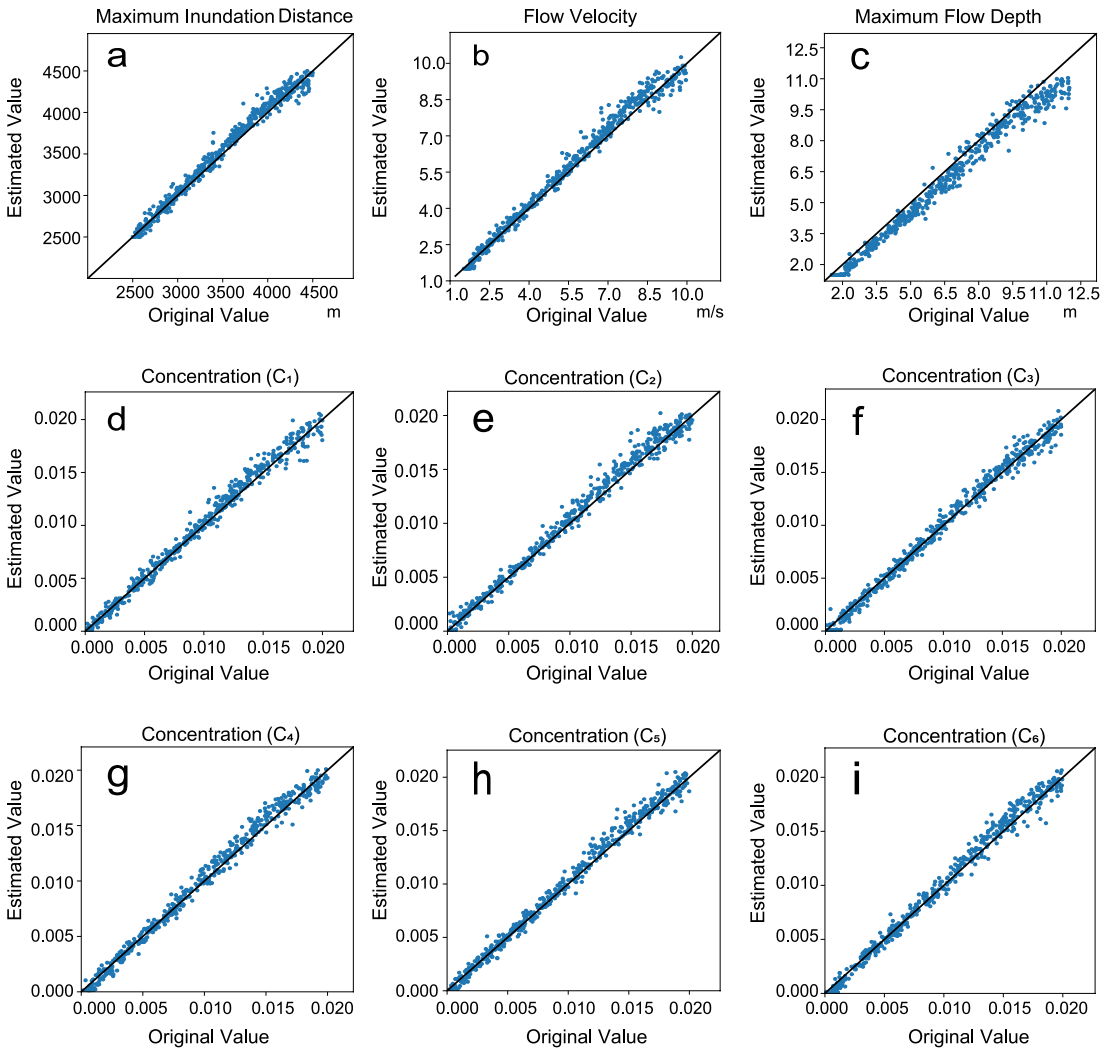

Figure 8: Verification of the performance of the model using artificial test data sets. The values estimated using the inverse model were plotted against the original values used for the production of the test data sets. The solid lines indicate a 1:1 relation and suggest good correlation. (a) Maximum inundation distance, (b) Flow velocity (c) Maximum flow depth, (d)–(i) Concentration of six grain-size classes.

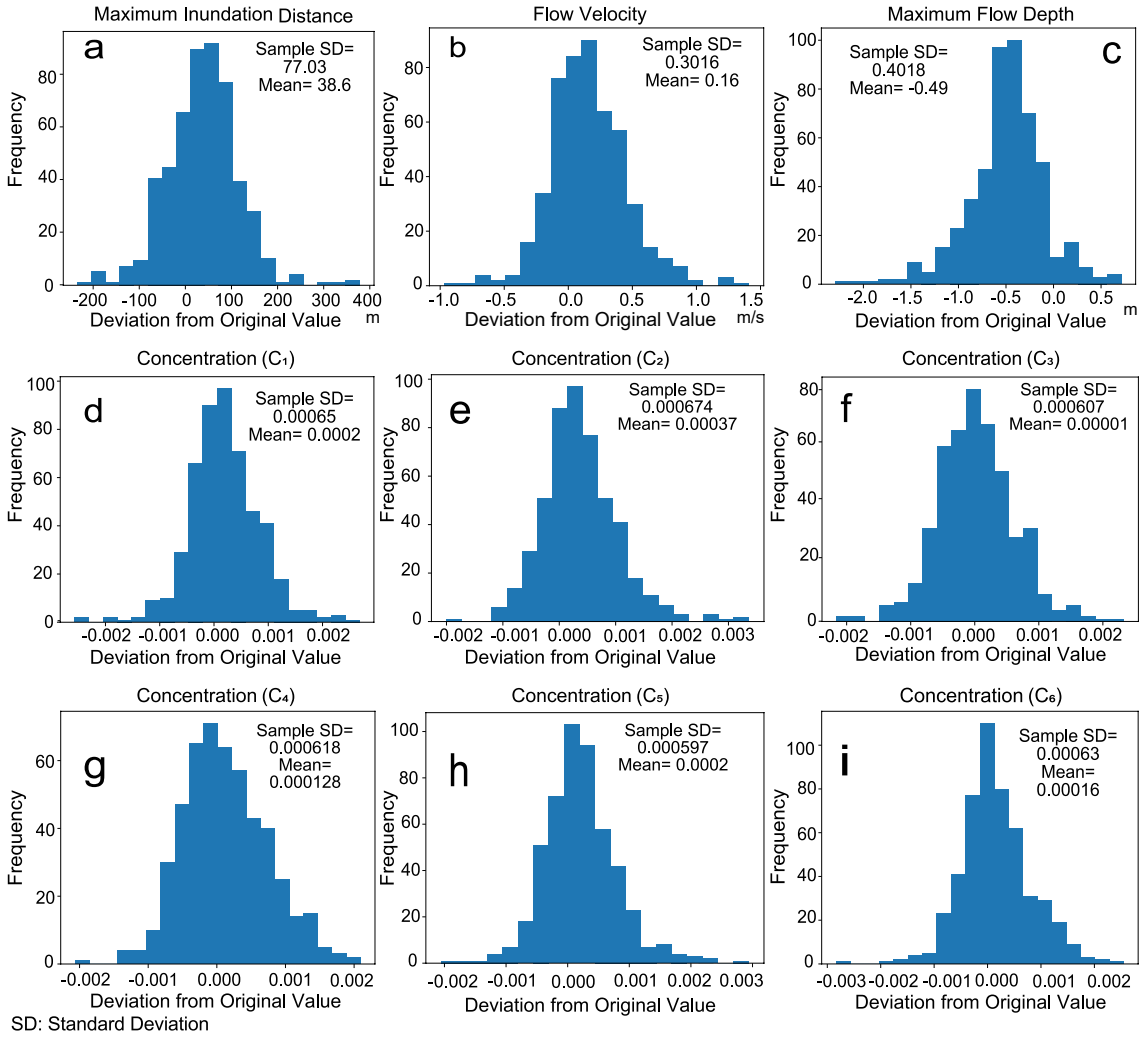

Figure 9: Histograms showing the deviation of the predicted results from the original values of the artificial test data sets. (a) Maximum inundation distance, (b) Flow velocity (c) Maximum flow depth, (d)–(i) Concentration of six grain-size classes.

2.4 Result of application to the 2011 Tohoku-oki tsunami deposit

The model was applied to the 2011 Tohoku-oki Tsunami deposits distributed around the Sendai Plain for the evaluation of the models. This region was extensively surveyed for hazard evaluation as well as tsunami deposits (Abe et al., 2012; Naruse and Abe, 2017), and thus, large amounts of field data are available for evaluating the inverse models. In this study, the field data used was the same as that used for the FITTNUSS model (Naruse and Abe, 2017), and therefore the inversion methodology can be compared with the previous study.

2.4.1 Field methods and settings for inverse analysis

Field work for obtaining these tsunami deposits and collect auxiliary data was conducted in June 2011 that was, three months after the tsunami event (Naruse and Abe, 2017). More details on the methods are provided in the studies of Abe et al. (2012) and Naruse and Abe (2017). The study area (Figure 10) mainly consists of a long sandy beach backed by a high onshore seawall, aeolian sand dunes, coastal forests, and long flat rice-paddy fields (Naruse and Abe, 2017). The deposit samples were obtained every 50–100 m at 26 sites along the transect. The thickness of tsunami sand and mud layers ranged from 0.1 cm to 34 cm. Grain-size analysis of the tsunami deposit showed that the tsunami sand was primarily medium sand with a small amount of fine and very fine sand (Naruse and Abe, 2017). The measured grain-size distributions were then discretized to six grain-size classes (Figure 11), two more classes than used in the previous FITTNUSS model (Naruse and Abe, 2017). The representative diameters of the grain-size classes were 615, 406, 286, 177, 117 and 77 μm.

Parameters, such as flow velocity, estimated using the inverse model were verified by comparing them with the data obtained from aerial videos and observations of the Sendai Plain (Hayashi and Koshimura, 2013; Mori and Takahashi, 2012). It is difficult to evaluate the predicted sediment concentration data as it was not possible to obtain sediment concentration by direct field observation during that event.

2.4.2 Determination of length of sampling window

The sampling window was set at a region from 0 to 2000 m along the transect. Although the total distance of the transect for collecting the samples was approximately 3000 m, the measured bed thickness was very thin (several millimeters) and exhibited a large fluctua-

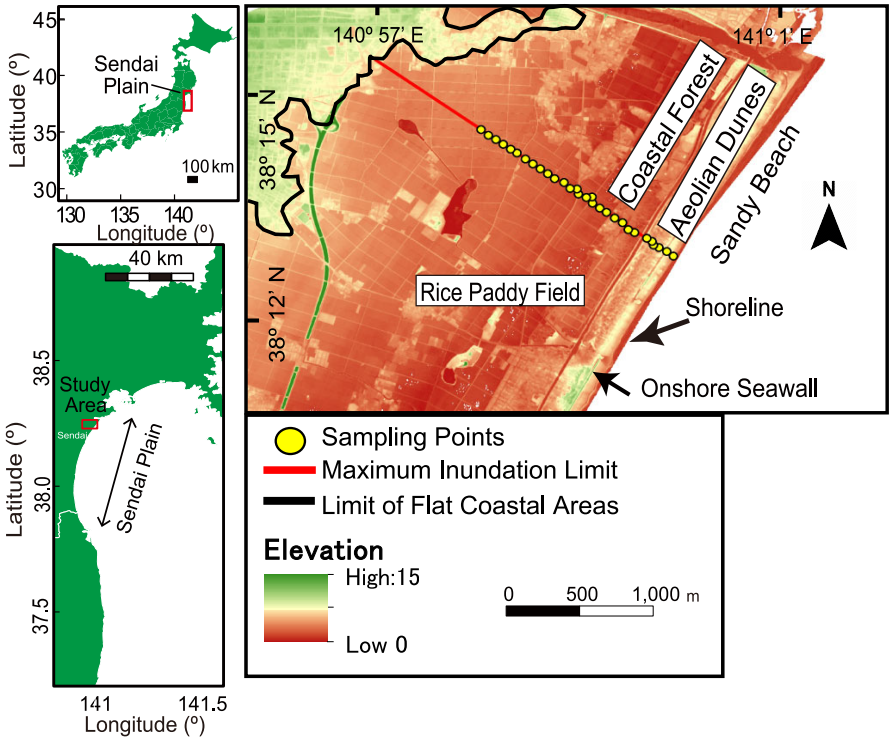

Figure 10: Location of the survey transect and sampling points on the Sendai Plain. The location of the surveyed transect is shown on the topographic map of the study area. The 4 km long transect was situated transverse to the shoreline, and the tsunami deposit was sampled at 27 locations along the transect (Naruse and Abe, 2017).

tion in the distal region (2000 to 3000 m) (Figure 15). Therefore, a 2000 m long sampling window was extracted from the sampling distance, which is 3000 m. This size of sampling window was also used for training the inverse model. For this situation, the number of spatial grids used for the inversion was 133 because the grid spacing in the fixed coordinates was 15 m. The selection of a sampling window of this size was checked based on a comparison with the results obtained using different sampling windows, and the results of the comparison suggested that 2000 m was the most suitable for obtaining stable results. Figure 13 shows the fluctuations of the jackknife standard error estimation of the parameters depending on the sampling window sizes. The equations related to jackknife standard error assessment are given in appendix. The majority of the parameters, such as flow velocity and sediment concentrations exhibited a decreasing trend in their estimation errors as the length of the sampling window was increased. In particular, the jackknife error of the flow

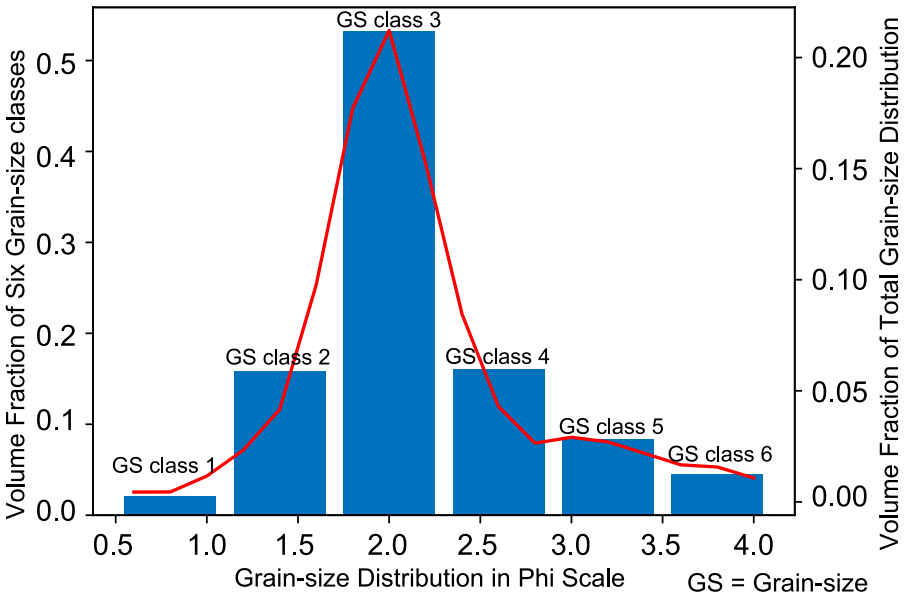

Figure 11: Total grain-size distribution of the tsunami deposits in the Sendai Plain and the discretized fraction of the sediments in the six grain-size classes.

velocity decreased significantly above a sampling window size of 1000 m in length. The estimates of the maximum inundation distance show large errors but it decreased suddenly at approximately 2500 m. In contrast, the error in the maximum flow depth increased above a sampling window size of 2000 m. Hence, it was decided that the size of the sampling window was set as 2000 m. It should be noted that the computation result for the maximum inundation distance was unstable at this selection.

2.4.3 Effect of irregularly spaced data sets on the accuracy of the inversion

In field investigations, sampling intervals are larger than grid spacing of the artificial training and test data sets, and are irregularly spaced. Therefore, it is necessary to check the effect of non-ideal data sets, such as incomplete field data sets on the results of inversion. In the model, 1D linear interpolation was applied to the field data set of Sendai Plain to fit locations of data points to the spacing of training data sets, but this interpolation can have some influence on the predictions of the inversion model. Hence, after the model was trained, subsampling of test data sets was performed at the outcrop locations of Sendai Plain. In this subsampling procedure, volume per unit area of sediment in the test data sets at the sampling locations were estimated by 1D linear interpolation, and these subsampled

data was subsequently interpolated again at the grids of the forward model. Therefore, the irregularly spaced data points were created from the original test data sets, and resulted in regularly spaced sampling locations due to repetition of 1D interpolation. The inverse analysis was conducted on this subsampled test data sets.

Finally, the model prediction was checked with both the true flow conditions and the inversion results using the original test data sets to examine the bias and variance caused by the incompleteness of spatial distribution of sampling locations. Figure 12a and 12b shows that the maximum inundation distance and flow velocity have a bias towards positive end and mean of bias were 210 m and 0.5 m/s respectively. The maximum flow depth has negative bias 0.9 m (Figure 12c). Considering that it already had a bias of 0.5 m in the inversion results of the original test data sets, the additional bias caused by incompleteness of data sets was 0.4 m towards negative end. Figure 12(d–i) shows that the bias in sediment concentrations were generally around 0.001.

2.4.4 Result of inversion

The inverse model reconstructed the flow conditions of the tsunami from the deposit of the 2011 Tohoku-oki tsunami in the Sendai Plain. The model estimated flow parameters that were close to the observed values. The maximum inland extent of tsunami deposits observed by Mori and Takahashi (2012), was up to 4.02 km beyond the shoreline and the tsunami had inundation height of 6.5 m above Tokyo Peil (mean sea level at Tokyo bay), which transported large amount of sandy sediments landward (Mori and Takahashi, 2012). The average flow velocity of the run-up flow was measured 4.2 m/s from an aerial video which varied landward from 6.9 to 1.9 m/s (Hayashi and Koshimura, 2013).

Table 2 shows the predicted hydraulic conditions of the 2011 Tohoku-oki tsunami of the Sendai Plain. The predicted result of the flow velocity was approximately 5.4 m/s with a range of uncertainty ±0.1 m/s using jackknife standard error calculation with a 95% confidence interval (Figure 14b). The value of the maximum flow depth was appoximately 4.1 m (±0.2 m uncertainty using jackknife standard error calculation (Figure 14c) with a 95% confidence interval).

The reconstructed total sediment concentration over six grain-size classes was 5.08%. The estimated value of the sediment concentration of each grain-size class ranged from 0.04% to 2.19% (Figure 14d–14i).

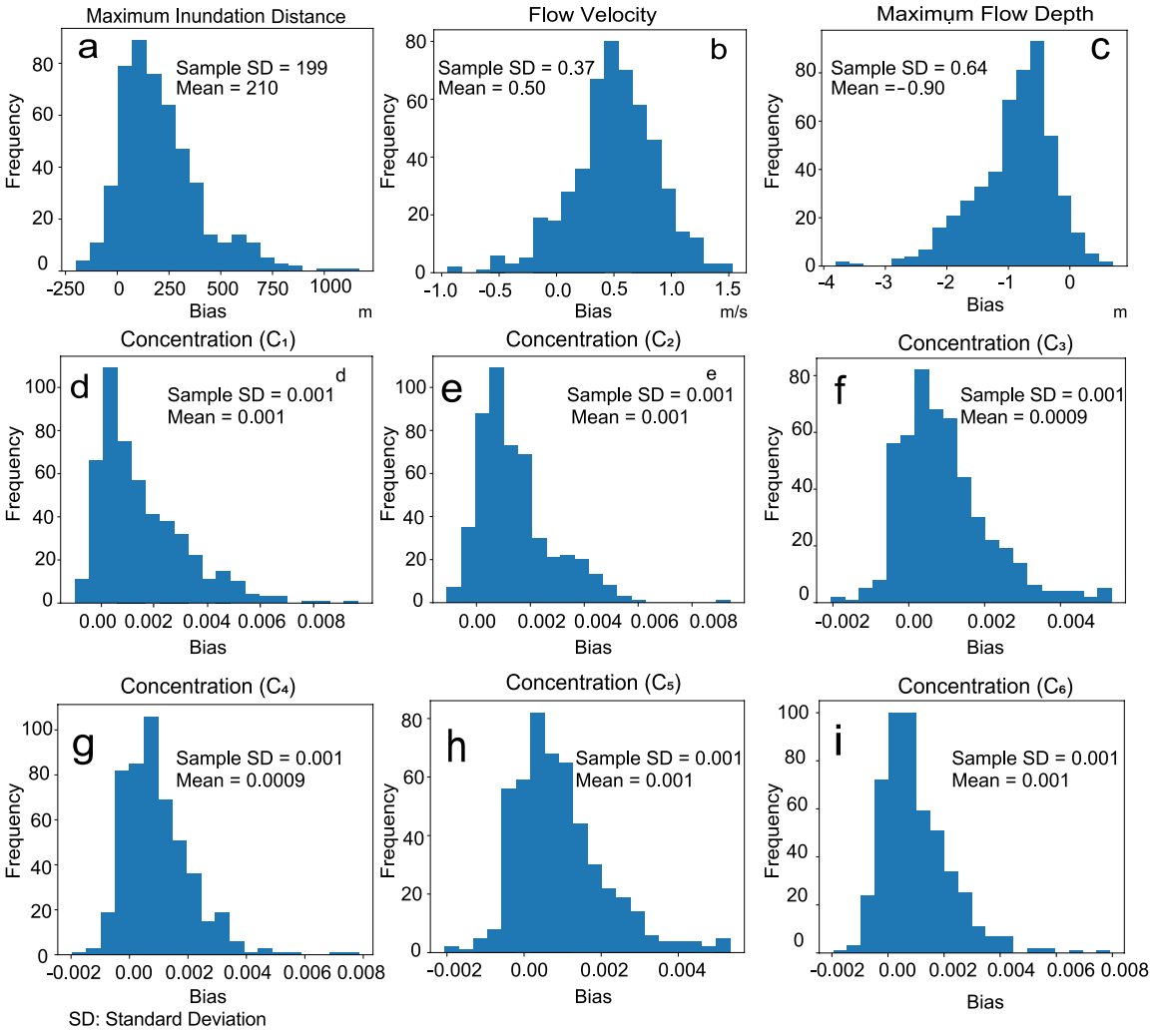

Figure 12: Histograms showing the variance and bias of predictions from the test data sets subsampled at the sampling locations in Sendai Plain. (a) Maximum inundation distance, (b) Flow velocity (c) Maximum flow depth, (d)–(i) Concentration of six grain-size classes.

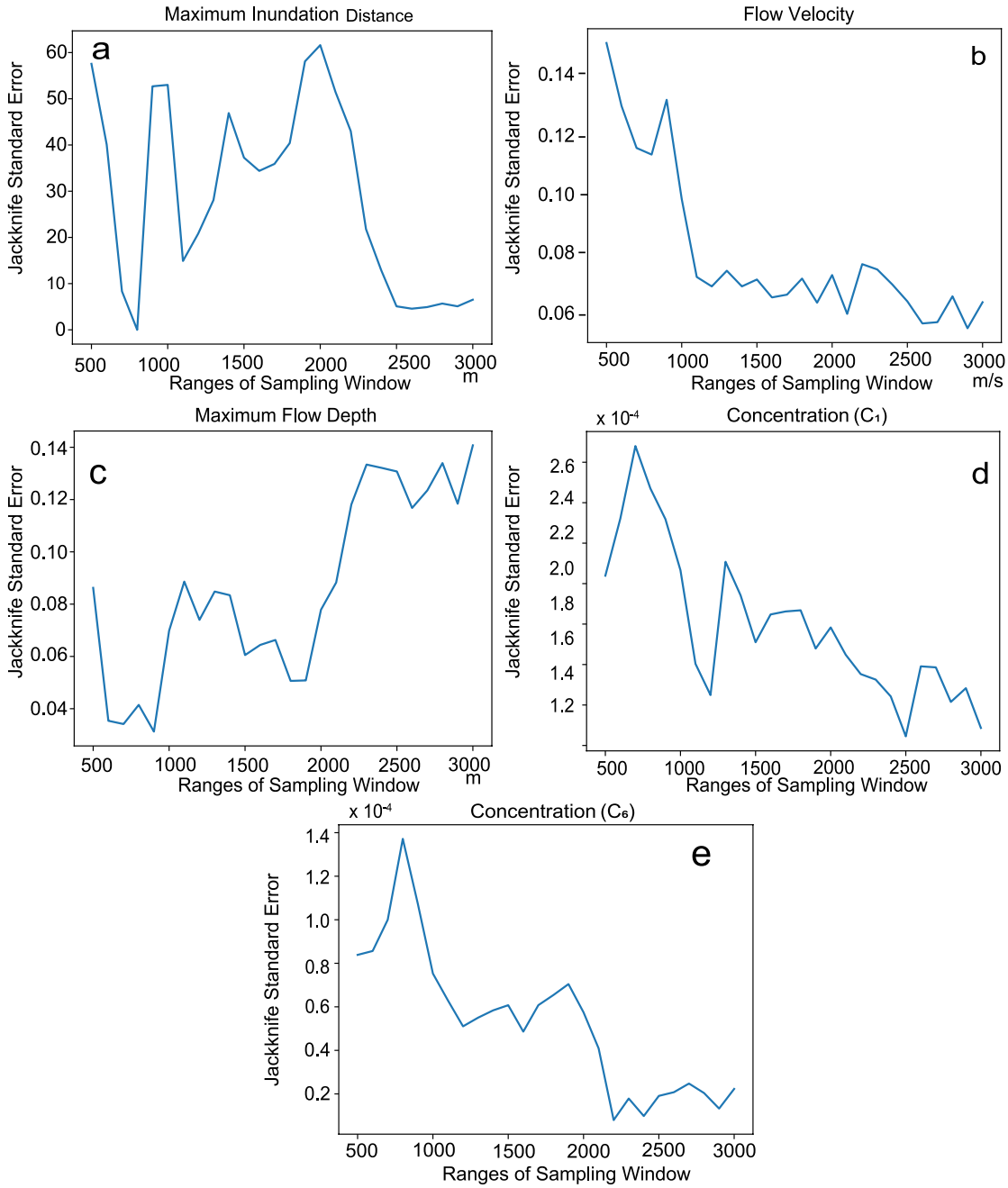

Figure 13: Variation of jackknife standard error with changing range of sampling window distance. (a) Maximum inundation distance, (b) Flow velocity (c) Maximum flow depth, (d) Concentration of the first grain-size class, (e) Concentration of the sixth grain-size class.

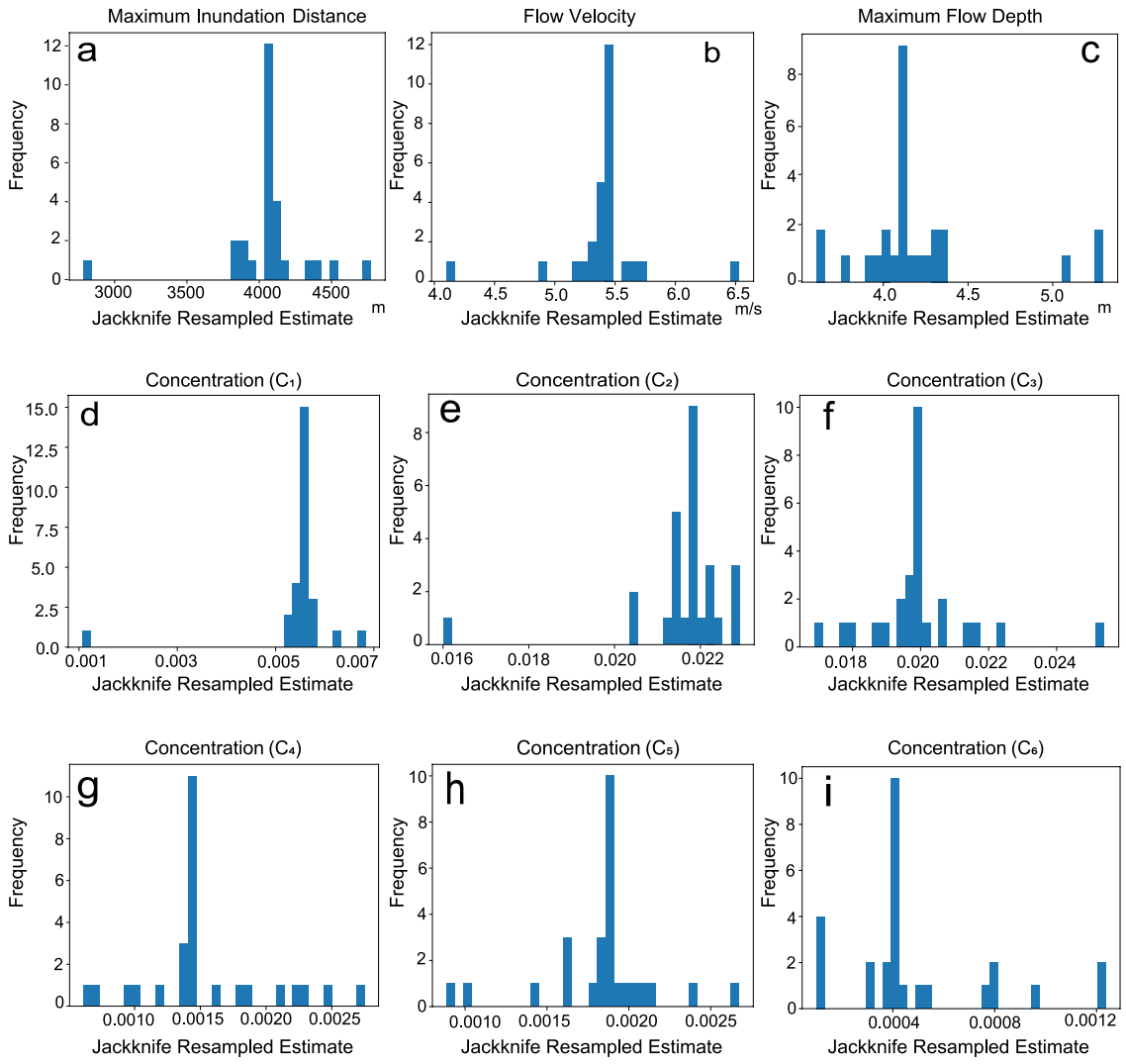

Figure 14: Jackknife estimates for the results predicted by the inverse model to determine the uncertainty of the model. (a) Estimates for maximum inundation distance, (b) Estimates for flow velocity (c) Estimates for maximum flow depth, (d)–(i) Estimates for Concentrations of six grain-size classes.

Table 2: Predicted results by inverse model applied to 2011 Tohoku-oki tsunami deposit data obtained from Sendai Plain

Parameters	Predicted Results	Mean bias
Maximum inundation distance	4045 m ± 121 m	210 m
Flow velocity	5.4 m/s ± 0.1 m/s	0.5 m/s
Maximum flow depth	4.1 m ± 0.2 m	-0.9 m
Concentration of C_1 (615 μm)	0.55% ± 0.034%	0.1%
Concentration of C_2 (406 μm)	2.19% ± 0.048%	0.1%
Concentration of C_3 (268 μm)	1.98% ± 0.058%	0.09%
Concentration of C_4 (177 μm)	0.1% ± 0.018 %	0.09%
Concentration of C_5 (117 μm)	0.18% ± 0.012%	0.1%
Concentration of C_6 (77 μm)	0.04% ± 0.011%	0.1%

The model predicted the maximum inundation distance of the tsunami from the deposit, as approximately 4045 m with a ± 121 m jackknife standard error with a 95% confidence interval (Figure 14a). The actual inundation distance was 4020 m (Naruse and Abe, 2017), which is consistent with the reconstructed value. Table 2 also shows, mean bias which are the mean of the bias estimates for 9 parameters, caused large and irregular spacing of the sampling points. The maximum inundation distance shows 210 m bias and flow velocity shows 0.5 m/s bias towards positive end, whereas the maximum flow depth shows total 0.9 m bias towards negative end. Bias in the sediment concentration was around 0.001.

Finally, using the reconstructed initial conditions of the tsunami, the forward model was used to calculate the spatial distribution of the thickness and grain-size composition for a comparison with the measured distribution. Figure 15 exhibits the thickness and grain-size distribution with the distance for the measured data and simulated results. The measured values of volume per unit area for each grain-size class matched the simulated results except in the case of the finest grain-size class, where the predicted values were larger than the actual measurements.

2.5 Discussion

2.5.1 Tests of inverse models

The tests of the inverse models performed using the artificial data sets of tsunami deposits demonstrated that the models built using NN can predict the flow velocity and the concentration of six grain-size classes, maximum inundation distance reasonably. The scatter dia-

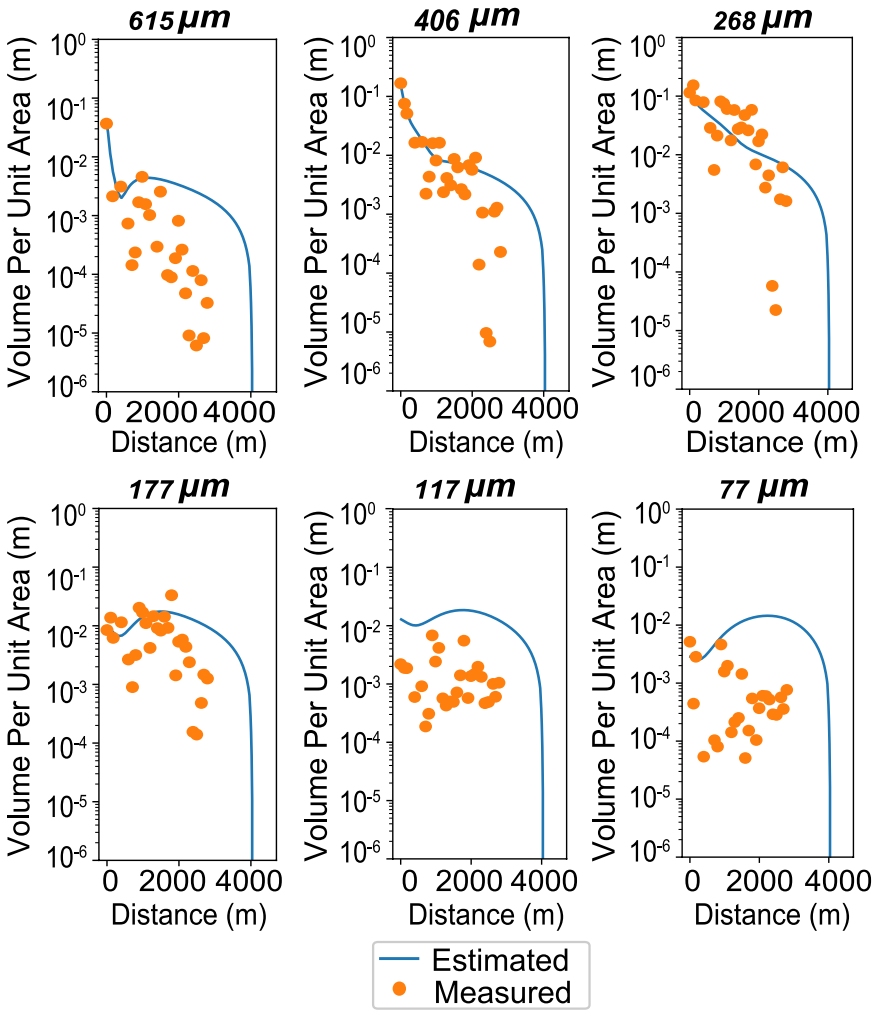

Figure 15: Spatial variation of the thickness of the tsunami deposit. Spatial distribution of volumes per unit area of six grain-size classes is presented. The solid circles indicate the values measured by Naruse and Abe (2017), and the lines indicate the results of the forward model calculation obtained using parameters predicted by the inverse model.

gram of the predicted parameters against the true conditions indicates excellent correlation (Figure 8). For example, 95% confidence interval of the estimation error of the maximum inundation distance was 121 m, and the range of true values was 2500–4500 m (Figure 14). Thus, the precision of estimates is only the order of approximately 5%. More importantly, there was no large deviation of mode of predicted values from true conditions except for the maximum flow depth. Especially in cases of estimates of sediment concentration, mean of the estimation errors ranges within 1.0×10^{-3}. These results imply that the inverse model has the ability to possess the prediction of hydraulic conditions satisfactorily.

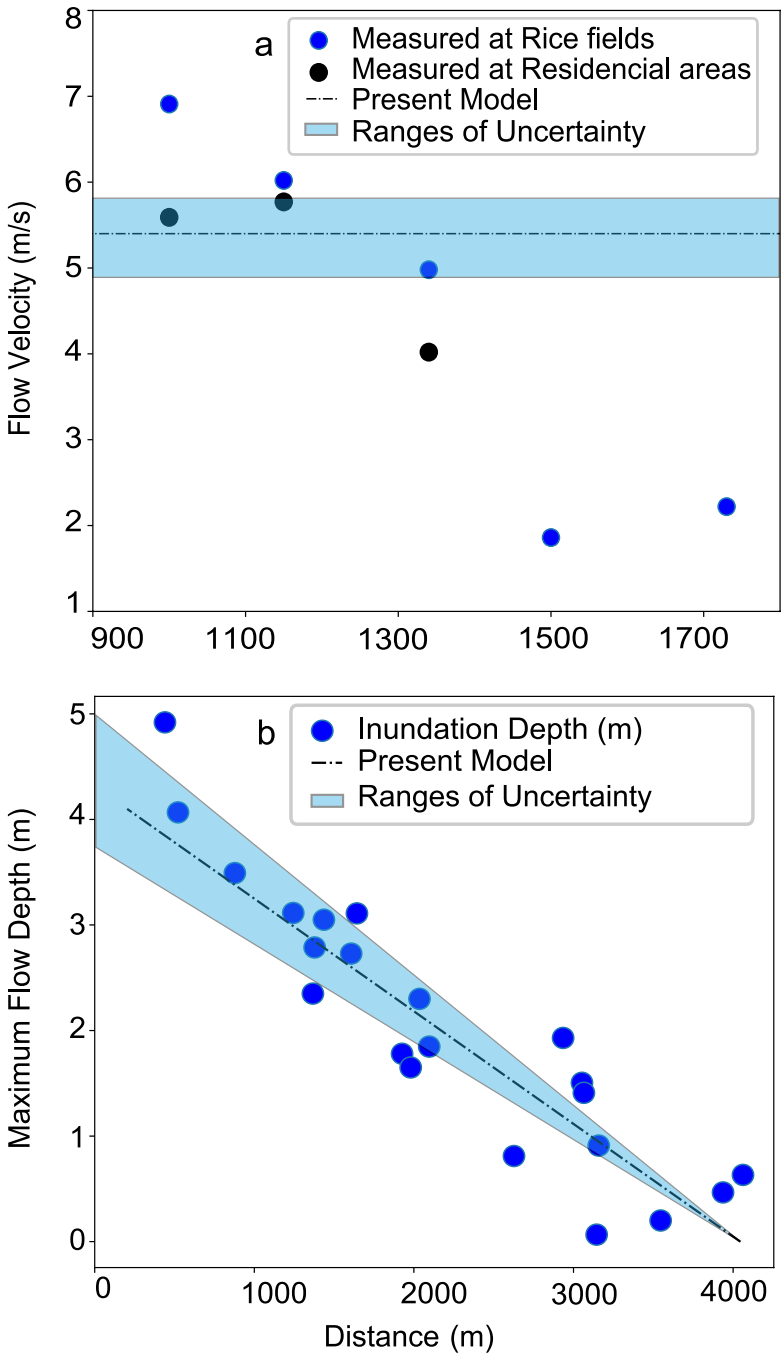

Figure 16: Comparison between field observation and results of inverse analysis of the 2011 Tohoku-oki tsunami. The solid dots are measured values by field observation, and the lines are results of the inverse analysis of this study. (a) Velocity of run-up flow of the 2011 Tohoku-oki tsunami on Sendai Plain. (b) Maximum flow depth of the 2011 Tohoku-oki tsunami on Sendai Plain. Values measured from the aerial videos are indicated by the solid and open circles (Hayashi and Koshimura, 2013), and the results of the inverse analysis are shown by the lines.

However, the model tends to estimate maximum flow depth values that are approximately 0.5 m lower. As a result, in the comparison of the predicted values and original values of the maximum flow depth plotted in the histogram, the deviation shows a positive bias, and the mode value was approximately 0.5 m towards the negative side. Despite the skewness, it is possible to correct the final result of the maximum flow depth by adding 0.5 m with the final reconstructed value from original field data.

2.5.2 Reconstruction of the flow parameters of the 2011 Tohoku-oki tsunami

After applying the inverse models to the 2011 Tohoku-oki tsunami, the predicted results of the flow velocity and the inundation depth were close to the values observed in the aerial video and field measurements (Figure 16), which indicates the effectiveness of the proposed method in applying the actual tsunami deposits.

The subsampling test showed (Figure 12) that the inversion model has slight bias for maximum inundation distance, flow velocity and the maximum flow depth because of the effect of large and irregular interval of sampling locations. The flow velocity shows 0.5 m/s mean bias towards the positive end. Therefore, the predicted value of flow velocity 5.4 m/s could be approximately 4.9 m/s considering the bias correction. Figure 16 shows that the observed inundating flow velocity of the 2011 Tohoku-oki tsunami measured by video records varies spatially from 1.9 to 6.9 m/s (Hayashi and Koshimura, 2013), and the reconstructed values along with the jackknife uncertainty estimates (4.8–5.8 m/s) are in the range of observed values.

The predicted inundation distance was 4045 m which is close to the original maximum inundation distance of approximately 4020 m. However, the mean bias for this parameter caused by incompleteness of field data sets was 210 m (Figure 12; Table 2). Hence, the bias corrected reconstructed values of the maximum inundation distance could be approximately 3835 m which is still close to the maximum inundation distance measured in the field (Naruse and Abe, 2017). The range of the estimated concentration for each grain-size class was 0.04–2.19 vol.%, and the total concentration was 5.08 vol.%. There was no direct observation of the sediment concentration in the inundating tsunami flows, and thus, it is impossible to compare the reconstruction with the actual observation.

The predicted results for the maximum flow depth were close to the observed maximum flow depth in the field data (Figure 16). The model predicted 4.1 m that approximates

the observed values well. The uncertainty analysis performed using the jackknife method indicated that the error of estimates for maximum flow depth ranges from 3.8 m to 4.4 m, which is reasonably narrow for an assessment of the magnitude of the tsunami. However, considering the total mean bias caused by both original and interpolation of the field data sets, 0.9 m should be added to the maximum flow depth predicted by the inverse model (Figure 16). Thus, the reconstructed value obtained can be corrected to 5.0 m, which is closer to the observed data set.

This is to be noteworthy that the effect of the friction coefficient (C_f) on the results of inversion was investigated to check forward model influence on the inversion results. Estimates of flow velocity varied from 5.5 to 3.1 m/s in response to the variation of C_f from 0.002 to 0.01. The present study uses C_f value 0.004 as the same was used in the FITTNUSS model (Naruse and Abe, 2017). The variation of reconstructed values of inundation depth varied only from 4.8 to 5.0 m and sediment concentration in response to varied C_f was negligible. To summarize, the result obtained using a largest value of friction coefficient (C_f) corresponds to the higher velocity in inversion results, but other flow characteristics were not influenced largely. Therefore, it is important to specify realistic friction coefficient value in the forward model to estimate flow velocity. The influence of number of grain-size classes on the inversion results was also checked. The variation of the results was negligible for all reconstructed values. Hence, the assumptions in the forward model have least influence on the inversion results.

2.5.3 Comparison with existing models

In the present study, I presented the use of a deep-learning NN as an inversion technique with a modified FITTNUSS forward model to obtain the initial tsunami hydraulic condition based on tsunami deposits. The advantages of this new methodology are that (1) it can employ a more realistic forward model than previous methods, and (2) the performance of the inverse model can be tested before its application to actual deposits by using artificial data sets. In addition, (3) it is possible to conduct an uncertainty analysis of the inversion using the resampling method owing to the computational efficiency of the model. However, the data set of the 2011 Tohoku-oki tsunami deposits in Sendai Plain is one of the best records of tsunami deposits in history. The data set contains high resolution samples as well as observational records of flow velocity and flow depth. However, further verification

of the methodology using other case studies is strongly needed in future studies for proving wide applicability of the method.

First, the DNN inverse model can employ the forward model, which is computationally expensive. The new inverse model requires only a limited number of iterations of the forward model calculation for producing the training data sets, and these iterations can be parallelized. The calculation for producing each training data set is independent. In contrast, the previous inverse models, including the FITTNUSS model (Naruse and Abe, 2017), employed the optimization method (e.g., LBFGS) in which the forward model calculation depends on the result of the previous iteration, and thus, this trial and error procedure cannot be parallelized. It was time consuming to obtain the best solution and was difficult to improve the computational efficiency in the previous methodology. Therefore, the previous inverse model only employed the largely abridged forward models, such as the "moving-settling tube" (Soulsby et al., 2007) or sudden settling from equilibrium uniform flows (Jaffe and Gelfenbuam, 2007). The recent inverse model TSUFLIND (Tang et al., 2018; Tang and Weiss, 2015) also probably employed a similar simplified assumption because of this computational load problem. Tang et al. (2018) proposed the inversion model with uncertainty analysis using TSUFLIND-EnKF method but this method shares the same limitations of TSUFLIND in the assumption of the forward model. In addition, optimization by EnKF requires iteration of calculation that cannot be parallelized, while production of training data sets in this method can be easily parallelized so that it can employ computationally expensive models (Tang et al., 2018).

In the new inverse model, this limitation is diminished in the forward model, such that the former can potentially employ fully hydrodynamic models as the forward model. The present method of DNN is relatively robust against the sampling measurement errors as the uncertainty can be evaluated by jackknife method which was not applied to any other inverse models. Furthermore, the forward model can be easily replaced with the similar or other upgraded forward models to improve the inverse model. This phenomenon implies that the present inverse model is flexible for upgrades.

Secondly, the inverse model proposed herein can be tested prior to the actual analysis because each inversion (i.e., feed-forward calculation of the NN) is completed instantaneously in this method. In previous methods, such as FITTNUSS, each inversion requires a long time such that it was not realistic to iterate the inversion several hundred times for

testing the performance of the model. In addition, a modern statistical uncertainty analysis requires resampling procedures in which the iteration of the inversion is also required. Therefore, it was possible to apply the jackknife uncertainty analysis in the case of the DNN inversion in this study, but it is difficult to provide an error range of the estimates for the FITTNUSS method or other methods in a realistic time period.

The inverse model in this study uses inexpensive artificial data for training of the neural network to avoid the difficulties to gather large amounts of data sets of tsunami deposits with in-situ measurements of flow velocity and depth. Even if the measured values of tsunami characteristics are available, the overfitting of the inverse model should not be avoided because the number of those data sets must be limited. The random generation of artificial training data sets for different parameters was adopted to bypass the drawbacks of using real measurements to train the inverse model (Le et al., 2017; Tobin et al., 2017; Tremblay et al., 2018). Bias due to inaccuracy of the forward model may occur in this methodology as all of other inverse models, and thus it is necessary for accurate reconstruction to seek the forward model based on the appropriate assumptions for the field. As described above, the framework of inversion employed in this study is flexible to adopt a realistic forward model.

2.6 Limitation and scope of improvement

The present model shows promising results, but the reliability of this model is required to be validated by using more field data. The options and hyperparameters of the inversion, such as the sampling window size, can be tested using other examples of modern tsunami deposits with known flow parameters. Furthermore, it is necessary to apply this model to tsunami deposits in Tohoku and other regions along with older tsunami deposits in order to scrutinize the present model comprehensively and to develop a robust model that can be used in the relevance of hazard evaluation.

In addition, the model still has some limitations in terms of its applicability and accuracy. For example, the reconstructed values of the maximum flow depth showed a bias of -0.5 m, and the additional bias caused by the effect of irregularly spaced data sets on the inversion results. In future studies, improving the algorithm of the neural network structure might eliminate or reduce the bias of the parameter. Notwithstanding the bias in the predicted values of the parameters such as maximum inundation distance, flow velocity,

maximum flow depth, this model showed satisfactory results for tsunamis of any scale. Our model is not suitable for the regions with topographic lows and channels along with the high slope areas where return flow is strong. The assumption of quasi-steady run-up flow analysis will only work in regions where the topography is sufficiently smooth and slope can be regarded as constant. Also, the forward model assumptions are valid only at depositional areas. Thus, a coastal dike or problems in source areas are not necessary to consider (Naruse and Abe, 2017), and therefore the erosional areas must be excluded in the inverse analysis using our method. These simplifications are adequate for the Sendai Plain as suggested by verification of the inversion result. In future studies, it is needed for verify influence of degree of topography on the inversion results, and other forward models will be tested if necessary. The improvement of the model can be done by incorporating 2D shallow-water model in future.

It is to be noted that, in the present study considered thickness of the deposit for one run-up flow or layer. Thus, in case of deposits that exhibit multiple layers (Abe et al., 2020), one of the layers must be chosen for the analysis. Hence, if a single layer cannot be traced in a region, it is impossible to apply our model to that region. Since, the 2011 Tohoku-oki tsunami deposits on Sendai Plain were mostly observed to be a single sand layer formed by the first wave, it was possible to apply the model to Sendai Plain (Abe et al., 2012).

2.7 Conclusions

The new model presented in this study uses an artificial NN to derive the hydraulic conditions of a tsunami. It successfully reconstructed the flow conditions including the maximum inundation distance, flow velocity, maximum flow depth and sediment concentrations from artificial tsunami deposits produced by the forward model as well as the natural tsunami deposits of the 2011 Tohoku-oki tsunami. The reconstructed flow velocity and maximum depth were 5.4 m/s and 4.1 m respectively, which are in the ranges of observed values of the tsunami. The uncertainty of the results was determined using the jackknife method, which also shows that the model yields results that do not comprise large ranges of data. Thus, in future studies, it is expected that this model would be able to successfully reconstruct the flow conditions of modern and ancient tsunamis.

2.8 Code and Data availability

The source codes and all other data of the DNN inverse model are available in Zenodo (http://doi.org/10.5281/zenodo.3881964).

2.9 Copyright statement

3 Reconstruction of the flow conditions from the 2004 Indian Ocean tsunami deposits at the Phra Thong Island, Thailand

3.1 Introduction

On December 26, 2004, a Mw 9.1 earthquake triggered a devastating tsunami that affected the coastal areas and cities adjacent to the Indian Ocean, which resulted in extensive socio-economic damage and numerous fatalities in several countries including Thailand, Indonesia, Srilanka, India, and Myanmar (Satake et al., 2006; Sinadinovski, 2006; Rossetto et al., 2007; Pari et al., 2008; Satake, 2014; Philibosian et al., 2017). In Thailand, 8300 people lost their lives, with 70 lives and a village of households were lost on the Phra Thong Island in Phang-Nga Province (Satake et al., 2006; Masaya et al., 2019). In Thailand, the total damage was estimated to amount to around USD 508 million, which equates to approximately 2.2% of GDP while the number of deaths was 4225 in Phang Nga Province, with the injured and missing cases (Jayasuriya and McCawley, 2008, 2010; Suppasri et al., 2012).

An awareness of tsunami disaster prevention is the most essential criterion to reduce socioeconomic losses suffered by countries lying along the coastlines, such as Thailand, Japan, Indonesia, India and Srilanka etc. (Lin et al., 2012). Indeed due to the lower tsunami risk and the higher return period of high magnitude tsunamis (600 years) (Suppasri et al., 2015), the degree of preparedness, for example, effective evacuation techniques, and appropriate awareness are still in the early stage of development in Thailand (Suppasri et al., 2012). Suppasri et al. (2012) reported that, the nation has implemented post-tsunami precautionary measures such as the construction of evacuation shelters at a safe height and distance from the coastline along with the evacuation routes with evacuation regulations, memorial parks, appropriate structural design and land use management which were aimed at dealing with tsunami waves. Meanwhile, a careful building of sea walls, and breakwaters has also been suggested for the area.

To propose further regulations for evacuation plan and tsunami hazard mitigation, evaluating the extent of tsunamis with the flow velocity and the maximum height that the tsunamis could reach is important (Pignatelli et al., 2009). However, these flow parameters have not been directly measured, even for the 2004 Indian Ocean tsunami. It has been reported by Satake et al. (2006) that the maximum elevation that a tsunami reached

(tsunami height) in Thailand, was between 5 and 20 m, and Tsuji et al. (2006) reported 19.6 m flow height at Phra Thong Island, while Rossetto et al. (2007) reported a peak tsunami height of 11 m and Jankaew et al. (2008) reported a tsunami height of 5 to 12 m in this area. Meanwhile, other flow parameters, such as flow velocity and depth, remain largely unknown. From the video footage of the tsunami, Rossetto et al. (2007) reported a flow velocity of 6–8 m/s at the Khao Lak area and 3–4 m/s at Kamala beach. Other reported flow velocities from Thailand include 4 m/s at Phuket and 9 m/s at Khao Lak (Karlsson et al., 2009; Szczuciński et al., 2012b).

It is important to obtain the flow conditions essential to tsunami hazard mitigation in terms of devising future resilient structural measures by investigating tsunami deposits, which provide crucial information on the flow discharge and the extent of the tsunami inundation (Dawson and Shi, 2000; Sugawara and Goto, 2012; Furusato and Tanaka, 2014; Sugawara et al., 2014; Udo et al., 2016; Koiwa et al., 2018; Masaya et al., 2019). It has been suggested that, after distinguishing tsunami deposits through their sedimentological characteristics (Morton et al., 2007; Switzer and Jones, 2008; Szczuciński et al., 2012b), they can be used to reconstruct tsunami flow conditions (Jaffe and Gelfenbuam, 2007; Smith et al., 2007; Paris et al., 2009; Sugawara and Goto, 2012; Naruse and Abe, 2017; Tang et al., 2018). The preservation of sedimentary bedforms in the sand sheet, capping bedforms, sedimentary structure, texture, and facies models provides the evidence of flow direction and changes in flow energy and hydrodynamic aspects, such as flow height and inundation distance (Choowong et al., 2008a; Switzer and Jones, 2008; Costa et al., 2011; Szczuciński et al., 2012b; Moreira et al., 2017). Other reconstructions of the tsunami flow conditions at Khao Lak were completed using eyewitness reports, aerial videos, and photographs, while the extent of the damage was analyzed using field measurements and satellite imagery (Karlsson et al., 2009). In addition, analysis of the sediment geochemistry and the diatom assemblages, also provided insights into the flow conditions of the 2004 Indian Ocean tsunami (Sawai et al., 2009; Sakuna et al., 2012; Andrade et al., 2014).

To reconstruct quantitative values of tsunami characteristics from the deposits, various numerical forward and inverse models which incorporate sediment dynamics, and transport and depositional equations have been established (Li et al., 2012; Sugawara and Goto, 2012; Jaffe et al., 2012; Johnson et al., 2016; Yoshii et al., 2018). Recently, the deep neural network (DNN) inverse model was proposed (Mitra et al., 2020) and was proven to be

effective for reconstructing flow conditions via an examination of the deposits of the 2011 Tohoku-oki tsunami. This model also provides some insight into the uncertainty quantification of the estimated flow parameters using the jackknife method. The DNN inverse model predicted the tsunami flow conditions, such as maximum inundation distance, flow velocity, maximum flow depth and sediment concentration from the natural tsunami deposits. The reconstructed inundation distance was 4,045 m which is close to the original maximum inundation distance of approximately 4,020 m, values of run-up flow velocity were 5.4 m/s which was close to the spatial average of the measurements which ranged from 1.9 to 6.9 m/s, and the estimations of the maximum flow depth was 4.1 m which was also within the range of the in-situ measured values from Sendai Plain (Mitra et al., 2020). Thus, this model has reasonable potential to estimate the hydraulic conditions from the 2004 Indian Ocean tsunami that were not measured directly.

The Phra Thong Island is one of the locations where the tsunami deposits were preserved without a great amount of topographic irregularities with almost no anthropogenic disturbances in the island. The coastlines of Phra Thong Island were severely eroded and retreated by the 2004 tsunami. However, the presence of widespread mangrove forests with other waterborne plant debris helped in the identifications of the extent and direction of the flow (Fujino et al., 2008, 2010). Historically the island is an important location for the study of tsunami deposits, with pre-2004 tsunami deposits preserved in inter-ridge swales and an overall extensive distribution of paleotsunami deposits having been reported (Jankaew et al., 2008; Fujino et al., 2009). In fact, paleotsunami deposits have been identified at Phra Thong Island, Thailand by several research teams (Jankaew et al., 2008; Fujino et al., 2008; Sawai et al., 2009; Fujino et al., 2010; Brill et al., 2012b; Pham et al., 2017; Gouramanis et al., 2017; Masaya et al., 2019).

Here, I conduct an DNN inverse analysis of the tsunami deposits measured at Phra Thong Island and reconstruct the flow conditions, such as the maximum inundation distance, flow velocity, maximum flow depth and sediment concentrations of five grain-size classes. The inverse model was based on the forward model, which was proposed by Naruse and Abe (2017). The forward model calculations were iterated at random initial flow conditions to produce artificial training data sets that represent depositional characteristics, such as the spatial distribution of thickness and grain-size composition. Using the artificial training data sets, the DNN was then trained to establish a relation between the depositional

characteristics and the flow conditions. The post-trained DNN model was ready to predict flow conditions from the tsunami deposits after the performance of the trained DNN was verified using test data sets. The 1D cubic interpolation was applied to the field data sets of Phra Thong Island to fit the data set to model grids. Finally, this DNN inverse model was applied to the field data sets from the Phra Thong Island, Thailand to reconstruct the flow conditions of the 2004 Indian Ocean tsunami. This inverse model was already validated to be effective for the 2011 Tohoku-oki tsunami deposits distributed in Sendai Plain (Mitra et al., 2020). In case of Phra Thong Island, I validated the results by the field measurements of the tsunami flow depth. Also, the estimated thickness and grain-size distribution of tsunami deposits were compared with the actual measurements. The inverse analysis results could be used for designing future tsunami hazard assessments and disaster mitigation strategies in Thailand.

3.2 Study area

The study area is the Phra Thong Island, situated off the west coast of Phang-Nga Province (north of Phuket island) and the west coast of southern Thailand (Figure 17a), and is adjacent to the Indian Ocean (Rodolfo, 1969). This study investigated the tsunami deposits distributed in the eastern coast of Phra Thong Island, where the topography near the coastline is a flat plain that mainly consists of shore-parallel beach ridges with intervening swales (Brill et al., 2012a). The 2004 Indian Ocean tsunami flooded the area with waves higher than 6 m and an inundation limit of approximately 2 km inland (Tsuji et al., 2006; Fujino et al., 2010). The tsunami left a widespread sand sheet with a thickness of 5–20 cm (Jankaew et al., 2008; Fujino et al., 2010). Meanwhile, the presence of wet, peaty swales helped in the preservation of the tsunami deposits (Jankaew et al., 2008; Fujino et al., 2009; Gouramanis et al., 2017). Given its natural topography with few artificial features, Phra Thong Island is a rare case, that is useful for verifying tsunami sediment transport calculations with less uncertainty (Brill, 2012).

Figure 17b shows the location of Phra Thong Island and the adjacent areas in Thailand where the tsunami deposits have been reported. I considered samples from 29 locations along the transect shown in Figure 17c and Figure 18. The distance from the pre-event the coastline to each sampling site was calculated by projecting of the sites to a flow parallel reference line (Fujino et al., 2010). Tsunami heights of 6.6, 7, and 12 m were reported near

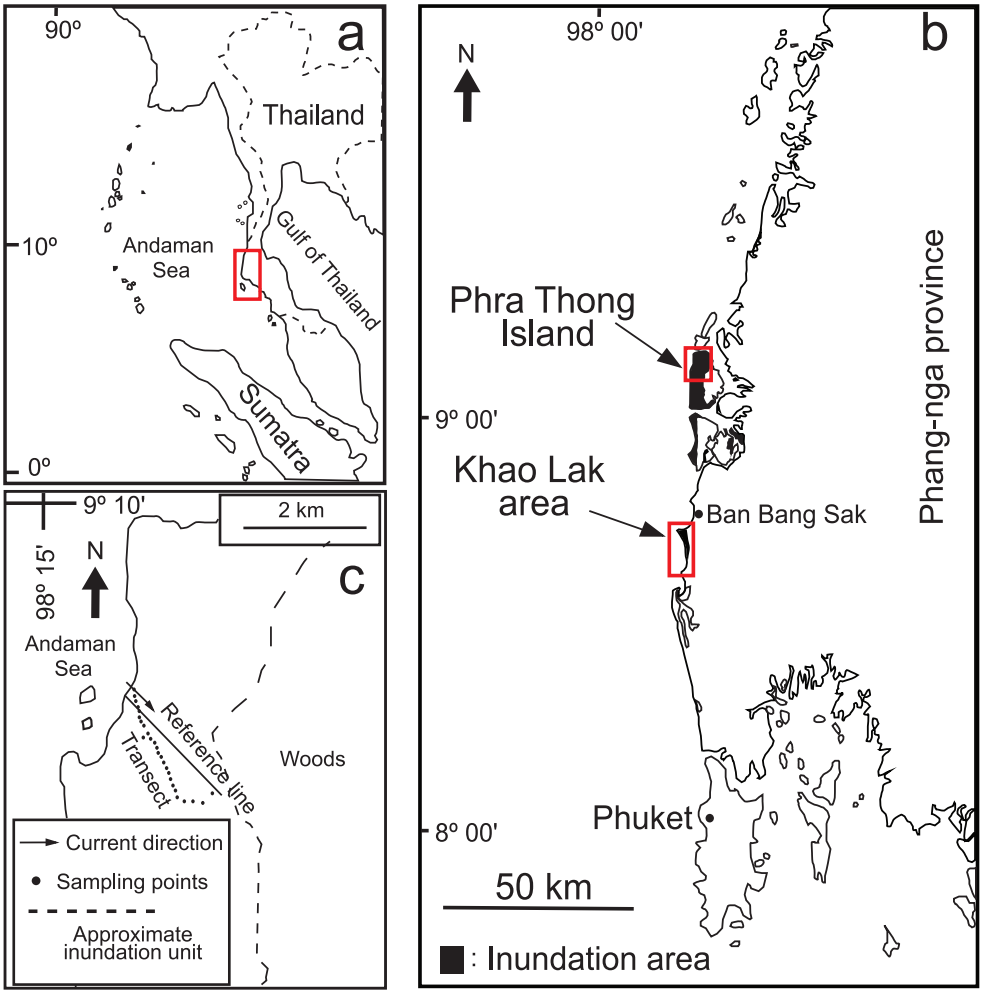

Figure 17: (a) Location of study area in southwestern Thailand.(b) Phra Thong Island and adjacent landmark areas where 2004 Indian ocean tsunami inundated. (c) Locations of study sites at Phra Thong Island. The 2004 tsunami inundated about 2 km inland.

the transect where the coast was extensively eroded and had retreated several hundreds of meters (Jankaew et al., 2008; Fujino et al., 2010). The sediment from shallow seafloors were transported and deposited in large volumes of sand sheet deposition widely along the coast, with the deposit is largely composed of medium to fine sand. The deposit became thinner and finer in a landward direction, becoming very fine at the landward limit of the inundation.

The maximum inundation distance was measured about 2000 m inland (Fujino et al., 2008, 2010) and the thickness of the tsunami deposits at a maximum of 12 cm, while this did oscillate a great deal for the first 1300 m from the shoreline. Meanwhile, the exponentially

Figure 18: Google Earth image showing locations of sampling points investigated for 2004 Indian Ocean tsunami of Phra Thong Island described in this paper.

landward thinning of the deposits was observed along the transect. For more details on the thickness and grain-size distribution of the tsunami deposit, see the description of the transect of Phra Thong Island provided by Fujino et al. (2010).

The mean grain-size and overall grain-size distribution of the tsunami deposits from Phra Thong Island are shown on Figure 19b. The overall thickness of the tsunami deposits along the transect are presented in Figure 19a and the measured grain-size distributions were discretized to five grain-size classes for every location of sampling sites. It should be noted that along the transect, the initial locations of the sampling points of Figure 19a and 19b were adjusted to start from the 0 m distance from the shoreline. Figure 19c and 19d represents the volume fractions of five grain-size classes and total grain-size distribution.

3.3 Methodology

This model uses the forward model of FITTNUSS (the framework of inversion of tsunami deposits considering transport of nonuniform unsteady suspension and sediment entrainment) (Naruse and Abe, 2017) to calculate the sediment transport and deposition from input parameters including the maximum run-up length, the depth-averaged flow velocity, the

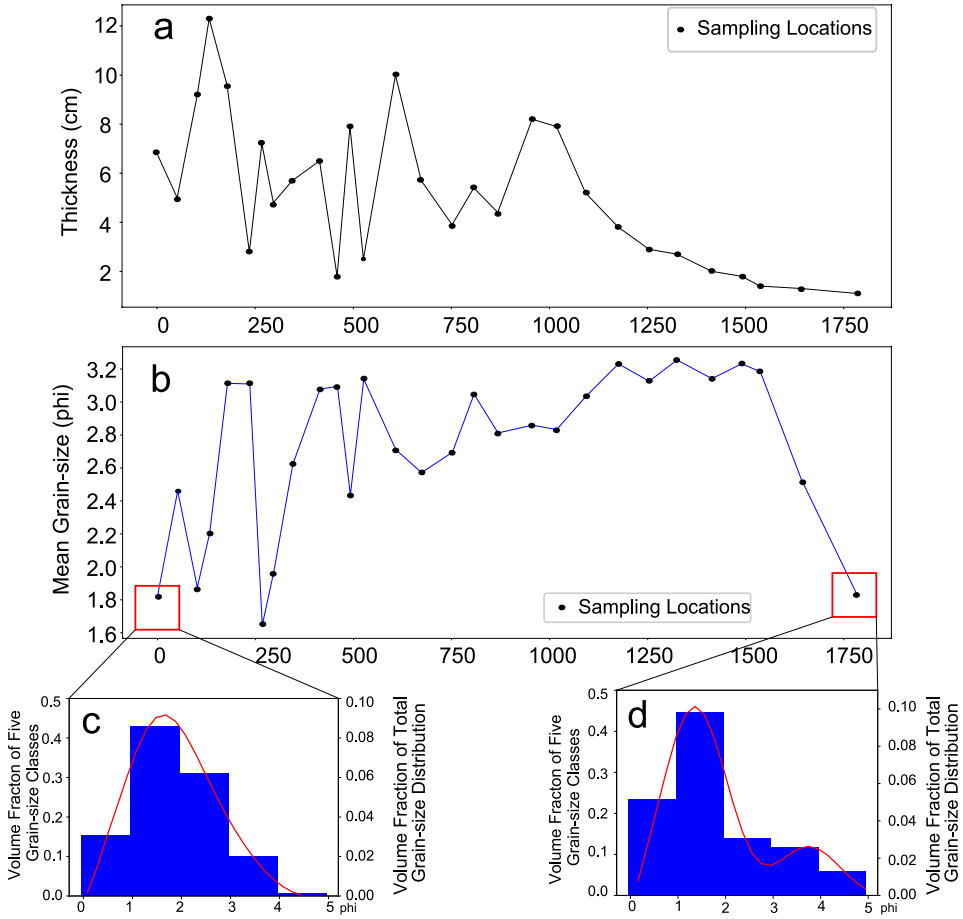

Figure 19: (a) Variations of grain-size parameters and thickness of tsunami deposits for the sites along transect of Phra Thong Island.(b) Mean grain-size distribution of the tsunami deposits along the transect. (c) and (d) Total grain-size distribution at first and last locations at Phra Thong Island and the discretized fraction of the sediment in the five grain-size classes.

maximum flow depth, and sediment concentration at the seaward end. The forward model can calculate the thickness and grain-size distribution along an 1D shoreline normal transect, which is used to train the DNN inverse model. Here, I present a brief overview of the FITTNUSS forward model and the inverse model.

3.3.1 Forward model

The FITTNUSS forward model is based on the layer-averaged one-dimensional equations (Equation 1 and 2). This model incorporates sediment conservation equation (Equation 3), which includes several parameters, such as the volume concentration in the suspension of

the *i*th grain-size class (C_i), the settling velocity (w_{si}), sediment entrainment coeffientcient (E_{si}), ratio of near-bed to layer-averaged concentration of the *i*th grain-size class (r_{0i}) and volumetric fraction of the sediment particles in the bed surface active layer (F_i), above the substrate (Hirano, 1971). For the sedimentation of tsunamis, the Exner equation of bed sediment continuity (Equation 4) was used.

Finally, using the scheme to simplify the tsunami hydrodynamics proposed by (Soulsby et al., 2007), the velocity of the run-up flow of the tsunami, U is assumed as uniform and steady, but the inundation depth varies in time and space (Figure 21). Hence, this model simplification is called the quasi-steady flow assumption (Naruse and Abe, 2017) and the flow dynamics of tsunamis were simplified in the model with the application of a transformed coordinate system and the implicit Euler's method of the equations to increase the computational efficiency. The details of the equations and the parameters and variables are provided in the previous chapter and Naruse and Abe (2017). A few researchers recently reported that tsunami induced boundary layers may span only a fraction of water length formula (Lacy et al., 2012; Williams and Fuhrman, 2016; Larsen and Fuhrman, 2019). The importance of the resistance law for the inverse analysis, considering such non-steady conditions, may be a subject for future study.

The forward model reproduces the spatial variation of the thickness and grain-size distribution of the tsunami deposit from the input values of the following (1) maximum distance of horizontal run-up (maximum inundation distance), (2) maximum flow depth, (3) run-up velocity, and (4) sediment concentration of each grain-size class at the seaward boundary (Naruse and Abe, 2017). The grain-size classes selected for this inverse analysis were 726, 364, 182, 91 and 46 μm respectively.

3.3.2 Inverse Model

The DNN inverse model (Mitra et al., 2020) accepts grain-size and thickness distribution at an input layer of neural network (NN). The nodes in the input layers receive the values of the volume per unit area of all grain-size classes at the grid points of the forward model. Then, following the feed forward mechanism, the NN outputs the tsunami characteristics through the several hidden layers (Figure 20a) (Mitra et al., 2020). The details of DNN architecture and hyperparameters are provided in the Chapter 2 and Mitra et al. (2020).

Before applying the DNN inverse model to the measured tsunami deposits, it was

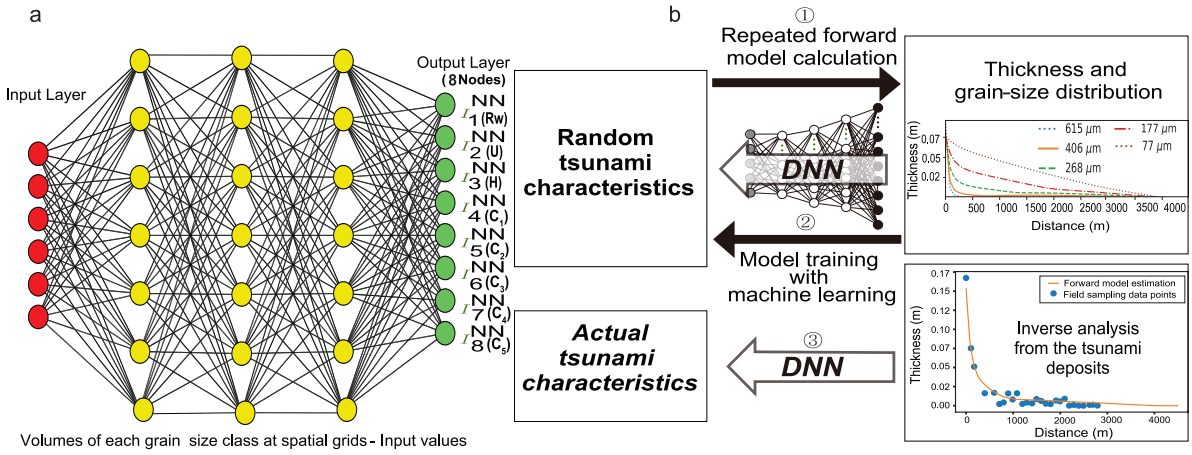

Figure 20: (a) NN architecture of the DNN which predicts output maximum inundation distance (R_w), flow velocity (U), maximum flow depth (H) and concentration of five grain-size classes (C_1 to C_5) (modified from Mitra et al. (2020)) (b) Flow chart of the inverse model (modified from Mitra et al. (2020))

trained using artificial training data sets of tsunami deposits produced by the repetition of the forward model calculation with randomly generated input values. Figure 20b shows the workflow for training and to applying the inverse model. First, the tsunami characteristics values were randomly produced, and the repetition of the forward model calculations using the generated tsunami characteristics produced artificial data sets of the thickness and grain-size distribution of the tsunami deposits to train the NN. The model prediction was evaluated according to the loss function (Eqaution 10), which quantifies how close the NN was to an ideal inverse model.

The weight coefficients in the NN were optimized to minimize the loss function in the training process (Wu et al., 2018; Mitra et al., 2020). Following the training process, the model could be applied to a measured data set of tsunami deposits. The details of the hyperparameter selection and the step-by-step procedures of the model training are provided in the Chapter 2 and Mitra et al. (2020).

To generate the training data sets, the present inverse model involves the ranges of input parameters that are the maximum inundation distance, maximum flow velocity, maximum

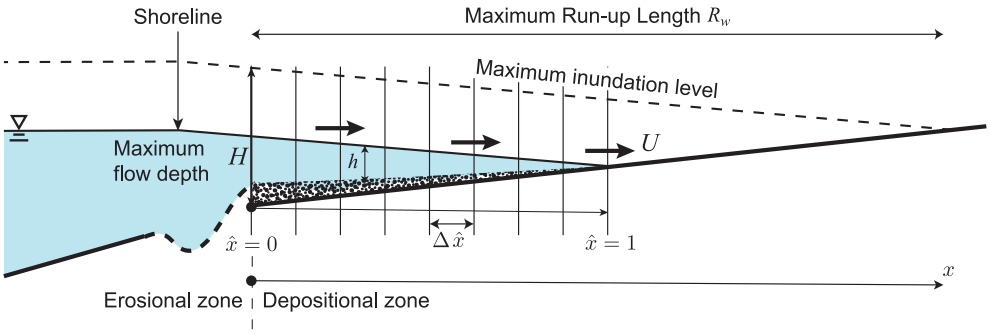

Figure 21: Explanation of model domain configuration. The assumption of velocity of tsunami run-up U is constant in time and space. The inundation depth h increases constantly until it reaches its maximum value H at the seaward boundary. R_{w} is the maximum inundation distance. The bed-attached streamwise coordinate x is set transverse to the shoreline and is positive landward. Within the applied transformed coordinate system, the moving front edge of the tsunami is located at a fixed value of the dimensionless spatial coordinate $\hat{x} = 1$ (modified from Naruse and Abe (2017)).

flow depth and sediment concentrations of five grain-size classes for generating the training data sets, which were 1700–4500 m, 2.0–10 m/s, 1.5–12 m and 0–2% respectively. The range of maximum inundation distance can be modified depending on the field evidence of the extent of the tsunami deposit distribution. The range of parameters adopted in this study is applicable to most of the large-scale tsunami-inundated areas as the ranges have been selected with several case studies of tsunamis that includes mostly field measurements, survivor video and numerical analysis (Wijetunge, 2006; Fritz et al., 2006; Matsutomi and Okamoto, 2010; Mori et al., 2011a; Szczuciński et al., 2012b; Abe et al., 2012; Nandasena et al., 2012; Goto et al., 2014).

A sampling window to select the region for applying the inverse model from the entire distribution of the data sets had to be set, given that, in certain cases, the field measurements along the transect do not cover the entire distribution. In addition, the measurements at the distal part of the transect may contain large errors since the tsunami deposits in that area

may be too thin for precise observations. The model had to be trained on a specific sampling window, and precision of the model prediction depending on the sampling window size was tested using the validation data sets. For more details on the significance and applicability of the sampling window, please refer to Mitra et al. (2020).

I have selected a sampling window size of 1700 m for the present case which was chosen on the basis of the comparative results obtained from tests using different sampling window sizes as described in the results section. For this study area, the grid spacing in the fixed coordinates was 15 m, meaning the number of spatial grids used for the inversion was 113.

To apply the inverse model to the measured values of field data set from Phra Thong Island in 1D vectors, the collected data points must be fit into that fixed coordinate system of the model. Here, an 1D cubic interpolation was used on the measured data set that provides values at the positions between the data points of each sample. Since this procedure may have led to additional errors or bias in the results, checking the influence of the interpolation on the predictions of the inverse model using the subsampling of the artificial data sets at the location of the outcrops was essential (Mitra et al., 2020).

The inverse model predicts the flow conditions, and the precision of the results was evaluated using the jackknife method. This method estimates the standard error of the statistics or a parameter of a population of interest from a random sample of data. The jackknife sample is described as the "leave-one-out" resample of the data. If there are N observations, there are N jackknife samples, each of have a sample size of $N - 1$. If the sample of N observation is a set denoted as $x_1, x_2, ..., x_N$, the nth jackknife sample is $x_1, ..., x_{n-1}, x_{n+1}, ..., x_N$. The pseudo-value estimation of the nth observation was then computed and an estimate of the standard error from the variance of the pseudo-values was obtained (Abdi and Williams, 2010; Mitra et al., 2020).

3.4 Results

3.4.1 Training and testing of the inverse model

The DNN was trained using artificial data sets which were the depositional characteristics, such as volume per unit area and grain-size distribution. The number of training data sets was chosen to be 5000 in this study. Figure 22a presents a plot graph of the relationship between the number of training data sets and the loss function of the validation data set. The performance of the inverse model improved as the number of training data sets increased

(Figure 22a), but there was only a slight improvement after the iteration of the forward model calculation exceeded 3000.

The training process proceeded with a certain number of epochs that indicates the iterations of the optimization calculation by the full data set. Figure 22b shows that the present model was reasonably converged over 2000 epochs for both the training and validation performances. The loss function values of training and validation at the first epoch were 0.09 and 0.06, respectively. The final and lowest loss function at the final epoch was 0.0036 for the training data sets and 0.0013 for the validation data sets.

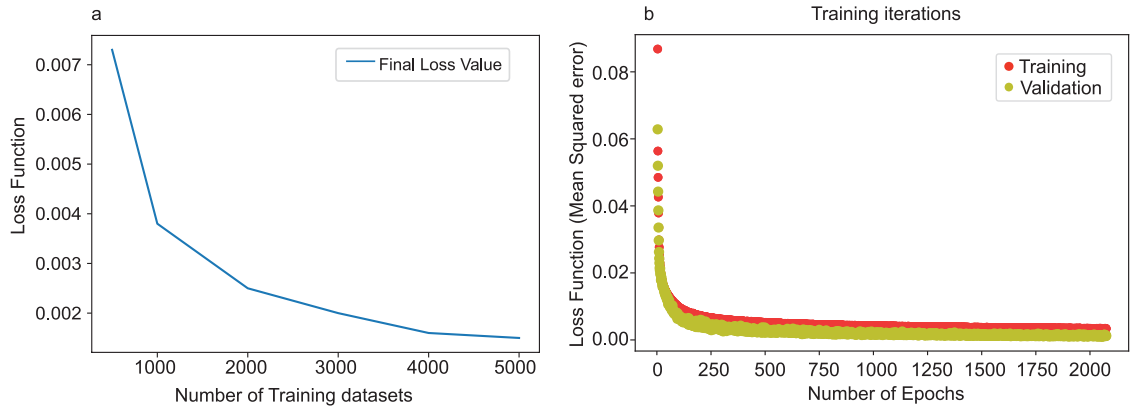

Figure 22: (a) Relationship between the loss function of the validation and the number of training data sets selected for the inverse model. The results of the training improved as the number of training data sets increased, while it slightly varied after 5000 training data sets. (b) History of learning indicated by the variation of the loss function (mean squared error). Both values of the loss function for the training and validation data sets reached a minimum value, indicating that overlearning did not occur.

After training the model, the predictions of the inverse model for the test data sets were plotted against the original values used for producing the data sets. Figure 23(a–h) shows that the eight predicted parameters from the artificial test data sets were distributed along the 1:1 line in the graph indicating that the test results were correlated well with the original inputs. Figure 24(a–h) shows the histograms of the deviation of the estimated values predicted from the original values. Deviations were distributed in a relatively narrow range without large biases in relation to the true conditions, except in the case of the maximum

flow depth which was slightly biased. The values of the predicted maximum flow depth were approximately 0.4 m lower than the input values.

3.4.2 Application of the DNN inverse model to the 2004 Indian Ocean tsunami

Inversion results The inversion method was applied to the measured grain-size distribution of tsunami deposits along the transect of Phra Thong Island in view of reconstructing the flow conditions from the deposit of the 2004 Indian Ocean tsunami. The 1D cubic interpolation was applied to the data set measured along the transect of Phra Thong Island, before the inversion method was applied to the field data set.

I selected 1700 m as the length of the sampling window, which allowed for minimizing the uncertainty of the inverse analysis quantified via the jackknife method (Figure 25). The jackknife standard error was calculated for different sampling window sizes of the data sets. Figure 25 represents that the error decreased as the sampling window was increased, with the exception of the region above 1700 m. However, an increasing trend was observed for maximum flow depth, while the jackknife standard error became stable after 1500 m (Figure 25c). Thus, the 1700 m sampling window provided the best results in terms of the precision of the inversion. As described in the method section, the interpolation of the measured data sets at the computational grids may result in additional bias or errors from the inverse model. The subsampling analysis was thus conducted using artificial data sets. This test was done to check the effect of irregularly spaced field data sets on the accuracy of the inversion. The details on the subsampling procedure is given in Mitra et al. (2020).

The subsampling test demonstrated that the inversion model had a mean bias of 10.8 m for maximum inundation distance (Figure 26) while the predicted result by DNN was 1700 m. Likewise the predicted results for the flow velocity was 4.6 m/s and it was 4.8 m for the maximum flow depth, with the mean bias obtained from the subsampling results being 0.1 m/s for flow velocity and -0.4 m for maximum flow depth, which were exactly in line with the values obtained from the testing of the trained DNN model without the subsampling test.

Table 3 shows the predicted flow conditions with a 95% confidence interval calculated by jackknife method (Figure 27). When using the jackknife standard error calculations, the maximum inundation distance was 1700 m with 8.1 m range of uncertainty (Figure 27a). Meanwhile, the estimated flow velocity was 4.6 m/s and the maximum flow depth

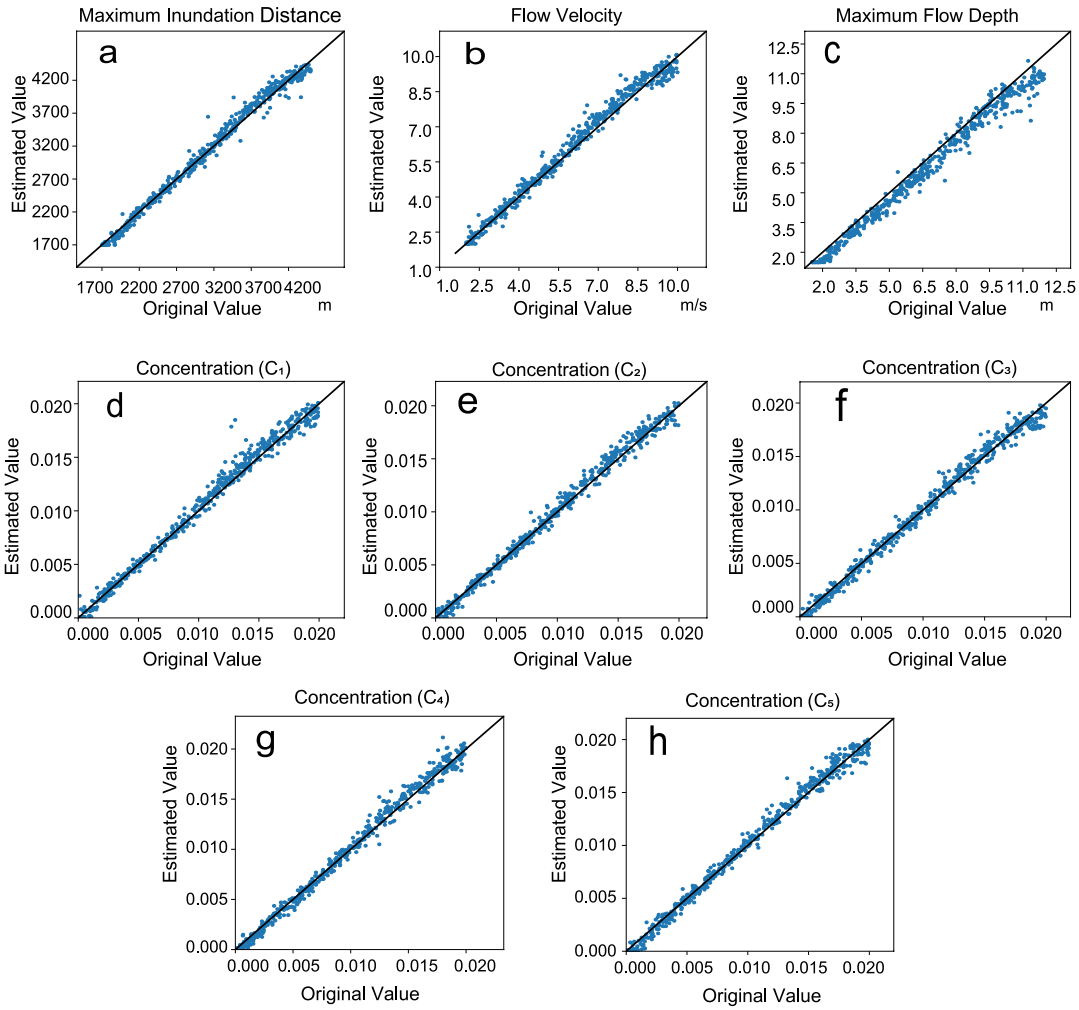

Figure 23: Performance verification of the model using artificial test data sets, indicating that the values estimated using the inverse model were plotted against the original values used for the production of the test data sets. Solid lines indicate a 1:1 relation and suggest good correlation. (a) Estimates for maximum inundation distance, (b) Estimates for flow velocity (c) Estimates for maximum flow depth, (d)–(h) Estimates for Concentrations of five grain-size classes.

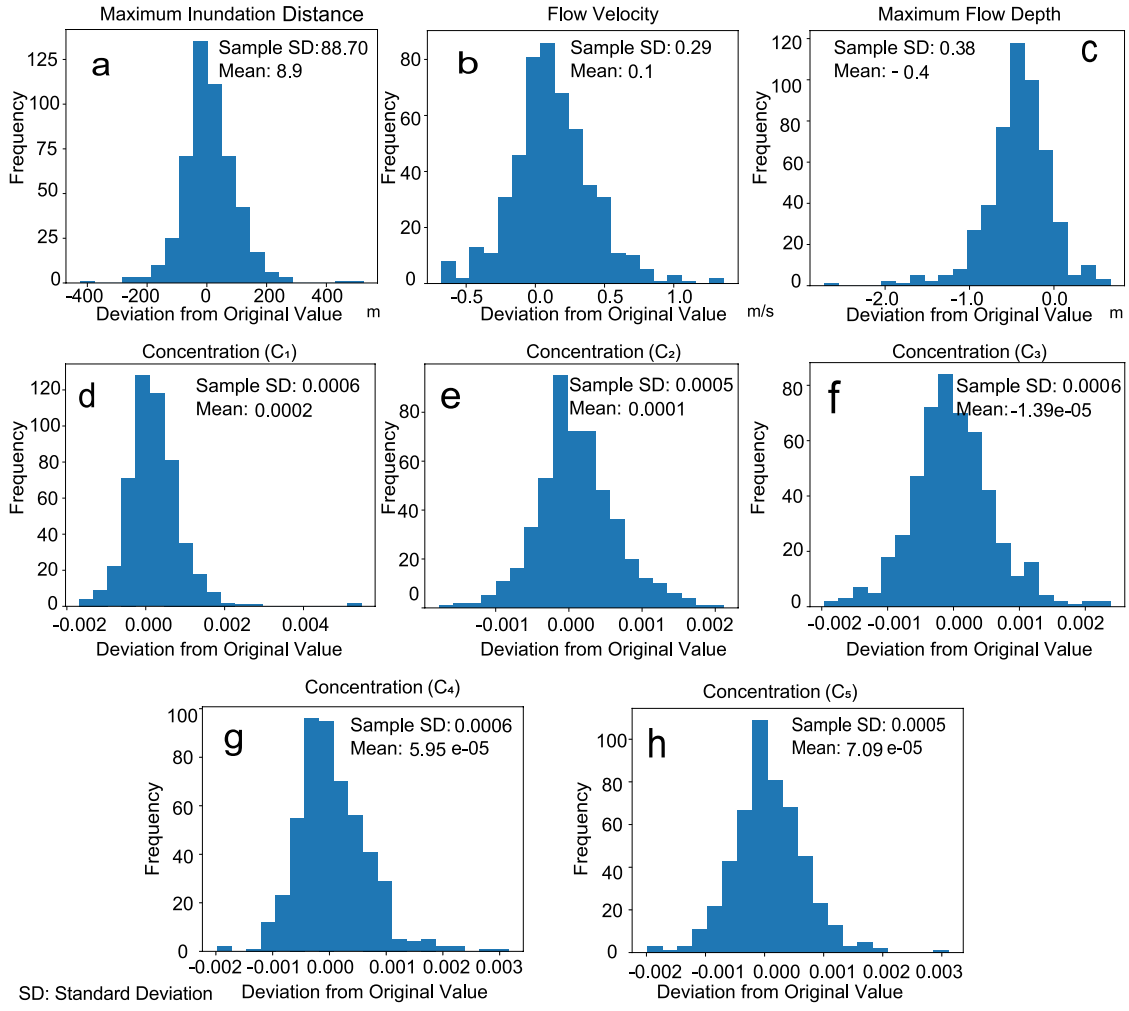

Figure 24: Histograms showing the deviation of the predicted results from the original values of the artificial test data sets. (a) Maximum inundation distance, (b) Flow velocity (c) Maximum flow depth, (d)–(h) Concentration of five grain-size classes.

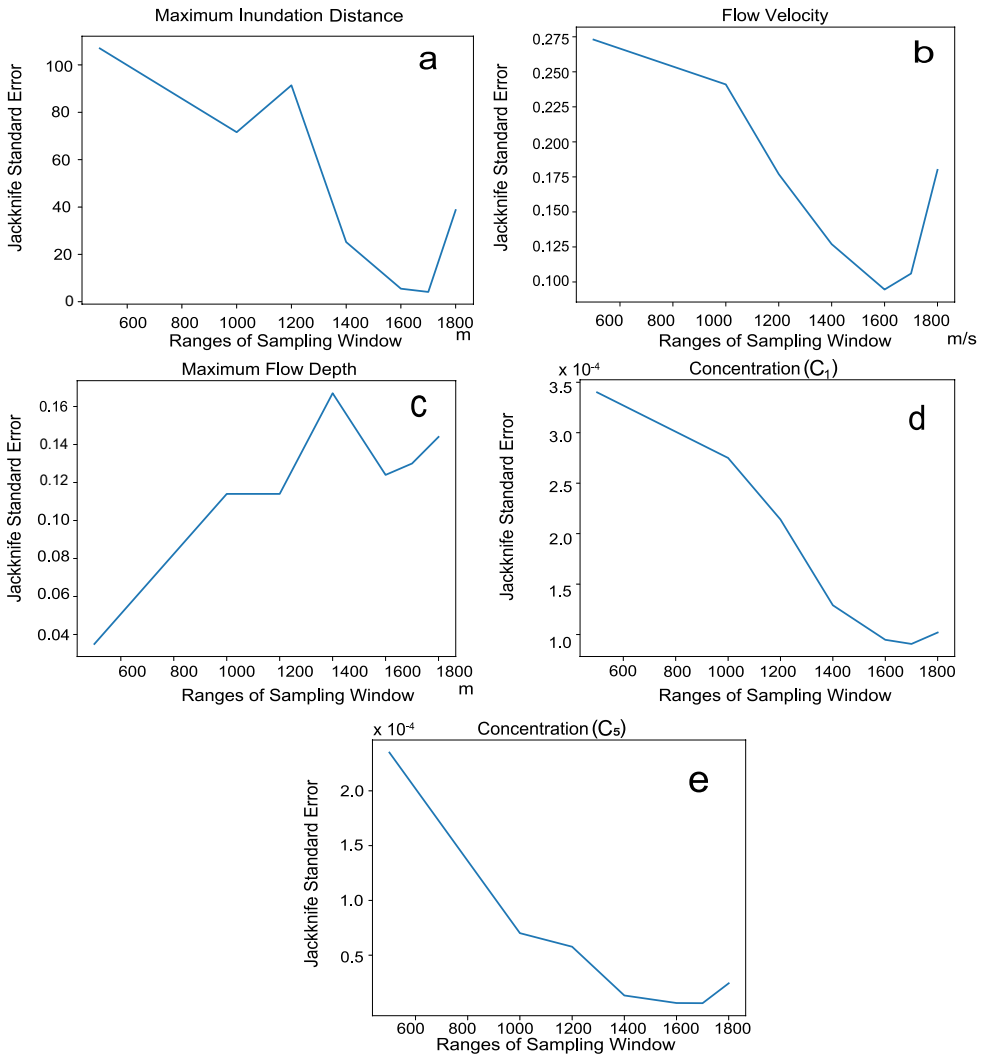

Figure 25: Propagation of jackknife standard errors with different range of sampling window distances. (a) Maximum inundation distance, (b) Flow velocity, (c) Maximum flow depth, (d) Concentration of the first grain-size class, (e) Concentration of the fifth grain-size class.

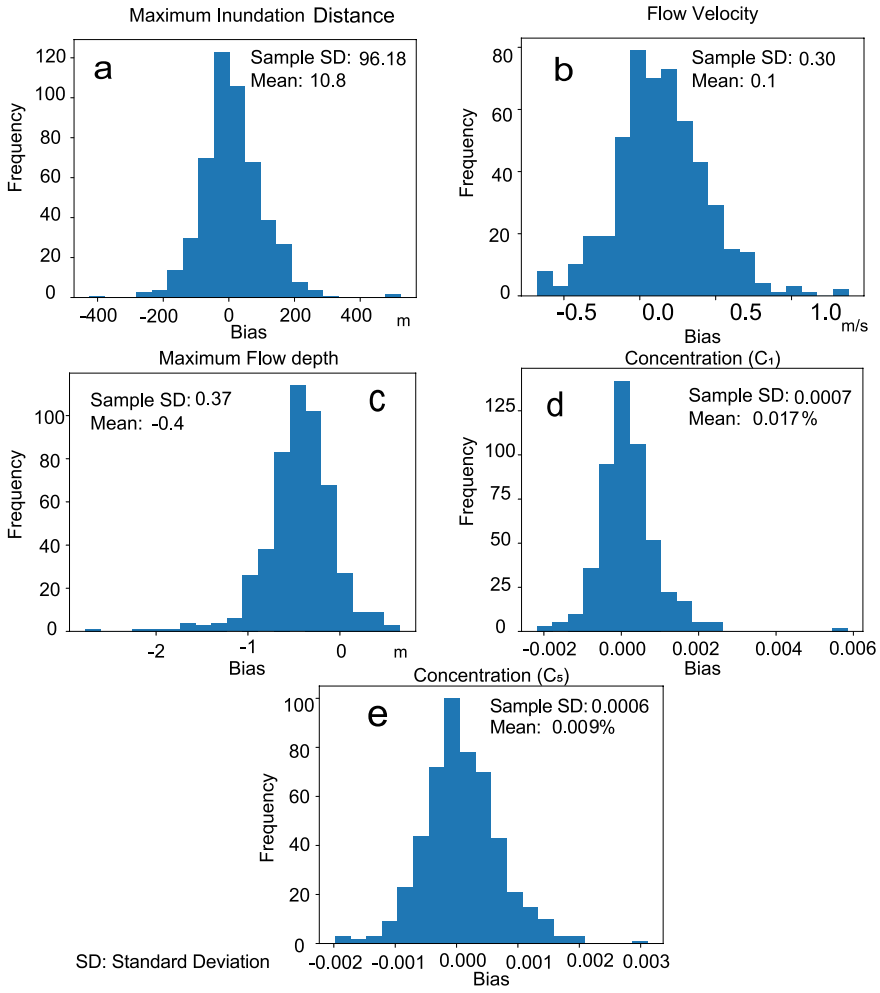

Figure 26: Histograms showing the variance and bias of predictions from the test data sets subsampled at the sampling locations of the transect in Phra Thong Island. (a) Maximum inundation distance, (b) Flow velocity (c) Maximum flow depth, (d) Concentration of the first grain-size class, (e) Concentration of the fifth grain-size class.

Table 3: Predicted results from the inverse model when applied to the 2004 Indian Ocean tsunami data obtained from Phra Thong Island, Thailand. All reported standard error calculations were performed using a 95% confidence interval.

Parameters	Predicted Results	Mean Bias
Maximum inundation distance	1700 m ± 8.1 m	10.8 m
Flow velocity	4.6 m/s ± 0.2 m/s	0.1 m/s
Maximum flow depth	4.8 m ± 0.3 m	−0.4 m
Concentration of C_1 (726 μm)	0.17% ± 0.018%	0.017%
Concentration of C_2 (364 μm)	0.22% ± 0.017%	0.009%
Concentration of C_3 (182 μm)	0.17% ± 0.032%	-3×10^{-4}%
Concentration of C_4 (91 μm)	0.27% ± 0.011%	0.007%
Concentration of C_5 (46 μm)	0.01% ± 0.001%	0.009%

was 4.8 m with jackknife standard error uncertainty values 0.2 m/s and 0.3 m, respectively (Figure 27b,c). The reconstructed total sediment concentration over five grain-size classes was approximately 0.8%, and the estimated values of each grain-size class ranged from 0.01%–0.27%. The jackknife error estimation shows the presence of errors were low, such as 0.001% (Table 3).

Finally, the forward model calculation was performed using the reconstructed flow conditions to estimate the spatial distribution of the volume per unit area and grain-size composition, and it was compared with the measured values from the transect of Phra Thong Island. Figure 28 shows the predicted spatial grain-size distribution was in line with the actual values from field measurements.

3.5 Discussion

3.5.1 The model's inversion performance

The training and testing of the DNN inverse model demostrated that this model has reasonable ability to predict tsunami characteristics, such as maximum inundation distance, flow velocity, maximum flow depth and sediment concentrations. The final loss function values for the training and validation were 0.0036 and 0.0013 respectively which were close (0.0040 and 0.0018) to those reported by Mitra et al. (2020). The testing of the DNN inverse model was evaluated using artificial data sets of tsunami deposits. The scatter diagrams (Figure 23) of the predicted and true conditions indicate a good correlation, with no large deviation in the mode of the predicted values except for a slight bias in the maximum

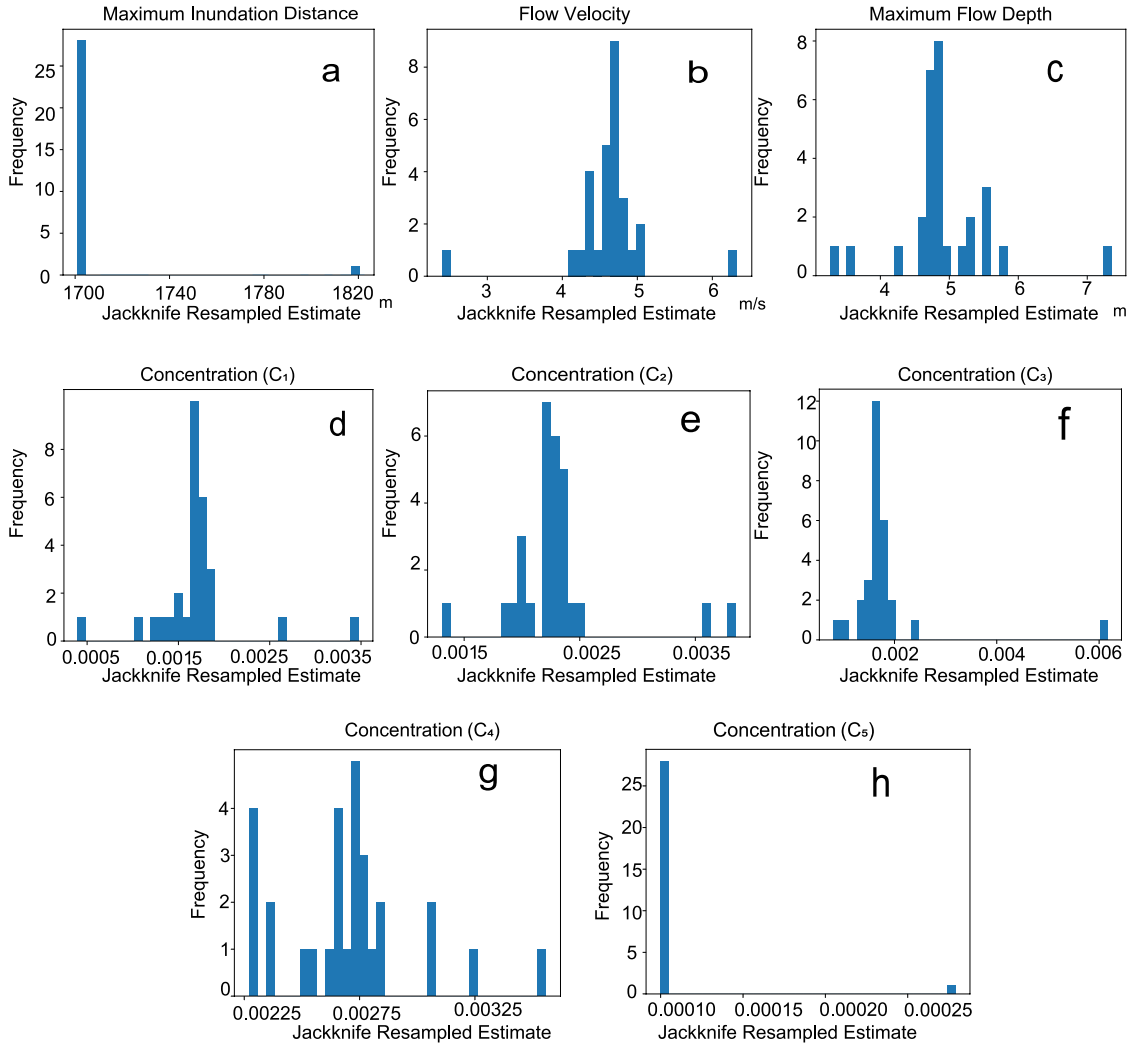

Figure 27: Jackknife estimates for the results predicted by the inverse model at the 1700 m sampling window, used to determine the uncertainty of the model. (a) Estimates for maximum inundation distance, (b) Estimates for flow velocity (c) Estimates for maximum flow depth, (d)–(h) Estimates for concentrations of the five grain-size class.

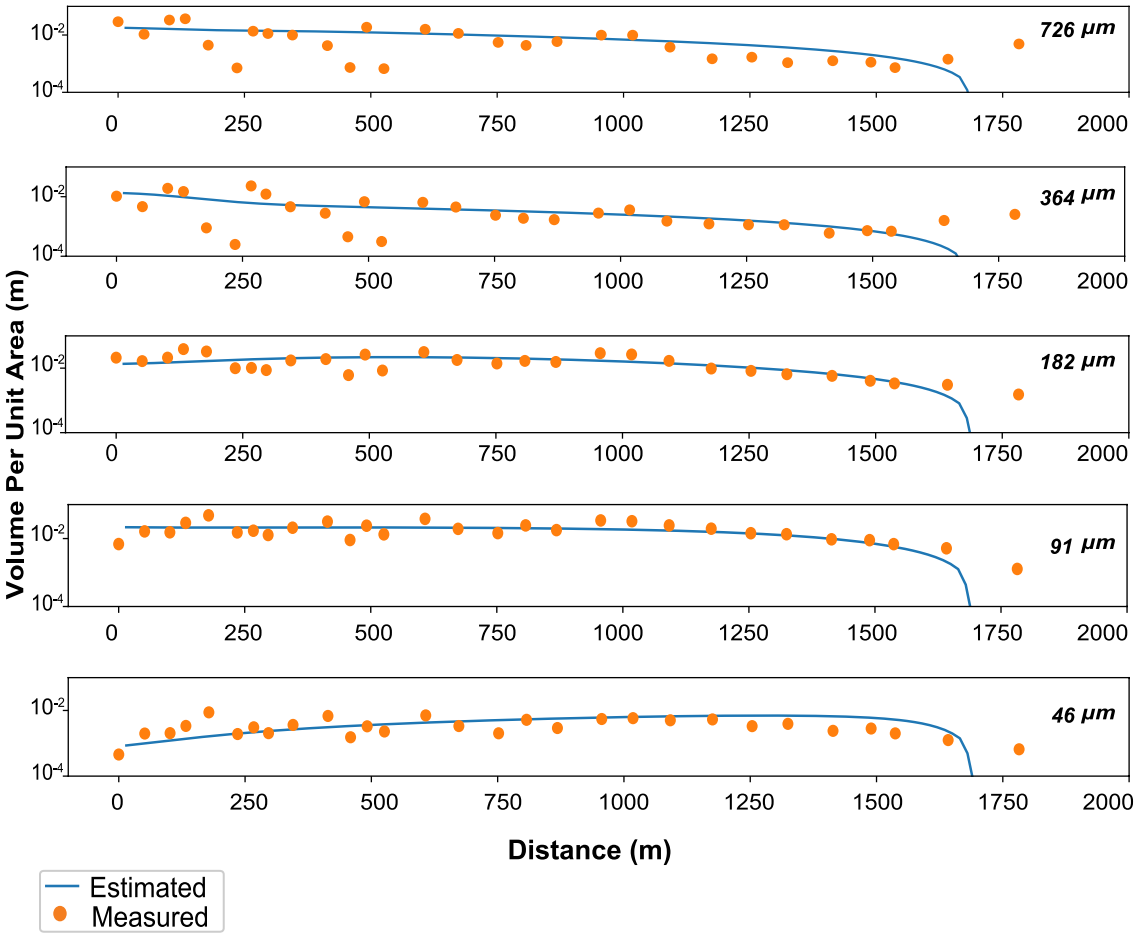

Figure 28: Spatial distribution of volume per unit area of five grain-size classes. Solid circles indicate the values measured by Fujino et al. (2010), and lines indicate the results of the forward model calculation obtained using parameters predicted by the DNN inverse model.

flow depth. While the model tended to estimate the maximum flow depth values approximately 0.4 m lower on average, correcting the final results by adding the bias to the final reconstructed values from the original field data was possible. In Mitra et al. (2020), the reported bias for the maximum flow depth was approximately 0.5 m, while the sample standard deviation was around 0.40, which is close to the value in the present study (0.38 m). The bias during the testing of the model was caused by the internal algorithm and neural network structure, but I hope the bias of maximum flow depth will be sorted if the neural network structure can be improved in the future. In future studies, the algorithm of the neural network structure can be improved to eliminate or reduce the bias of the parameter.

Regarding the deviation of the predicted values from the true values which are artificial test data sets, the sample standard deviation values were relatively small for all parameters. The sample standard deviation for the maximum inundation distance was as low as 88.70 m for a range of true values of 1700–4500 m, while that for flow velocity was 0.29 m/s for a range of true values of 2.0–10 m/s. Meanwhile, the average value for sediment concentration was around 0.05%. All these values were close to those reported by Mitra et al. (2020) (e.g., maximum inundation distance, 77.03 m; flow velocity, 0.30 m/s, sediment concentration, 0.06%).

After the model was trained and tested, the test data sets were subsampled at the sampling locations on Phra Thong Island to investigate the bias in the predicted flow conditions due to the irregular distribution of the sampling points. The results implied that the irregularity of the sampling distribution had little effect on the bias and errors. In fact, the bias values for maximum inundation distance, flow velocity, and sediment concentration were very small (Figure 26a–e), while that for the maximum flow depth in the subsampling tests indicated no additional bias, implying that the sampling interval on Phra Thong was sufficient for the inverse analysis using the DNN model.

To summarize, the performance of the trained DNN inverse model was identical to that of the model reported in Mitra et al. (2020) which successfully reconstructed various characteristics of the 2011 the Tohoku-oki tsunami. It is noteworthy that Mitra et al. (2020) used different numbers of grain-size class than used in this study, and they also employed different ranges of initial parameters for flow velocity and maximum inundation distance. The modifications in the current study were necessary since the grain-size distribution of the tsunami deposits measured at Phra Thong Island was considerably coarser than that

measured in the Sendai Plain. This change had close to zero effect on the performance of the inverse model, implying that the inverse method employed in this study is adaptable to various environments.

3.5.2 Verification of inversion results for the tsunami deposits

After the testing of the inverse model described above, I applied the model to the data sets obtained along the transect (Figure 17), and obtained the first quantitative estimates of the tsunami characteristics in Phra Thong Island. While in situ measurements of the 2004 Indian Ocean tsunami's activity on in Phra Thong Island are not abundant, several surveys have reported the attendant inundation heights and run-up length of the tsunami in this region. Here I compare the inversion results with these in situ measurements of the 2004 Indian Ocean tsunami.

The inversion results or the tsunami flow depth in this study were in the range of the in situ measurements. The DNN inverse model reconstructed the maximum flow depth as 4.8 ± 0.3 m at the sampling site, which was located approximately 684 m from the shoreline, when measured in the direction parallel to the flow direction (N154°E). This value does not contain the additional bias −0.4 m. The data of tsunami inundation height, which present a sum of the flow depth and topographic height, were measured at Phra Thong Island by several research groups including Tsuji et al. (2006) and Korean Society of Coastal and Ocean Engineers (KSCOE) groups (Choi et al., 2006) (`http://www.nda.ac.jp/~fujima/TMD/fujicom.html`). The data points reported by the latter were 50 and 400 m from the shoreline, and were relatively close to the sampling site 1 (distances of 1.40 km and 1.37 km away from the sampling site 1). The measured values of the tsunami inundation heights at these sites were 7.1 and 6.7 m. The KSCOE group also reported the inundation heights at four sites in Phra Thong Island, which were 30–130 m from the shoreline, and relatively far from the transect (ca. 2.55 km from the sampling site 1), with the inundation heights found to be between 5.5–6.0 m at these sites. Meanwhile, the averaged elevation around the study area which was calculated from the topographic profiles provided by Jankaew et al. (2008, 2011); Brill et al. (2012b), was approximately 2.9 m. The most seaward locations of the transect in Jankaew et al. (2008, 2011) were around 400 m from sampling site 1 in the study area. The maximum and measured flow heights from Phra Thong Island were reported 7.1 m and 5.5 m respectively

(http://www.nda.ac.jp/~fujima/TMD/fujicom.html). The corresponding maximum and minimum values of elevation are 3.1 and 1.1 m respectively (Jankaew et al., 2008, 2011; Brill et al., 2012b). Hence, the approximate estimate of measured maximum flow depth is ranged from 2.4 m to 6.0 m. Considering the bias correction of 0.4 m, the reconstructed value of maximum flow depth (5.3 m) falls within the range of measured maximum flow depth values. Hence, when based on the 1700 m sampling window size, the maximum flow depth reconstructed in this study was close to the reported measurements. However, certain amount of measurement and calculation error may have existed due to the local topographical variations. The model also estimated a maximum inundation distance (1700 m) that was close to the observed value apprximately 2000 m, which was measured at the inland end of the transect (Fujino et al., 2010).

3.5.3 Characteristics of the 2004 Indian Ocean tsunami on Phra Thong Island

The inversion results for the tsunami characteristics on Phra Thong Island indicated that the tsunami inundation flow was typically uniform along the coastal area of Thailand. This study reconstructed the flow velocity of the tsunami as 4.6 ± 0.2 m/s. Given that no direct observation values have been reported for this specific transect in Phra Thong Island, this presented the first estimate for this region. The reconstructed flow velocity in this region was close to the observed velocity in other regions of coastal areas in Thailand, albeit that a larger velocity was reported in the Khao Lak area. Rossetto et al. (2007) reported video footage of the flow velocity, which was around 3-4 m/s on Phuket island (118 km south of our study area) and 6-8 m/s in the Khao Lak area (43 km south of our study area). Given the values collected from the video footage (Rossetto et al., 2007) in relation to Phuket island, Khao Lak area and the results reported by Brill et al. (2014), it is clear that most of the flow velocity values were around 4–5 m/s, apart from in the Khao Lak area. In fact, the flow depth measurement data from Khao Lak area also had exceptionally high values (Tsuji et al., 2006; Karlsson et al., 2009), indicating that the tsunami inundation flow could have been locally enhanced by the topographic effects in this region. The flow velocity and depth of the 2004 Indian Ocean tsunami were similar in all other regions covering a 130 km area from Phuket to Phra Thong Island.

3.5.4 Comparison with the results of existing 2D forward model

While the inverse analysis of tsunami deposits provides estimates of the flow characteristics in specific regions, two or three dimensional forward modeling is required to infer the spatial distribution of the flow parameters on a regional scale (Li et al., 2012; Masaya et al., 2019). The horizontal two dimensional forward model TUNAMI-N2 was applied to the Phra Thong Island, to estimate the spatial distribution of the maximum flow depth in this area (Masaya et al., 2019). However, model appeared to have overestimated the maximum flow depth when compared with the measured values obtained by the KSCOE group (Choi et al., 2006), with the former returning a flow depth of 6–8 m and the latter returning a depth of 4.2–3.8 m. This model is based on a fixed-source model where the initial water levels for a whole region are set along with the specific fault parameters. The model's results strongly depend on these fault parameters which should be iteratively modified to fit the measurement or distribution of the actual tsunami deposits. In addition to the source model, this model also includes tsunami sediment transport calculation that consists of bed load layer and suspended load layer. However, the calculated value of the sediment thickness was overestimated as the assumption of movable bed for a large area caused excessive erosion of the ground (Masaya et al., 2019). Moreover, the model of Masaya et al. (2019) employed single grain-size class for the reconstruction of the parameters from a larger area, which could have resulted in an erroneous estimation as the distribution of grain-size of tsunami deposits varies due to sediment transportation and deposition (Sugawara et al., 2014). In contrast, the DNN inverse model does not involve predefined conditions or thresholds to deduce the maximum flow depth. Here, the estimated flow characteristics and thickness distribution of the deposits by the DNN inverse model fitted well with the measured values, but they only apply to a local region. However, the DNN inverse model can potentially accept any type of forward models that can produce the distribution of tsunami deposits as training data sets. The model calculation of Masaya et al. (2019) relies on the estimation of a single set of fault parameters, which were not widely explored to obtain the optimal parameters. In future, Model TUNAMI-N2 can be potentially used as the forward model in DNN inverse model to consider two-dimensional behavior of tsunamis. To do so, the model needs to be modified for considering sediment transport of multiple grain-size classes.

3.6 Conclusions

The DNN inverse model demonstrated its efficiency in successfully reconstructing the hydraulic conditions of the 2004 Indian Ocean tsunami from the Phra Thong Island, Thailand. The reconstructed maximum inundation distance was 1700 m, while the flow velocity and maximum flow depth were 4.6 m/s and 4.8 m respectively. The value of maximum flow depth including the additional bias correction was 5.3 m that was within the range 2.4 m to 6.0 m which was the approximate estimate of measured maximum flow depth at Phra Thong Island. The value of flow velocity was also close to the reported values using the video footage from the vicinity of the Phra Thong Island. The uncertainty of the results using jackknife method also indicated that simulated results did not contain a large range of values. Phra Thong Island was one of the most well preserved and historically important area for paleotsunami deposits. Hence, the application of the DNN inverse model was suitable to reconstruct flow conditions of the 2004 Indian Ocean tsunami from Phra Thong Island. The DNN inverse model also represented the comparison of the calculated and measured spatial distribution of volume per unit area along the transect at the island. This model can be applied to any areas of modern and ancient tsunami deposits consisting of low land or flat areas to successfully reconstruct the tsunami flow conditions and can serve as a tool for tsunami hazard assessment and disaster resilience at coastal cities.

3.7 Code and data availability

The source codes and all other data of the DNN inverse model are available in Zenodo (https://doi.org/10.5281/zenodo.4744889).

3.8 Copyright statement

4 Understanding flow characteristics from tsunami deposits at Odaka, Joban Coast, using a DNN inverse model

4.1 Introduction

The 2011 Tohoku-oki tsunami of Mw 9.0 occurred on March 11, 2011, and it affected a large region of eastern Japan. With a significant number of fatalities and losses, this tsunami is considered as one of the largest in Japan (Sato et al., 2014). Many studies of tsunami deposits have been conducted in and around the Sendai Plain (Naruse et al., 2012; Abe et al., 2012). Among them Naruse et al. (2012) estimated that the flow velocity of the 2011 Tohoku-oki tsunami on the Sendai Plain ranged from 2.4 to 2.7 m/s, based on the critical velocity for the bedload motion of the largest grain-size class in the deposits. Several field surveys, aerial video records, and satellite images were used to understand flow conditions of the 2011 Tohoku-oki tsunami by reconstructing the inundated area and the size of the tsunami (Hayashi and Koshimura, 2013; Tanigawa et al., 2014). The tsunami height at the transect (Naruse and Abe, 2017; Mitra et al., 2020) of Sendai Plain was comparatively low (6.5 above T.P) (Naruse and Abe, 2017), possibly caused by the divergence of wave reflection owing to the concave bathymetry and wide continental shelf (Sato et al., 2014). The flow velocity of 1.9–6.9 m/s was reported on the Sendai Plain using aerial video records (Hayashi and Koshimura, 2013). Several numerical models of sediment transportaion have been proposed to investigate the offshore propagation and inundation at the Sendai Plain (Sugawara et al., 2012, 2014).

The waves around the Odaka region at Fukushima Prefecture destroyed or damaged nearly all seawalls because of large tsunami height and co-seismic land-level subsidence (Sato et al., 2014). The inundation flow velocity in Fukushima was estimated to be higher than that in the Sendai Plain. Sanuki et al. (2013) estimated the flow velocity to be 10–15 m/s in the river and coastal plain from video images. Sato et al. (2012a) and Sanuki et al. (2013) conducted a numerical simulation of tsunami inundation and also estimated high velocity flows in the area. Sato et al. (2014) estimated a the flow velocity higher than 11 m/s from the collapse of buildings. Thus, extremely high velocity inundation flows were presumed in this region, but the precise measurements of tsunami inundation flows in the coastal areas of Fukushima area have not been well examined because of the Fukushima Daiichi Nuclear Power Plant disaster (Mori et al., 2011b; Mimura et al., 2011). How-

ever, post-tsunami surveys were conducted by several groups, such as the Tohoku Earthquake Tsunami Joint Survey Group (TETJSG, https://coastal.jp/ttjt/index.php) and Sato et al. (2012b), which estimated tsunami heights from the water mark. There are few studies of tsunami deposits around Minamisoma, as the area was restricted until June 2012 (Sato et al., 2014) because of nuclear radiation. Thus, the tsunami deposits have been well preserved, the restrictions prevented anthropogenic disturbances. Therefore, it is important to survey the Minamisoma area to quantitatively reconstruct the tsunami characteristics using numerical and experimental models for future tsunami hazard mitigation and to construct preventive structural measures (Shuto, 2019).

Here, I conducted an inverse analysis of tsunami deposits distributed in Odaka region of Minamisoma area, Fukushima, using the newly proposed method by Mitra et al. (2020, 2021) to estimate flow conditions of the tsunami inundation in the area. Several inverse and forward models have been proposed to reconstruct flow conditions (Jaffe et al., 2012; Li et al., 2012; Sugawara and Goto, 2012; Johnson et al., 2016; Yoshii et al., 2018). Recently Mitra et al. (2020, 2021) proposed a new 1D inverse model using the deep neural network (DNN) and predicted reasonable flow conditions of the 2011 Tohoku-oki tsunami and the 2004 Indian Ocean tsunami from measured grain-size distributions at different locations, such as the Sendai Plain and Phra Thong Island, Thailand. This inverse model utilizes a forward model that incorporates the non-uniform, unsteady transport of suspended sediments with turbulent mixing. The DNN model can effectively quantify the maximum inundation distance, flow velocity, maximum flow depth and sediment concentration. The major advantages of this model are that the hydrodynamic and sediment transportation settings of this model are more realistic than other models and the uncertainty calculation of the predicted results can be estimated using a jackknife method. The results of the inverse analysis were verified by field observations. Using this method for the 2011 Tohoku-oki tsunami at the Sendai Plain, the reconstructed inundation distance was 4,045 m which is close to the original maximum inundation distance of approximately 4,020 m; the values of the run-up flow velocity was 5.4 m/s, which was close to the spatial average of the measurements that ranged from 1.9 to 6.9 m/s; and the estimated the maximum flow depth was 4.1 m, which was also within the range of the in-situ measured values from the Sendai Plain (Mitra et al., 2020). For the 2004 Indian Ocean tsunami at Phra Thong Island in Thailand, the reconstructed inundation distance was 1700 m, whereas the original inundation distance

was approximately 2,000 m, the flow velocity and maximum flow depth were 4.6 m/s and 4.8 m, respectively (Mitra et al., 2021).

In this study, despite the complex topography of the region, the flow properties of the 2011 Tohoku-oki tsunami were successfully reconstructed, and the results were corroborated by field observations. This provided a better understanding of tsunami inundation flow in Froude supercritical and subcritical conditions, which vary depending on the region and topographical settings. There are few studies that deal with the supercritical or subcritical conditions of tsunami inundation flows (Qi et al., 2014; Sakakiyama, 2014) quantitatively. This study focuses on the ability of the DNN model to estimate the flow conditions, such as flow velocity, flow depth etc., and how those parameters can be used to delineate the Froude number (Fr) to understand the type of prevailing flow, such as subcritical ($Fr < 1$) or supercritical ($Fr > 1$), during tsunami inflow at different regions. Hence, the DNN inverse analysis results could be used to construct appropriate preventive structural measures for tsunami and mitigation strategies around the Minamisoma area.

4.2 Topographic Setting and Tsunami Characteristics in Study Area

This study used the samples from Odaka District of Minamisoma City (Figure 29), which is located at Fukushima Prefecture (Oota et al., 2017; Koff et al., 2012). The tsunami flooded a wide area with the river, which caused major damage to the properties in the Odaka lowland (Koff et al., 2012). The topographical features of the area include the gentle slope of the coastal plain, beach ridges, marshes, lagoons and sea dikes (Sawai et al., 2012; Koff et al., 2012). A co-seismic subsidence of 0.5–0.8 m has been reported from a few places in the Odaka region (Sato et al., 2012b, 2014) and this event caused a reduction of the sea-wall heights. The shoreline along Minamisoma was convex with the presence of alternating coastal cliffs and plains which were associated with terrace-like seafloors consisting of steeper ascending slopes near the coastline (Tsuruta et al., 2017).

Precise velocity measurement is absent in this area. The inundation heights were measured by Sato et al. (2014) and the TETJSG at the Odaka region around the Joban Coast. Large variations in inundation heights along the coastal line were observed within short distances in the region (Sato et al., 2014). This variation in inundation heights was caused by the complex coastal topography in Minamisoma City. Figure 30a and b shows the measured tsunami inundation heights around the Joban Coast and the Sendai Plain, and it is

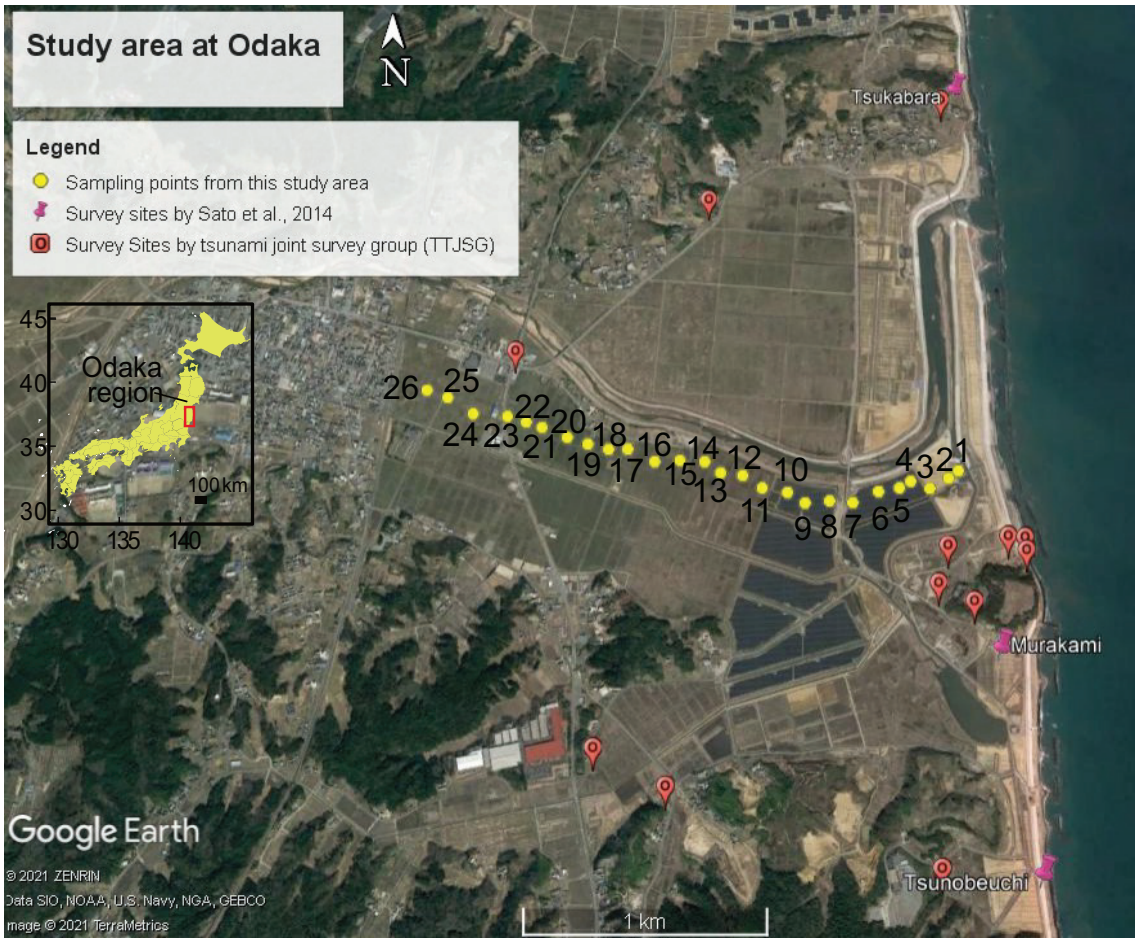

Figure 29: Google map showing the study area at Odaka and surrounding locations.

evident that the former shows a poor correlation with the best fit regression line, whereas the latter shows a strong correlation. The data of inundation heights around the Odaka region were collected from the TETJSG (http://www.coastal.jp/tsunami2011) and Sato et al. (2014). The topographic elevation for the TETJSG data sets were calculated with a 5 m mesh DEM (GSI) which was acquired by the light detection and ranging (LiDAR) technology in 2012 and using several methods using 3D analyst tool and spatial analyst tool. For 3D analyst tool method, "add surface information" was selected from the functional surface option and the the feature class (measured point) with DEM was provided as input. In this method, the elevation was extracted. Another method was extract values to points from the spatial analyst tool using the same input as the previous method and finally, the values were used to calculate a measured flow depth from the measured inundation height. However, it

should be noted that, the calculated values of maximum flow depths were approximation from the area.

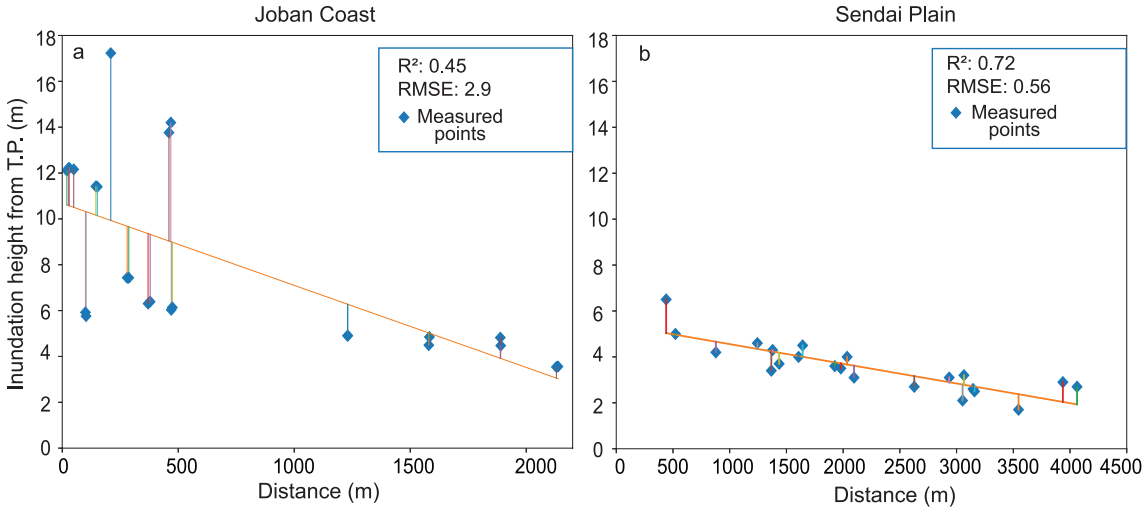

Figure 30: Plots showing the measured inundation height from the Tokyo Peil (T.P) (a) Measured flow depth of the 2011 Tohoku-oki tsunami around the Joban Coast and Root mean square error (RMSE) and R^2 values show that the data points are away from the best fit line (b) Measured flow depths at Sendai Plain show that the measured flow depth of the 2011 Tohoku-oki tsunami and Root mean square error (RMSE) and R^2 values show that the data points are close to the best fit line.

In this study, the post-tsunami survey was conducted along the sampling transect (Figure 31), perpendicular to the shoreline, and the samples were collected from 26 locations along the transect as shown in Figure 29. This survey was conducted shortly after the site restriction was lifted in June, 2012. The sampling was done every 100–200 m, and the thickness of the deposits was measured accordingly at each site. Grain-size analysis was peformed using settling tubes with "the Stube application program" (Naruse, 2005) and procedures for the cleaning and pretreatment of samples followed the methods described in Naruse and Abe (2017).

4.3 Methodology

4.3.1 Forward model

The DNN inverse model incorporates the FITTNUSS forward model (Naruse and Abe, 2017), which is based on layer-averaged, 1D shallow water equations. This model calculates the spatial variation of the thickness and grain-size distribution of the tsunami deposits

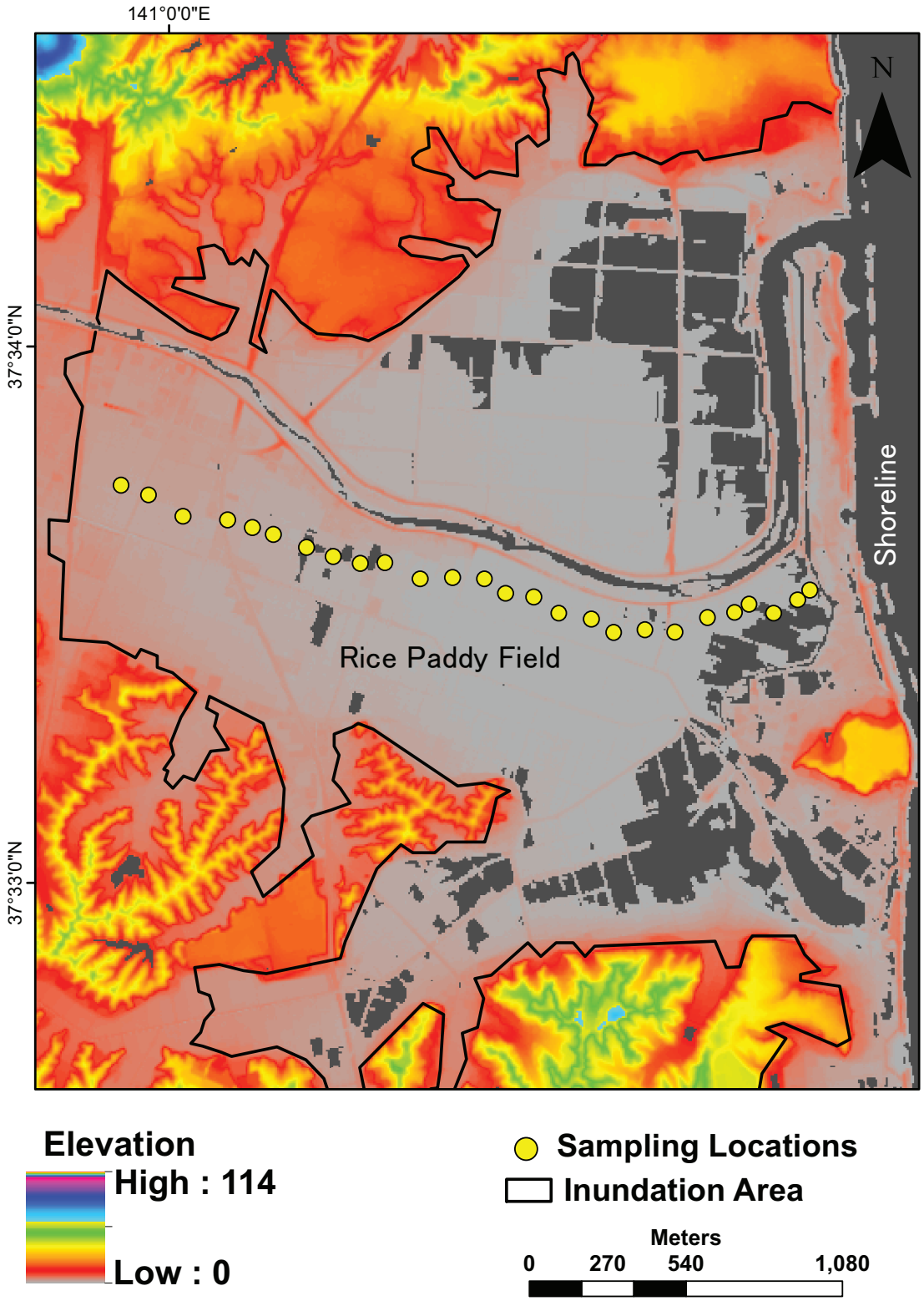

Figure 31: DEM map showing the topography around the study area at Odaka.

using the maximum inundation distance, flow velocity, maximum flow depth and sediment concentration as the input values.

The flow dynamics and sediment transport calculations include layer-averaged equations of the conservation of fluid mass, momentum, and sediment mass. The model works with the quasi-steady flow assumption that the velocity of tsunami run-up (U) is assumed to be constant, whereas the inundation depth increases at a constant rate until it reaches the maximum value at the seaward boundary. It was also assumed that the suspended sediment only exchanges with the bed sediment in the active layer on the surface of bed (Hirano, 1971). The model requires several empirical closure equations regarding flow dynamics and sediment transport including the entrainment rate of basal sediment, bed friction and stratification of sediment concentration described in Naruse and Abe (2017).

The grain-size distribution in this study was discretized to six grain-size classes with representative diameters of 841, 595, 420, 297, 210 and 149 μm. The sedimentation of the tsunami was calculated using the Exner equation of bed sediment continuity of the ith grain-size classes, and the time variation of the grain-size distribution in the active layer was considered in the model (Hirano, 1971).

This model assumes that sediment entrainment and deposition occur during the run-up phase and that all the suspended sediment settled during the stagnant phase after the inundation. The coordinate transformation was applied for the efficiency and stability of the calculation of the fluid dynamics. The finite difference method was employed to obtain the numerical solutions in this model. The in-depth details of all the equations are provided in Naruse and Abe (2017) and Chapter 2.

4.3.2 Inverse model

The DNN inverse model consists of the artificial neural network, with a total of five layers among them. There are three hidden layers and the input layer accepts the values of volume per unit area of grain-size classes at specific spatial grids. The number of nodes and other hyperparameters are the same as those used in Mitra et al. (2020, 2021). Finally, the output layer of the neural network predicts the flow conditions such as maximum inundation distance, flow velocity, maximum flow depth and sediment concentration.

Figure 32 shows the workflow of the DNN inverse model which was trained using the artificial data set of depositional characteristics, such as thickness and grain-size distribu-

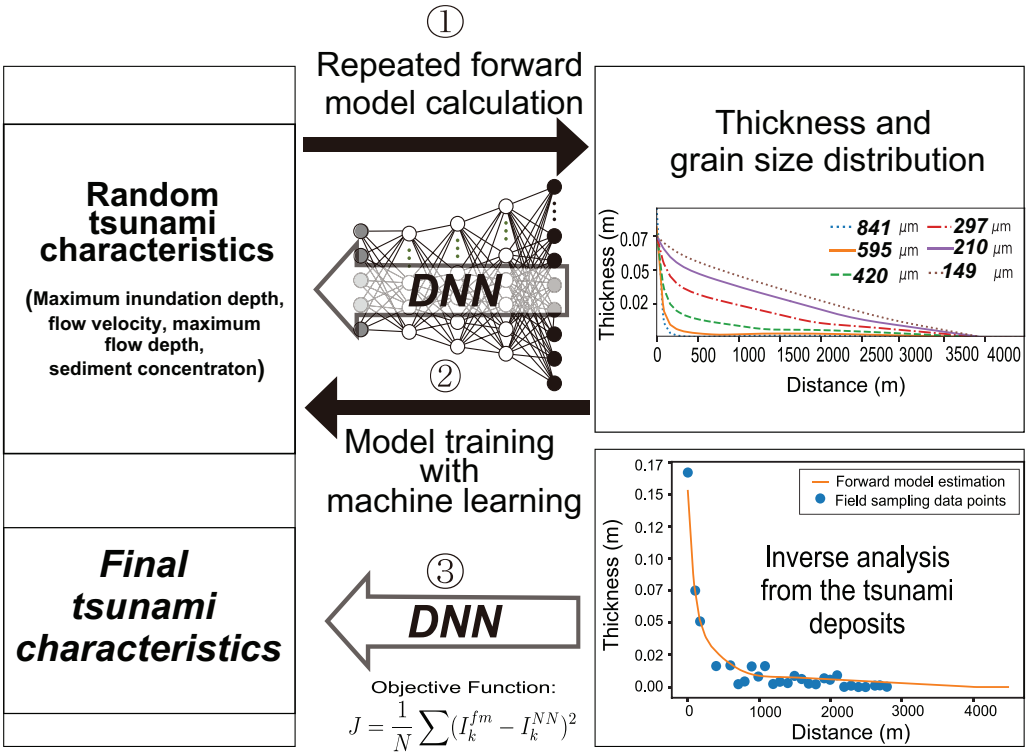

Figure 32: Workflow of DNN inverse model (modified from Mitra et al. (2020)).

tion, which were produced by random and repetitive calculations of the forward model. This was followed by the validation of the performance using the artificial test data sets. A sampling window around the proximal part was used on the entire volume per unit area distribution to apply the inverse model as the distal part may contain large error owing to thinning of the deposits and field measurements potentially not covering the entire distribution of the deposits. The performance of the model was provided in the appendix 8.2 as the performance results were almost similar with the results provided in Mitra et al. (2020, 2021).

After training and validation, the model was ready to apply to the field data set from Odaka region. To reconstruct the flow condition of the 2011 Tohoku-oki tsunami, I have

selected a sampling window size of 1800 m for our study which was chosen based on the comparative results obtained from tests using different sampling window sizes as described in the results section. For this study area, the grids spacing in the fixed coordinates was 15 m, meaning the number of spatial grids used for the inversion was 120. After the model was trained, subsampling of test data sets was performed at the sampling locations of Odaka region (Figure 33a–i). In this test, volume per unit area of sediment in the test data sets at the sampling locations were estimated by 1D cubic interpolation, and these subsampled data were subsequently interpolated again at the grids of the forward model and the inversion was applied on the subsampled data set. Hence, the model prediction was checked with both the true and the inversion result values using the original test data sets to examine the bias caused by the irregularities in spatial distribution of sampling locations.

4.4 Training and testing of the inverse model

The training and testing of DNN inverse model has already provided evidence that the model has the promising ability to reconstruct tsunami flow characteristics. The final loss function values for the training and validation were 0.0039 and 0.0013, respectively which were close to the previously reported values in Mitra et al. (2020, 2021). The sample standard deviation for predicted and true values for the maximum inundation distance was small, that is 81.82 m, and it was only 0.26 m for flow velocity. There were no large deviations for any parameter. However, for the maximum flow depth, the model tended to estimate approximately 0.4 m lower (see appendix 8.2) than the original values on average, which is also very similar to 0.4 m and 0.5 m bias in Mitra et al. (2021, 2020) respectively. Correcting the final results by adding this bias to the model estimated values, the reconstructed results were compared with the field measurements. Before applying the model to the actual field data sets, to investigate the bias that was caused by the effect of interpolation on irregularly spaced sampling locations, the test data sets of the model were subsampled at the outcrop locations. As a result, the mean bias and sample standard deviation caused by irregularity in sampling spacing was -16.9 and 98.86 m for the maximum inundation distance, respectively, and 0.2 and 0.32 m/s for the flow velocity, respectively. The maximum flow depth had a mean negative bias of 0.5 m (Figure 33 and considering that the parameter already had a bias of 0.4 m in the inversion results of the original test data sets, the additional bias caused by incompleteness of data sets was 0.1 m toward negative end. Fig-

ures 33d–i show that the overall mean bias in sediment concentrations was approximately around 0.01%.

The jackknife error variations were checked for different sampling window sizes. I chose a sampling window 1,800 m for our study. Maximum inundation distance (Figure 34a), maximum flow depth, and concentration (Figure 34c–e) shows a decreasing trend with the sampling window size, but the flow velocity shows an increasing trend (Figure 34b). The change in the estimation error was very small after the sampling window size of 1,700 m.

4.5 Results

4.5.1 Grain-size and thickness of tsunami deposits

The maximum inundation distance in this study area was observed 2,818 m from the shoreline along the survey transect, and tsunami deposits were present from 183 to 2,563 m from the shoreline. The tsunami deposits primarily consisted of sand-sized particles with an overlying mud layer. Mud layers ranged in thickness from 0.2 to 13.5 cm, and the overall sand thickness ranged from 0.5 to 22 cm. Sand layers were primarily composed of coarse to fine sand, with rip-up clasts and broken roots of vegetation. The spatial variation of grain-size distribution in the tsunami deposit was characterized by landward fining and thinning (Figure 35a). The tsunami deposits had a 22 to 6 cm (Figure 35a) thickness from the shoreline to around 1,600 m, whereas thinning of the deposits was observed after 1,600 m, ranging from 2 to 0.5 cm to the maximum extent of the deposit at the landward side. The mean grain-size distribution from this region varies from 1.5 phi to 2.6 phi around the study area at Odaka. The tsunami deposits in this area were characterized by a single layer of a fining upward sequence.

4.5.2 Inverse analysis of the 2011 Tohoku-oki tsunami deposits at Odaka

The maximum inundation distance at Odaka was reconstructed to be 2,897 m with a mean subsampling bias of −16.9 m (Table 4). The predicted flow velocity and maximum flow depth were 12.1 m/s and 2.4 m respectively with the mean subsampling bias of 0.2 m/s and −0.5 m. The total concentration of the sediment was 6.4% with the concentration of coarsest grain and finest grain-size classes were 0.5% and 2.1% respectively (Table 4). Figure 36 shows the jackknife error estimates for different parameters which were predicted by DNN

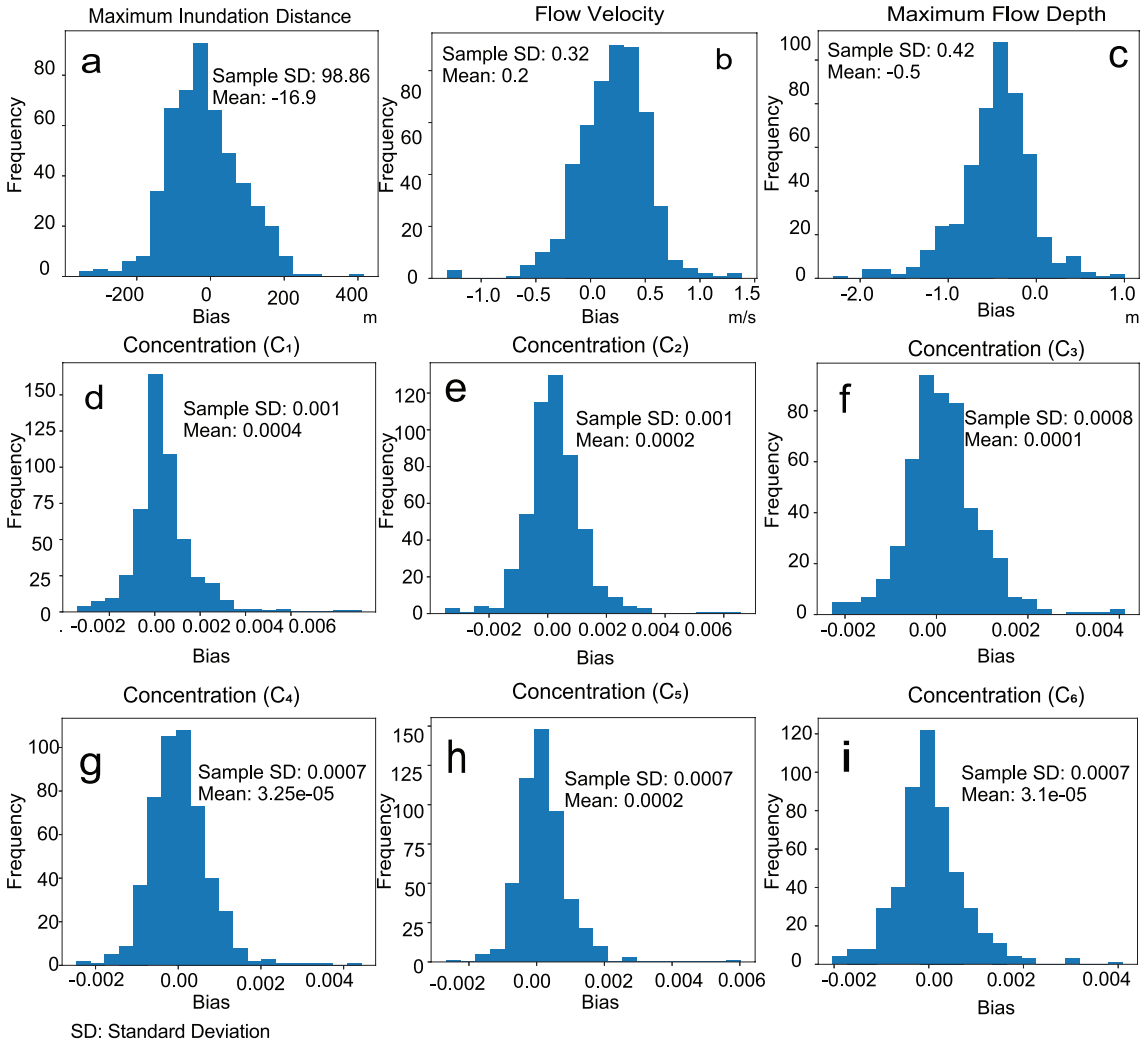

Figure 33: Histograms showing the variance and bias of predictions from the test data sets subsampled at the sampling locations of the transect at the Odaka region. (a) Maximum Inundation distance, (b) Flow velocity, (c) Maximum flow depth, (d)–(i) Concentrations of the six grain-size classes

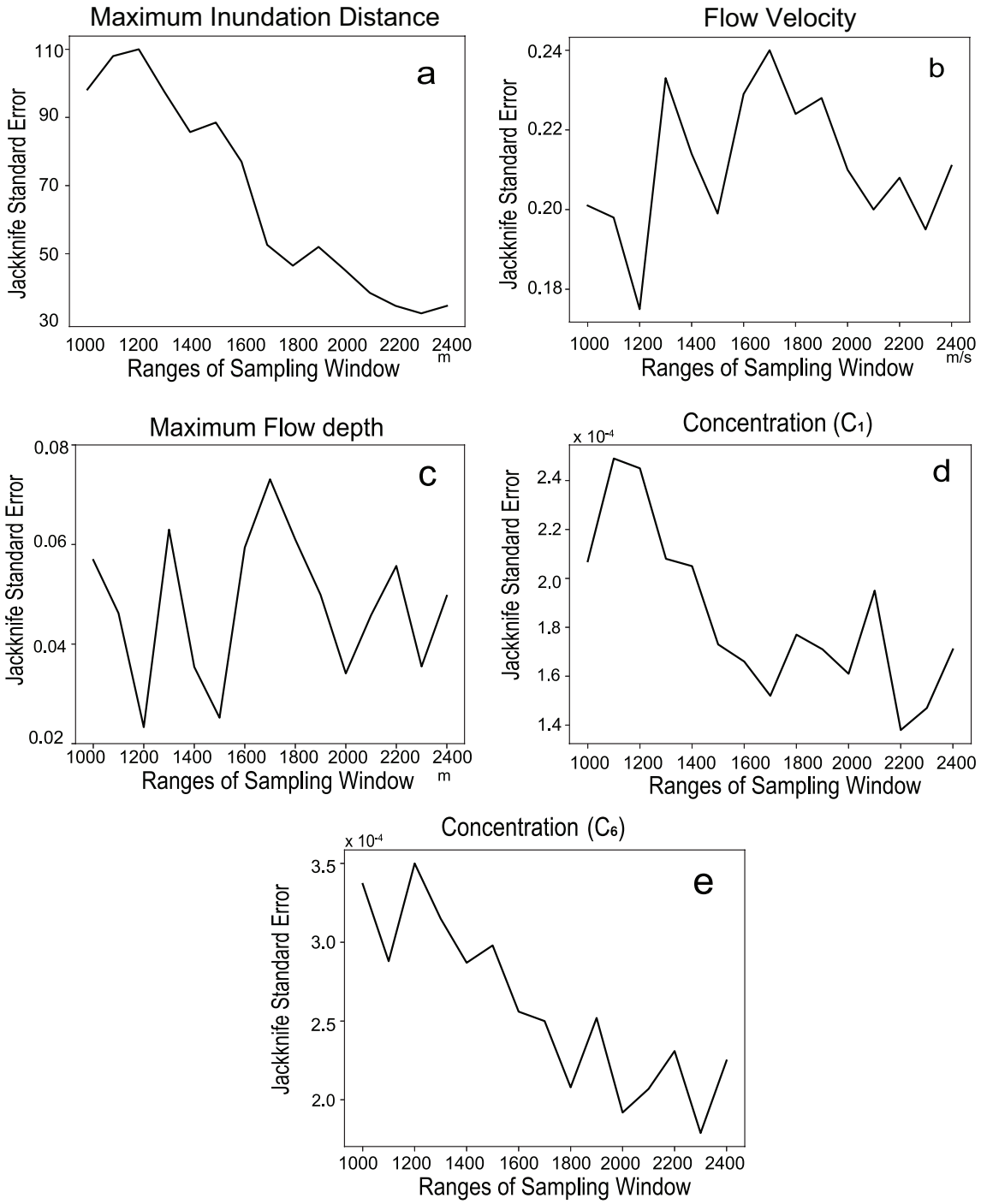

Figure 34: Changes of jackknife standard error with different sampling windows for different parameters. (a) Maximum inundation distance, (b) Flow velocity (c) Maximum flow depth, (d) Concentration of the first grain-size class, (e) Concentration of the sixth grain-size class.

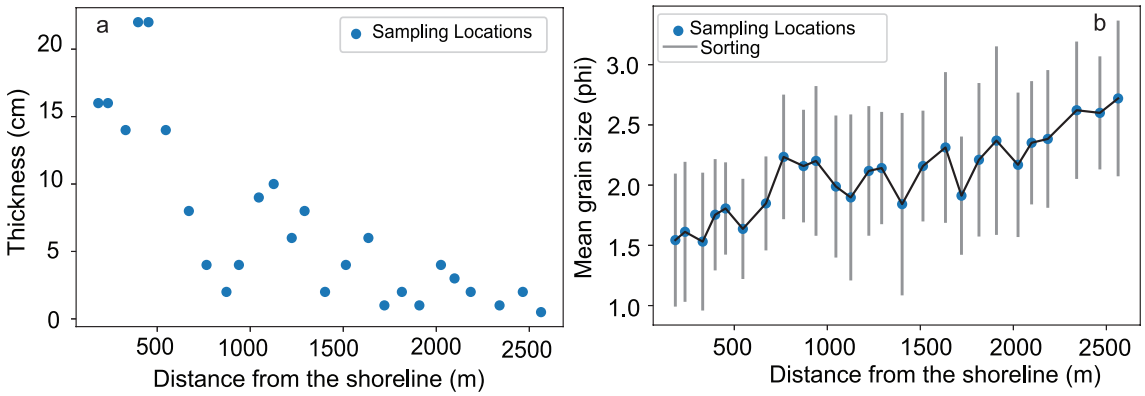

Figure 35: (a) Thickness of the deposits from the shoreline measured along the transect at Odaka. (b) Mean grain-size distribution and sorting of the deposits along the transect.

Table 4: Predicted results from the inverse model when applied to the 2011 Tohoku-oki tsunami data obtained from Odaka, Joban Coast. All reported standard error calculations were performed using a 95% confidence interval.

Parameters	**Predicted Results**	**Mean Bias**
Maximum inundation distance	2897 m ± 91.1 m	−16.9 m
Flow velocity	12.1 m/s ± 0.4 m/s	0.2 m/s
Maximum flow depth	2.4 m ± 0.1 m	−0.5 m
Concentration of C_1 (841 μm)	0.5% ± 0.03%	0.04%
Concentration of C_2 (595 μm)	0.6% ± 0.02%	0.02%
Concentration of C_3 (420 μm)	1.3% ± 0.04%	0.01%
Concentration of C_4 (297 μm)	2.1% ± 0.04%	0.003%
Concentration of C_5 (210 μm)	1.3% ± 0.05%	0.02%
Concentration of C_6 (149 μm)	0.6% ± 0.04%	0.003%

model. For example, 95% confidence interval of the estimation error of the maximum inundation distance was 91.1 m. The estimation error for the flow velocity was 0.4 m/s, and that for the maximum flow depth was 0.1 m (Figure 36a–c). The jackknife error estimates for sediment concentration were all very small, ranging around 0.02–0.05% (Figure 36 d-e).

Using the reconstructed flow conditions of the tsunami by the DNN inverse model, the forward model was used to calculate the spatial distribution of the thickness and grain-size composition, and the measured distribution was compared with the calculated distribution. Figure 37 shows the volume per unit area, and the grain-size distribution of measured and estimated values. The measured values of volume per unit area for each grain-size class matched the predicted results for all grain-size classes.

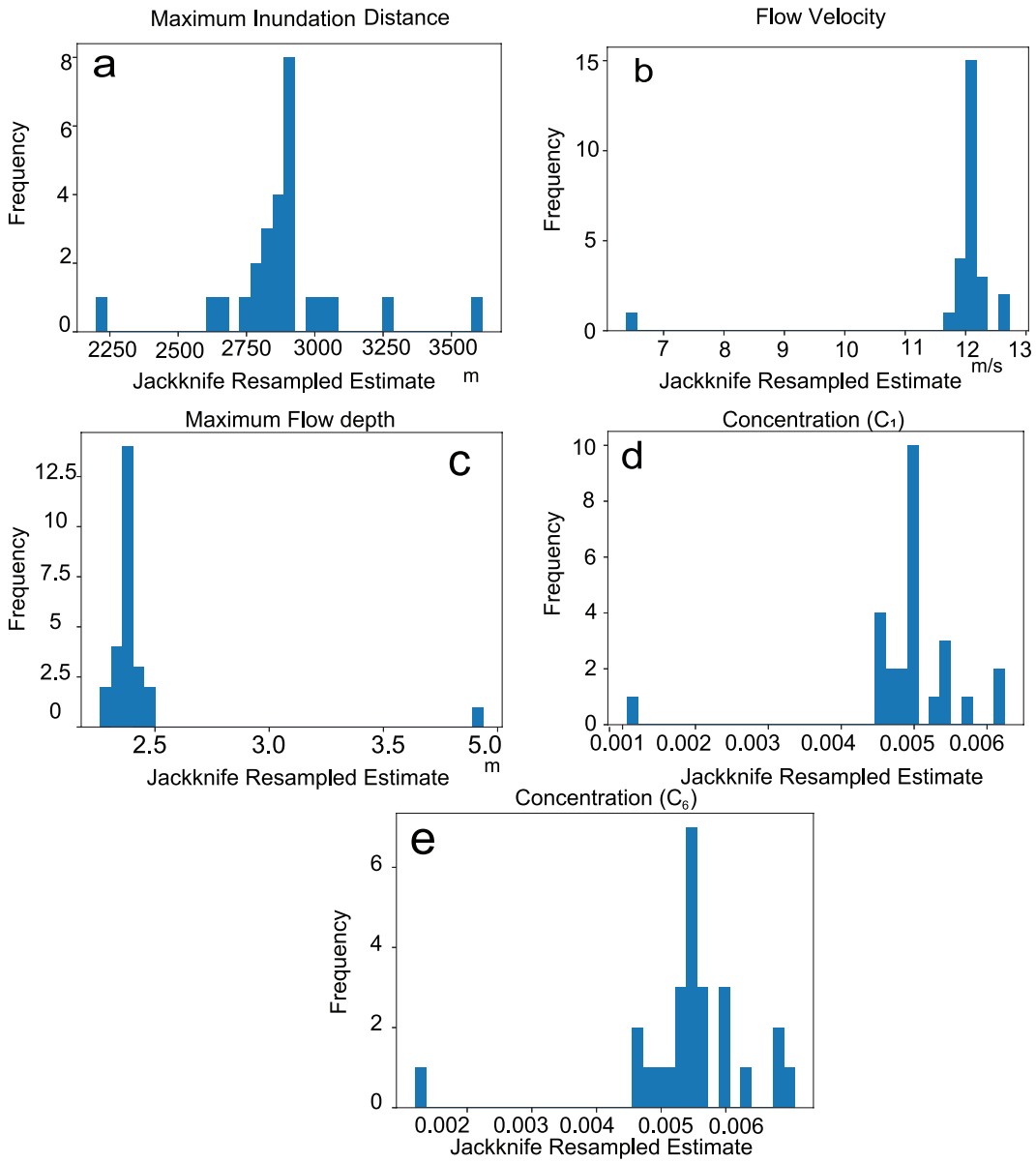

Figure 36: Jackknife resampled estimates for a sampling window size of 1,800 for different parameters. (a) Maximum inundation distance, (b) Flow velocity (c) Maximum flow depth, (d) Concentration of the first grain-size class, (e) Concentration of the sixth grain-size class.

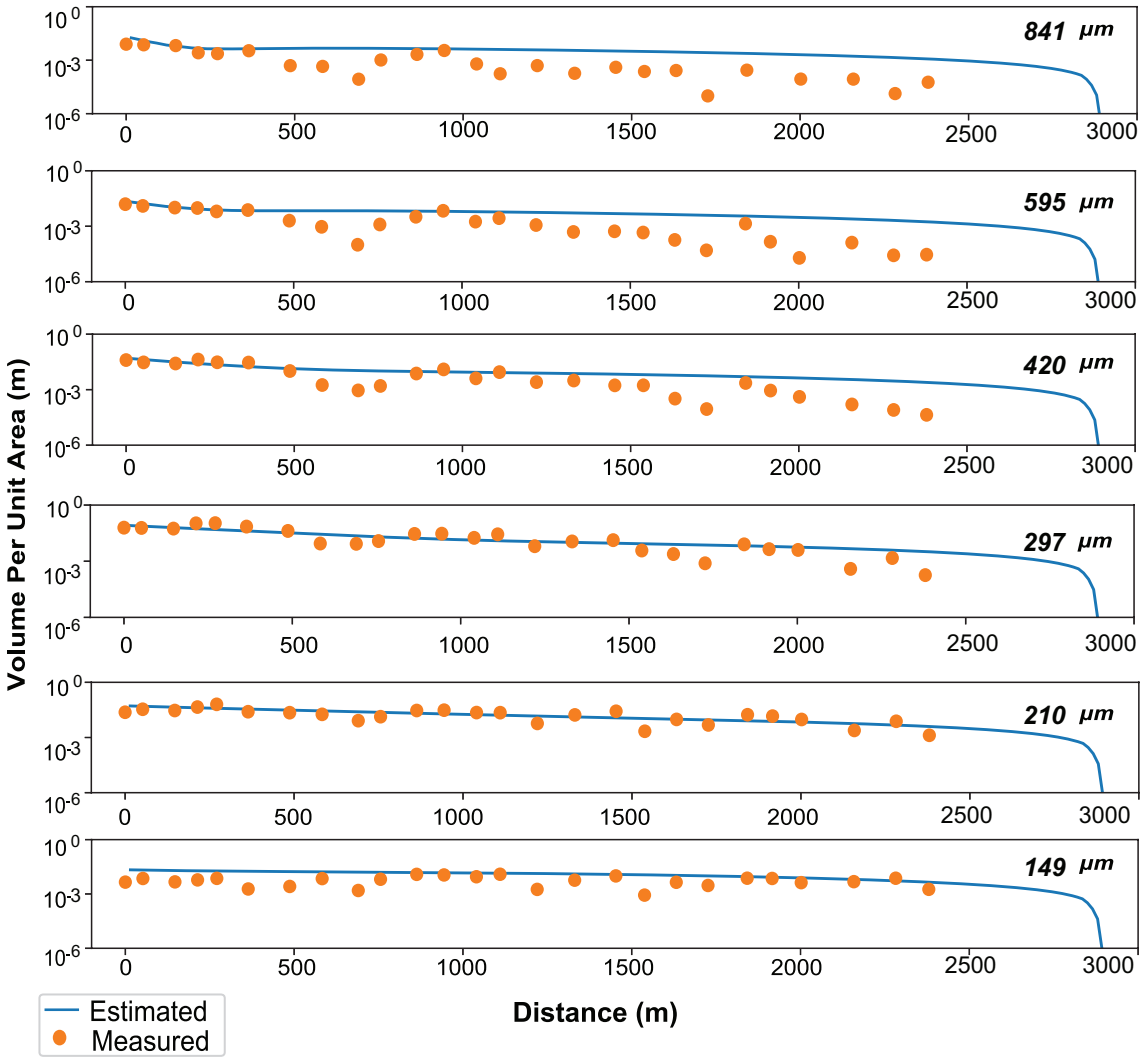

Figure 37: Spatial distribution of the volume per unit area of five grain-size classes. Solid circles indicate the values measured from the study area at Odaka, and lines indicate the results of the forward model calculation obtained using parameters predicted by the DNN inverse model.

4.6 Discussion

4.6.1 Verification of the tsunami characteristics reconstructed by DNN inverse model with measurements

To verify our results, I compared the maximum flow depth reconstructed by the DNN inverse model with the measured values by TETJSG and Sato et al. (2014) (Figure 38a and b). The locations measured by TETJSG widely covers the study area (Figure 30a). Sato et al. (2014) surveyed the surrounding areas around our field location, which are the Murakami, Tsunobeuchi, and Tsukabara areas. The Murakami and Tsunobeuchi areas are situated approximately 870 m, 1,600 m south, respectively from the transect of this study, whereas Tsukabara is situated approximately 1,560 m north from our field location. Sato et al. (2012b) measured the tsunami height using mudlines, damage marks on the artificial structures and trees. TETJSG also measured the height using water marks soon after the event took place and before anthropogenic disturbances occurred from recovery. Figure 38a shows that although there was a large variability in the measured values of the flow depths, the reconstructed result, 2.4 ± 0.1 m, reproduced the measured values approximately around Tsunobeuchi, Murakami, and Tsukabara (Figure 30a). According to the reported values by TETJSG and Sato et al. (2014), the maximum and minimum value of the meausured flow heights were approximately 17 m and 3.5 m around those areas. It should be noted that the flow depths (Figure 38) were calculted from the flow heights using the elevation extracted from 5 m DEM (acquired in 2012) and approximated ground elevation provided in (Sato et al., 2014). The scatters in Figure 38a can be explained by the accuracy of flow depth estimation, due to reliability of the tsunami measurements and precision of the interpolated ground elevation.

Regarding the flow velocity, the estimated velocity by the DNN inverse model was 12.1 m/s, which was higher comparing to the reconstruction in the Sendai Plain (Mitra et al., 2020). The flow velocities of the 2011 Tohoku-oki tsunami run-up flow were measured 4.2 m/s on average, ranging from 1.9 m/s to 6.9 m/s from the aerial video records of the Sendai Plain (Hayashi and Koshimura, 2013). In the 2004 Indian Ocean tsunami, flow velocities of 6–8 m/s at the Khao Lak area, 3–4 m/s at Kamala beach, 4 m/s at Phuket and 9 m/s at Khao Lak were observed (Rossetto et al., 2007; Karlsson et al., 2009; Szczuciński et al., 2012b). The velocity measured from the survivors' videos of the December 26, 2004 Indian Ocean tsunami at Banda Aceh, Indonesia, was in the range of 2–5 m/s. (Fritz et al., 2006).

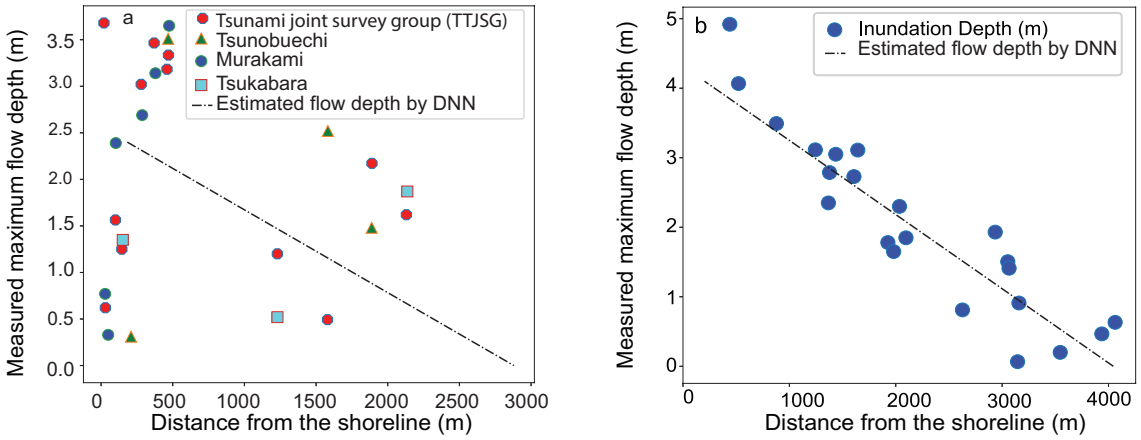

Figure 38: (a) Flow depths measured at neighboring areas are denoted by the markers and the flow depth estimated by the DNN inverse model is shown by the black line. (b) The flow depth measured at the Sendai Plain is marked by the blue solid circle and the black line shows the estimation by the DNN inverse model.

No direct observations of the flow velocity were made in this study area; however, the velocity was comparable with the values reported near the study area. Sanuki et al. (2013) used video footage analysis around the mouth of the Kido River, which is located 30 km away from our field location but along the same coastline. They reported that the inundation flow was 14–11 m/s inside the river channel, whereas it was around 15–10 m/s in the coastal plain. Moreover, Sato et al. (2014) estimated that the overtopping flow on the seawall crown reached 11–17 m/s in velocity at the Idagawa area which is located approximately 3 km south of the study area, based on the Bernoulli's theorem. Hence, reconstruction of the flow velocity by DNN inverse model is said to be reasonable, suggesting that the exceptionally high flow velocity occurred in this area.

The maximum inundation distance was also comapred with the measured value from the field study. The reconstructed maximum inundation distance was 2,897 ± 91.1 m, which was close to the observed extent of tsunami propagation that was around 2,818 m.

4.6.2 Influence of inundation by Froude supercritical flows

The reconstructed tsunami characteristics in the Odaka region using the DNN inverse model suggested that the type of inundation flow was a Froude supercritical condition. Here the Froude number is defined as $Fr = U/\sqrt{gh}$, which represents the ratio of inertia to gravity forces. U denotes the layer-averaged flow velocity as defined above. The parameters g and

h are the gravitational acceleration and flow depth respectively. The DNN inverse model for the Joban Coast suggested that the flow velocity U and the depth h are 12.1 m/s and 2.4 m, respectively, so that Fr is 2.5 (Table 4). This Fr value clearly indicates that the flow condition in the study area was the supercritical condition ($Fr = 2.5 > 1$). On the other hand, for the 2011 Tohoku-oki tsunami in the Sendai Plain, the flow velocity and depth were 5.4 m/s and 4.1 m, respectively in the reconstruction by Mitra et al. (2020), indicating that the flow type was subcritical ($Fr = 0.9 < 1$).

In general, $Fr < 1$ indicates subcritical flows ($Fr < 1$) that are relatively slow in velocity or thick in flow depth, and the water surfaces of the subcritical flows are flat and stable. The undulation of a subcritical flow surface exhibits an out-of-phase relationship with the shape of topography. In contrast, $Fr > 1$ indicates supercritical flows, which behave as a rapid or thin and unstable flow (Charvet et al., 2017), with low flow resistance and high sediment transport (Phantuwongraj and Choowong, 2012). In some cases, supercritical flow can result in a hydraulic jump that causes the local dissipation of high flow energy (Muste and Hoitink, 2017; Retsinis and Papanicolaou, 2020). The water surfaces of supercritical flows exhibit an in-phase relationship with the topography, and the shape of the flow surface shows a large fluctuation that emphasizes the shape of the bottom surface. Therefore, if the tsunami inundated the area as a supercritical flow, the flow depth could be high locally because of topographic influences.

The inundation flows of the large-scale tsunamis, such as the 2004 Indian Ocean tsunami, have been observed as subcritical or supercritical, with the range of the reported Froude number varying ranged from 0.7 to 2.0, depending on place (Matsutomi et al., 2005). Choowong et al. (2008b) reported that deposits of the 2004 Indian Ocean tsunami indicated a supercritical flow condition based on the sedimentary structures, and this flow regime was dominant during the inflow. The occurrence of anti-dunes at the Andaman Coast of Thailand suggested a supercritical flow condition at the depositional area, and the bed maintains an in-phase relationship with the free water surface (Simons et al., 1960; Middleton and Hampton, 1973; Kennedy, 1963). Thus, judging from the sedimentary structure, the supercritical flow condition was maintained in this area during the inundation of the tsunami. In contrast, no dominant sedimentary structure was observed along the Sendai Plain and in Odaka region, only plane-parallel stratification was observed, which can also be formed at the supercritical flow condition (Paola et al., 1989; McArthur et al., 2020). The inverse

analysis revealed that such supercritical flow inundation of the large-scale tsunami also occurred in the Odaka region, whereas it did not occur in the Sendai area.

The difference in flow conditions between Odaka and Sendai is shown clearly in the measurements of inundation heights. Figure 30a indicates that the measured flow heights fluctuating largely along the transect at Odaka, compared with those at Sendai (Figure 30b). This difference can be interpreted as the result of supercritical flow conditions with topographical complexities in the Odaka region. Since the inundation flow was presumably subcritical in the Sendai Plain, the water surface would have been stable even if there were local topographic changes. In the Odaka region, the water surface of the inundaiton flow fluctuated largely in response to local topographic variations because of its Froude supercritical condition. The the flow heights also varied to a great extent, such as in Idagawa, where they were exceptionally high (Sato et al., 2014).

Other possible reasons of local fluctuations in flow depths could be the formation of hydraulic jumps, particularly in the Odaka region. The fluctuations in the tsunami inundation depths in the Odaka District in the Minamisoma area could be due to the presence of a lagoon in that area, which caused the transition from a supercritical to a subcritical flow resulting in a hydraulic jump (Matsutomi et al., 2001; Yamaguchi and Sekiguchi, 2015; Ali Hasan Muhammad and Tanaka, 2019).

The reason for the large differences in tsunami characteristics between Odaka and Sendai has not been determined yet, but several possibilities may explain it. First, it could be due to the offshore steeper bathymetry in the Odaka region than that in the Sendai Plain (Tsuruta et al., 2017; Ikehara et al., 2014; Abe et al., 2012) and the convex-shaped shoreline, which possibly decreased tsunami energy dissipation (Sato et al., 2014). In contrast, the offshore bathymetry of the Sendai Plain is gentle, and the possible reason for the subcritical flow in the Sendai Plain could be the presence of a coastal forest which reduced the flow velocity significantly (Kusumoto et al., 2020). In some cases, the flow velocity becomes extremely high behind the coastal dikes near the shoreline and the energy decreases gradually owing to the presence of different obstacles along the way (Sugawara, 2020). However, in the case of Odaka or the Joban Coast the supercritical flow has been observed in the depositional area, similar to the Andaman Coast in Thailand (Choowong et al., 2008b).

4.7 Conclusion

In this study, flow conditions were reconstructed, such as the maximum inundation distance, flow velocity, maximum flow depth, and sediment concentration, of the 2011 Tohoku-oki tsunami, around the Odaka District, Minamisoma, at the Joban Coast. Despite having a gentle slope and complex topography, the DNN inverse model successfully predicted the flow conditions of the tsunami. The maximum inundation distance was 2,897 ± 91.1 m which was close to the observed extent of 2,818 m by field investigations. The flow velocity was 12.1 ± 0.4 m/s, which was similar to the values reported from the video image analysis and numerical simulation results by different researchers. The maximum flow depth was 2.4 ± 0.1 m, which also matched with the reported measured values of the maximum flow depth around the field study area. The flow condition along the transect was determined to be supercritical based on the results by the DNN inverse model, and the reason behind that might be the topographical undulations or a hydraulic jump. The fact that different flow characteristics of the 2011 Tohoku-oki tsunami varied depending on the location is the key feature of this study. Further studies are needed to improve the present inverse model algorithm to remove the computational bias, and the forward model could be updated as a 2D model or be replaced by another forward model. Thus, the DNN model involves a reasonable inverse analysis for different locations despite of having complex topography, and this model has the potential to be used as a tool for tsunami hazard mitigation and disaster management.

Our study incorporates the flow-type characterization phenomenon along with the reconstruction of the tsunami flow conditions for the area. Especially, for the Odaka region, it showed high flow velocity with shallow flow depth, which is typical phenomenon of a supercritical flow type. However, a detailed investigation of such a high flow velocity around the Joban Coast needs to be conducted in future studies, as supercritical flows with hydraulic jump can cause extensive damage to the artificial structures and livelihoods. For future studies, there is a need for considerable research on the influence of supercritical inundation flow of tsunamis in the coastal area.

4.8 Data and Code Availability Statement

The data sets and codes for this study can be found in the Zenodo (`https://doi.org/10.5281/zenodo.4764153`).

5 Preliminary results of DNN inverse analysis of the 869 Jogan tsunami deposits

5.1 Introduction

On July 13, AD 869, a large-scale tsunami was triggered by the earthquake, and damaged the low-lying coastal zones of northeast Japan (Usami, 1975). In the historical record, more than 1000 people were drown by this tsunami (Minoura et al., 2001). The magnitude of the earthquake was estimated approximately 8.6 or larger (e.g., Namegaya and Satake, 2014), based on comparison of tsunami deposit distribution and tsunami inundation simulations. The preliminary information of Jogan deposits were found from a historical document, Nihon Sandai-jitsuroku (e.g., Minoura et al., 2001; Sugawara et al., 2013), which states that Jogan tsunami caused extensive flooding in the Sendai Plain and this strong tsunami destroyed the town of Tagajo and its castle in Sendai.

Tsunami deposits of this event have been found on the Ishinomaki and the Sendai Plains, Miyagi, and Joban Coast, Fukushima (Namegaya and Satake, 2014). Tsunami deposits consisted of layers of gravels at the Sanriku Coast (Inoue et al., 2017), and of sand layers in the coastal lowlands of Sendai Plain and the Joban Coast (Abe, 1990; Sugawara et al., 2010, 2011, 2013; Suzuki et al., 2009; Minoura et al., 2001).

The 869 Jogan tsunami has been regarded as the possible precursor of the 2011 Tohoku-oki tsunami (Sugawara et al., 2012). It has been suggested that the distributions of this tsunami deposits are comparable with the deposits of the 2011 Tohoku-oki tsunami deposits from Sendai Plain. Based on the existing sedimentological data and numerical modeling, the maximum inundation distances were estimated around 2.6–3.3 km from the paleo-coastline for both events (Sugawara et al., 2013).

There are only a few estimates of the flow characteristics of the 869 Jogan tsunami. Several studies conducted the numerical simulation of Jogan tsunami using the 2D tsunami forward model, such as TUNAMI-N2 (e.g., Sugawara et al., 2011). On the assumption of various fault slip models, Namegaya and Satake (2014) estimated that the flow velocity was possibly close to the 2011 Tohoku-oki tsunami. However, there are no studies of the inverse analysis of tsunami characteristics based on the deposits of the 869 Jogan tsunami.

Here, I conducted the first inverse analysis of the 869 Jogan tsunami for understanding its flow characteristics and for verifying the hypothesis that the 2011 Tohoku-oki tsunami

is the recurrent event of the 869 Jogan tsunami. DNN inverse model by Mitra et al. (2020, 2021) showed that the model has the reasonable potential to elucidate on the tsunami characteristics with uncertainty analysis from deposits of large-scale tsunamis such as the 2011 Tohoku-oki tsunami and the 2004 Indian Ocean tsunamis. Here, I represent the applicability and the preliminary results of DNN inverse model for the 869 Jogan tsunami deposits at Sendai Plain. This study is important for the further mitigation strategies in future around the Sendai Plain.

5.2 Study area

Several field surveys of deposits of the 869 Jogan tsunami were conducted along shore-normal transect around Iwate, Miyagi and Fukushima Prefectures to detect maximum inland extent Jogan tsunami deposit (Sugawara et al., 2012).

For the present study I have considered tsunami deposits distributed in Sendai Plain tsunami deposits. The topography of the Sendai Plain around Jogan deposits is mostly formed by flood plains and beach ridges with lagoons. The ancient deposit of the 869 Jogan tsunami in this area were first identified as a sand layer with the association of peaty and muddy sediments at a relatively flat plain (Abe, 1990; Minoura and Nakaya, 1991). The event deposits were composed of well sorted medium grained sand dominantly. Rip-up clasts were present in the sandy deposits with underlying or overlying muddy deposits at different transects (Sugawara et al., 2010).

From several excavation sites in Sendai Plain, the thickness of Jogan deposits was estimated as 30 cm in maximum and was 8 cm in average (Sugawara et al., 2010) with the landward thinning trend. The landward limit of distribution of the Jogan tsunami deposits were 3–4 km from the present shoreline (Sugawara et al., 2013). The paleo-coastline during the 869 Jogan was estimated approximately 1 km landward of the present coastline (Ito, 2006; Sugawara et al., 2013). Hence, Jogan tsunami deposits at Sendai Plain was found around 2 to 3 km from the paleo-coastline (Figure 39).

The grain-size analysis results from transect F from Sugawara et al. (2010) (Figure 39), were considered for the application to DNN inverse model in order to reconstruct the tsunami characteristics from the 869 Jogan deposits. The maximum and minimum thickness of the event sand layer along this transect was 11 cm and 0.5 cm at a distance 1,768 m and 2,592 m respectively from the shoreline (Sugawara et al., 2010). For this study, the

spatial grain-size distribution from 8 sampling locations were considered. It should be noted there was a possible lagoon along the transect F (Figure 39). To avoid influence of local topography, only the sampling points at the depositional area beyond the lagoon were considered. Figure 40a and b shows the thickness and, the distribution of mean grain-size of Jogan tsunami deposits along the transect. The detailed field investigations and sedimentological characteristics from this transect of Sendai Plain have been reported in Sugawara et al. (2010).

5.3 Methodology

5.3.1 Forward model

The DNN inverse model uses FITTNUSS forward model (Naruse and Abe, 2017) which calculates the spatial variation of the thickness and grain-size distribution of the tsunami deposits using the input values, such as maximum inundation distance, flow velocity, maximum flow depth and sediment concentration. This model is based on layer-averaged one-dimensional shallow water equations including conservation of fluid mass, momentum and sediment mass. The model works with the quasi-steady flow assumption where the velocity of tsunami run-up (U) is assumed to be constant in while the inundation depth increases at a constant rate until it reaches the maximum value at the seaward boundary. The model assumes sediment entrainment and deposition during the run-up phase and coordinate transformation was applied for the efficiency and stability of calculation of the fluid dynamics. Finite difference method was employed to obtain the numerical solutions in the model. The forward model requires several empirical closure equations regarding flow dynamics and sediment transport including entrainment rate of basal sediment, bed friction and stratification of sediment concentration that were described in Naruse and Abe (2017). The forward model is repeated to produce the artificial data sets of spatial variation of the thickness and grain-size distribution of the tsunami deposits which were used to train the DNN inverse model.

To produce artificial data sets, random generation of the input parameters for the inverse model include the maximum inundation distance, flow velocity, maximum flow depth and concentration were used. The ranges of training data sets were 820–4000 m for maximum inundation distance, 1.5–10 m/s and 1.5–12 m for flow velocity and maximum flow depth respectively and 0 to 2% for sediment concentration. The produced data sets of spatial

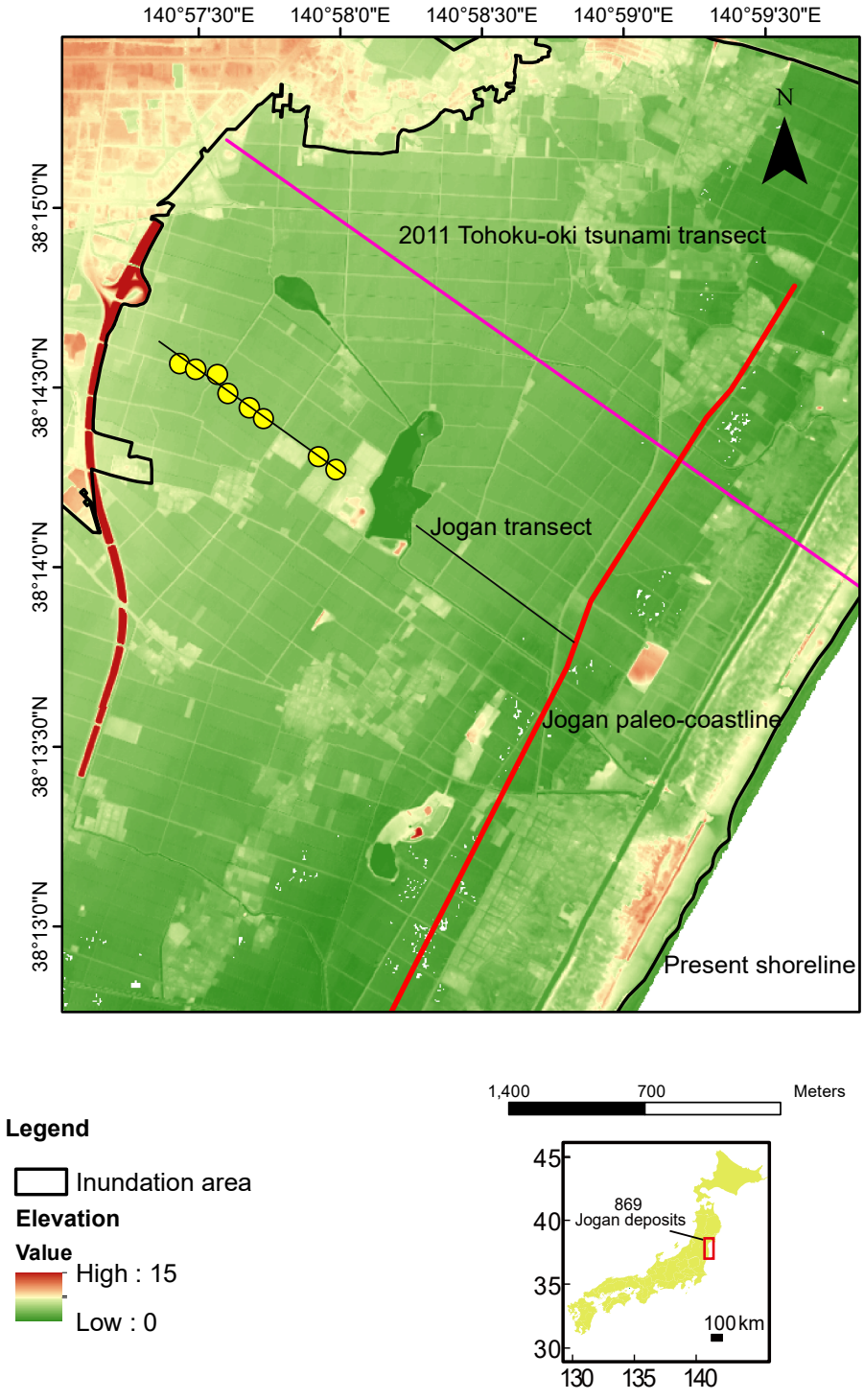

Figure 39: DEM map showing the elevation and topography around the 869 Jogan tsunami and the 2011 Tohoku-oki tsunami transects at Sendai Plain

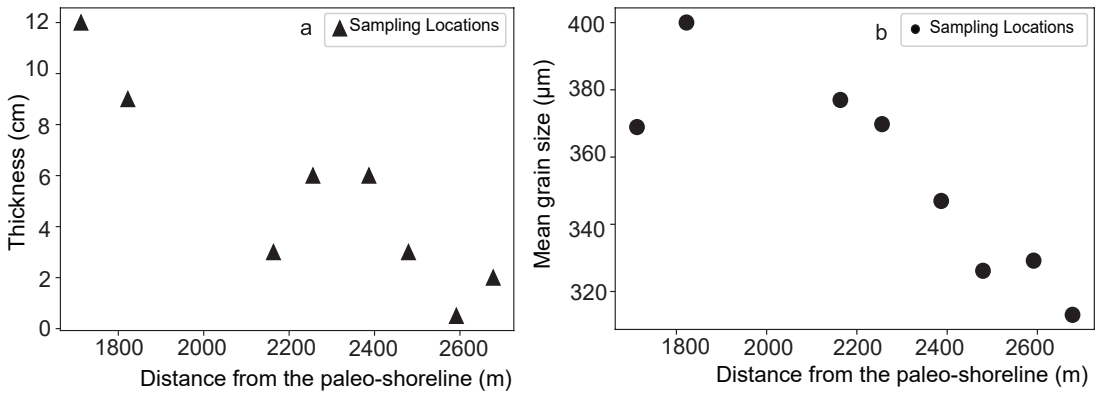

Figure 40: (a) Thickness of the deposits from the shoreline measured along the transect at Odaka. (b) Mean grain-size distribution and sorting of the deposits along the transect.

grain-size distribution using the above-mentioned parameter in forward model were used to perform the inversion. The grain-size classes used for this study were 500, 420, 354, and 297 μm respectively.

5.3.2 Inverse model

The DNN inverse model works in a feed forward mechanism. The hyperparameters of the DNN inverse model is same as described in Mitra et al. (2020). The input layer of the neural network takes the values of volume per unit area grain-size classes at specific spatial grids which goes through several hidden layers and hyperparameters and finally the output layer predicts tsunami characteristics, such as maximum inundation distance, flow velocity, maximum flow depth, and sediment concentration. This was followed by the validation of the performance using the artificial test data sets. The sampling window was used in this model to avoid problems due to thinning at the distal part of the transect and incompleteness of the data set along the transect. However, as the measured sampling locations of tsunami deposits were irregularly spaced, the effect of interpolation on the model was more than the previously mentioned in Mitra et al. (2020, 2021).

The model was ready to apply for the application to the field data sets of Jogan deposits upon post-training and validation performance. I have selected a sampling window size of 770 m for our study which was chosen based on the comparative results obtained from tests using different sampling window sizes as described in the results section. For this study area, the grids spacing in the fixed coordinates was 10 m, meaning the number of

spatial grids used for the inversion was 77. In the subsampling test (Figure 41), which was performed at the sampling locations of Jogan, volume per unit area of sediment in the test data sets at the sampling locations were estimated by 1D cubic interpolation, and these subsampled data were interpolated again at the forward model grids and the inversion was applied. Hence, the model prediction was checked to estimate the bias, caused by the irregular spacing in spatial distribution of sampling locations.

The training of the DNN inverse model has already proved that the model has the good potential to reconstruct the tsunami flow conditions. The final loss function values for the training and validation were approximately 0.0043 and 0.0032 respectively. There was no large deviation for all the parameters. However, for the maximum flow depth, the model tended to estimate approximately 0.6 m lower than the original values on average (see appendix 8.2).

During subsampling, irregularity in sampling spacing was checked and it presented the sample standard deviation and mean bias 847 m and 774 m (Figure 41) for the maximum inundation distance, 0.7 m/s and −0.3 m/s for the flow velocity. The maximum flow depth has mean negative bias of 0.9 m and considering that the parameter already had a bias of 0.6 m in the inversion results of the original test data sets, the additional bias caused by incompleteness of data sets was 0.3 m toward negative end.

5.4 Results

The reconstructed flow conditions, such as the maximum inundation distance at Jogan was reconstructed to be 5645 m with a jackknife standard error (95%) of 287 m (Table 5). The predicted flow velocity and maximum flow depth were 5.3 m/s and 3.9 m respectively with jackknife standard error (95%) of 1.5 m/s and 1.0 m. The total concentration of the sediment was 3.6% (Table 5). The jackknife error estimates for sediment concentration were small, ranging around 0.2–0.1%.

The forward model calculates the spatial distribution of the thickness and grain-size composition and I used the reconstructed flow conditions of the tsunami by DNN inverse model to compare the measured and predicted distribution. Figure 42 shows the volume per unit area, grain-size distribution of measured and predicted values. The measured values of volume per unit area for each grain-size class matched the DNN predicted results for all grain-size classes (Figure 42).

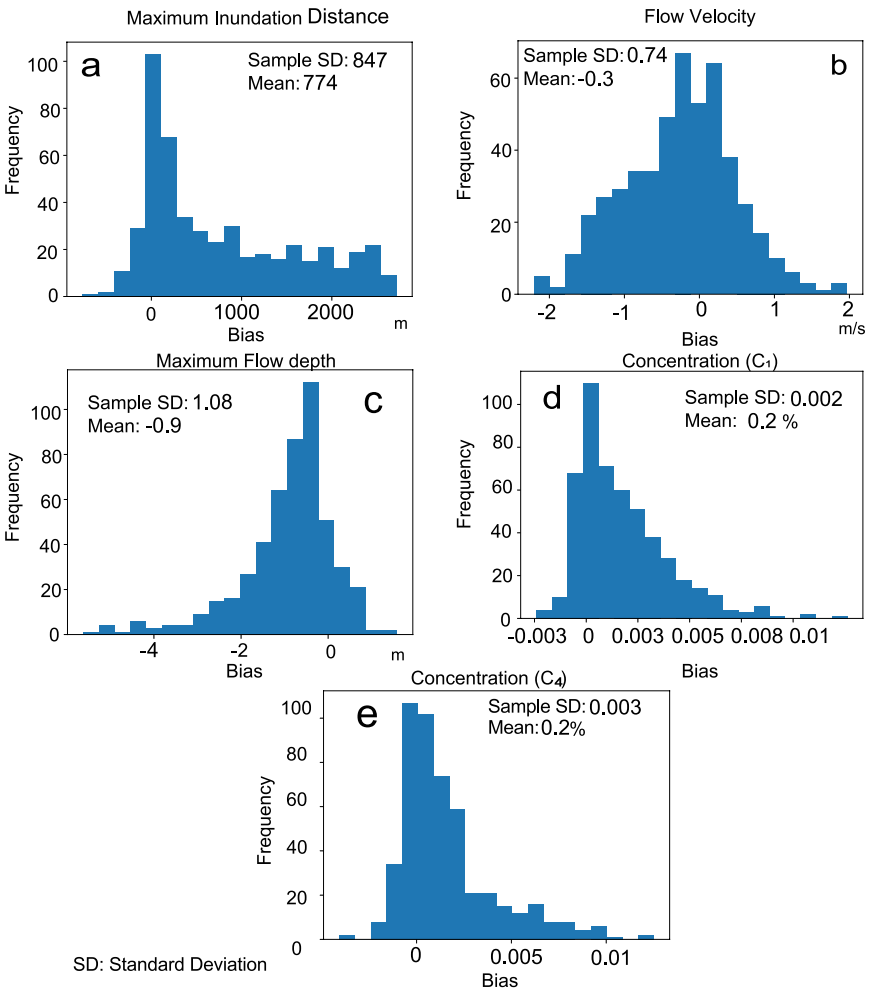

Figure 41: Histograms showing the variance and bias of predictions from the test data sets subsampled at the sampling locations of the transect at the Sendai Plain for the 869 Jogan tsunami. (a) Maximum inundation distance, (b) Flow velocity, (c) Maximum flow depth, (d) Concentration of the first grain-size class, (e) Concentration of the fourth grain-size class.

Table 5: Predicted results from the inverse model when applied to the 869 Jogan tsunami deposits obtained from the Sendai Plain. All reported standard error calculations were performed using a 95% confidence interval.

Parameters	Predicted Results	Mean Bias
Maximum inundation distance	5645 m ± 287 m	774 m
Flow velocity	5.3 m/s ± 1.5 m/s	−0.3 m/s
Maximum flow depth	3.9 m ± 1.1 m	−0.9 m
Concentration of C_1 (500 μm)	1.14% ± 0.22%	0.17%
Concentration of C_2 (420 μm)	1.10% ± 0.22%	0.14%
Concentration of C_3 (354 μm)	1.08% ± 0.22%	0.18%
Concentration of C_4 (297 μm)	0.30% ± 0.11%	0.16%

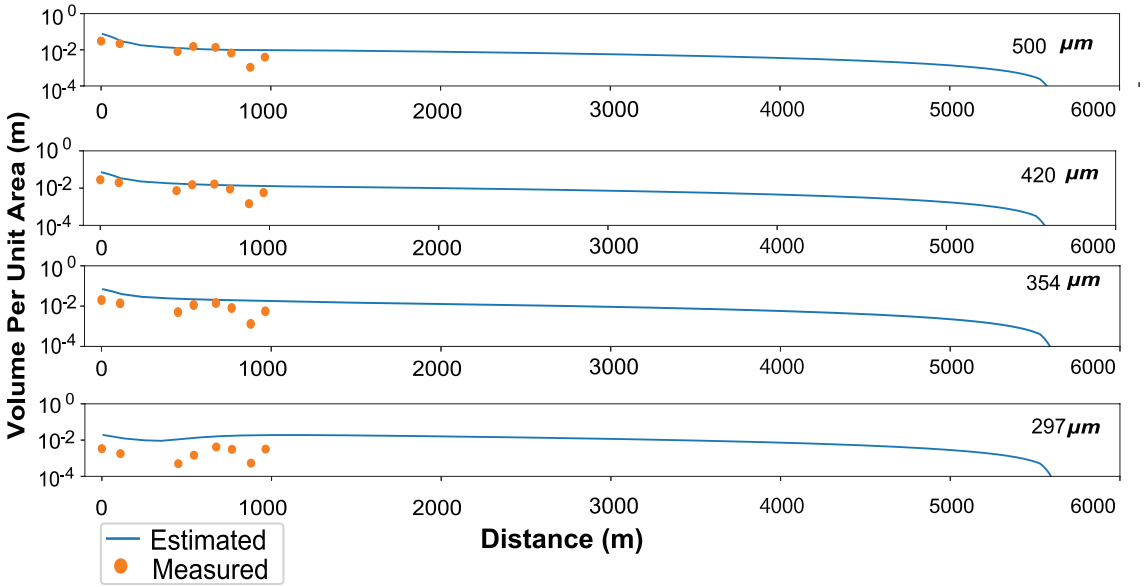

Figure 42: Spatial distribution of the volume per unit area of four grain-size classes of the 869 Jogan tsunami deposits. Solid circles indicate the values measured from the study area at the Sendai Plain, and lines indicate the results of the forward model calculation obtained using parameters predicted by the DNN inverse model.

5.5 Discussion

5.5.1 Comparison of the predicted results of the 869 Jogan tsunami with the existing models

This paper represented the preliminary results, estimating characteristics of the 869 Jogan tsunami from its deposits using the DNN inverse model. The DNN inverse model suggested 3.9 ± 1.0 m for the maximum flow depth at the seaward end of calculation domain (1,713 m from the shoreline). If the flow surface is extended to the paleo-shoreline, it is estimated that the maximum flow depth was 5.6 m. Also, the flow velocity of the 869 Jogan tsunami was estimated as 5.3 ± 1.5 m/s from the inverse analysis of this study. In addition, the DNN model predicted the inundation distance as 5,645 m from the seaward end of the calculation domain (1,713 m), and thus the estimated maximum inundation distance was 8,358 m from the present-shoreline and 7,358 m from the paleo-shoreline.

Here I compare these results with those of other sedimentological studies (Abe, 1990), as well as numerical models (Sugawara et al., 2011, 2013; Namegaya and Satake, 2014) that also presented the flow conditions of the 869 Jogan tsunami.

Several sedimentological studies estimated the maximum inundation depth and length of the 869 Jogan tsunami from distribution of the tsunami deposits. Abe (1990) identified the 869 Jogan tsunami deposit based on geochemical characteristics, sedimentary structures, amount of mud and sand deposits, volcanic ash and radiocarbon dating, indicating that the maximum elevation of the tsunami deposit was 2.5 to 3.0 m at the Sendai Plain. They estimated that the flow height at the shoreline was a few meters higher than this elevation. They also reported that inundation distance of tsunami inundation was reported around 3000 m from the shoreline (Abe, 1990). Sugawara et al. (2013) reported that the tsunami was around 2.6–3.3 km from the paleo-coastline which is situated around 1 km inland from the present shoreline. The DNN model predicted the maximum inundation distance, 5,645 m which was around 2,300 m more than the reported value. Thus, the predicted results by the DNN inverse model is higher than the estimated results by Sugawara et al. (2013). There are several possibilities that could explain the difference between the predicted and the observed inundation limits. First, it is possible that the performance of the inverse model is inadequate to analyze such a limited number of data, and that erroneous results are being obtained. Further verification of the precision of the inverse analysis is required. Second, the DNN inverse model estimates are based on the assumption that the

topography is infinitely flat. In reality, the slope changes at the inundation limit of both the 2011 Tohoku-oki and the 869 Jogan tsunamis. Thus, the inverse analysis results show the inundation area if the slope was constant outside the study area, and the change in slope could have prevented the tsunami inundation. Third possibility could be that the inundation limit of Jogan tsunami was actually further inland whereas the muddy part of the tsunami deposits near the inundation limit was lost due to diagenesis and/or bioturbation. Further field studies and improvement of the inverse model are needed to examine the plausibility of these possibilities.

Several numerical models with assumptions on the fault displacement regions also predicted the maximum inundation depth of the 869 Jogan tsunami. Minoura et al. (2001) conducted a numerical simulation using TUNAMI-N2 and delineated that tsunami wave height (i.e. the maximum flow depth at shoreline) was 8 m around Sendai Plain. Results showed that the tsunami inundated 2500 to 3000 m inland from the present shoreline. Later, Sugawara et al. (2013) evaluated the tsunami height (maximum flow depth) of 6–7 m near coastline using the similar model with the refined fault parameters. Similarly, Namegaya (2010) showed that the flow depth of Jogan tsunami at Sendai Plain was calculated around 3.5–5.5 m. Namegaya and Satake (2014) estimated the minimum flow depths and depth-averaged velocity from the Sendai Plain. They employed two values (0.030 and 0.040) for Manning's roughness coefficient to estimate of tsunami characteristics, obtaining that the flow depth ranged from 2 to 4 m and the depth-averaged flow velocity ranged from approximately 4.0 to 7.5 m/s. However, they assumed assumed a minimum flow depth of 1 m for the maximum inland extent of the Jogan sandy deposit, based on comparison of the 2011 Tohoku-oki tsunami inundation simulation and deposit observations (Namegaya and Satake, 2014). On the other hand, DNN inverse model estimated values of flow velocity and flow depth approximately 5.3 ± 1.5 m/s and 3.9 ± 1.1 m respectively and these values are the range of thier reported values.

It should be noted that three methodologies introduced here (sedimentological studies, numerical models with assumptions of fault slip models, and the DNN inversion model) reconstruct paleo-tsunami characteristics from different aspects. Numerical forward models can predict unsteady hydrodynamics of the tsunami but they examined a limited number of slip models. As it could be difficult to explore all range of possible parameters for slip model for ancient tsunamis, the models provide just an example of possible reconstructions.

The information on the tsunami deposits used to select an appropriate slip model is limited to their distribution range. In-depth sedimentological analysis also provide qualitative analysis of the ancient tsunamis. DNN inverse model showed promise for the reconstructions of tsunami characterics for the 869 Jogan event and provides single values of parameters precisely with jackknife uncertainty. However, the values for uncertainty and bias are more than modern tsunamis, especially for the maximum inundation distance and these drawbacks could be further improved by updating the internal algorithm of DNN inverse model and the forward model.

5.5.2 The similarity of the 869 Jogan tsunami in flow characteristics with the 2011 Tohoku-oki tsunami

The historical documents and field investigations by different researchers at Sendai Plain have suggested that the distribution, sedimentary features, geochemical signature, the maximum inland extent of deposits of the 869 tsunami are comparable with those of the 2011 Tohoku-oki tsunami (Shishikura et al., 2011; Goto et al., 2011; Chagué-Goff et al., 2012; Sugawara et al., 2013; Namegaya and Satake, 2014). However, there have only a few attempts to compare flow characteristics of both events based on tsunami deposits.

The results estimated by DNN inverse model is shown in Table 6 that shows that the flow velocity, maximum flow depth values of the 869 deposits are very close to the 2011 Tohoku-oki tsunami. The DNN inverse model estimate of Jogan tsunami deposits for flow velocity was approximately 5.3 m/s, whereas the the flow velocity for the 2011 Tohoku-oki tsunami was estimated around 5.4 m/s. Similarly, the maximum flow depth of the 2011 Tohoku-oki tsunami and the 869 Jogan deposits were 4.1 m and 5.6 m respectively. The maximum flow depth for the 869 Jogan event was calculated from the paleo-shoreline, considering that the DNN prediction was done from the seaward end of the calculation domain which was 1,713 m, which was measured from the paleo-shoreline. Thus, the result suggests that both events were of similar magnitude.

The grain-size distributions of tsunami deposits at Sendai Plain are quite different between two events (Figure 43), while the reconstructed flow characteristics of both events were almost similar. Tsunami deposits of the 869 event tend to be well sorted and fraction of grain-size classes finer than 2.0 phi, is scarce. In contrast, the grain-size distribution of the 2011 Tohoku-oki tsunami deposits show wider and positively skewed distribution.

Table 6: Estimation of flow velocity and maximum flow depth of the 2011 Tohoku-oki and the 869 Jogan tsunami, using DNN inverse model. Predicted values of the 869 Jogan tsunami are estimated approximately from the present shoreline.

Event name	Flow velocity	Maximum flow depth
869 Jogan tsunami (from the paleo- shoreline)	5.3 m/s	5.6 m
2011 Tohoku-oki tsunami	5.4 m/s	4.1 m

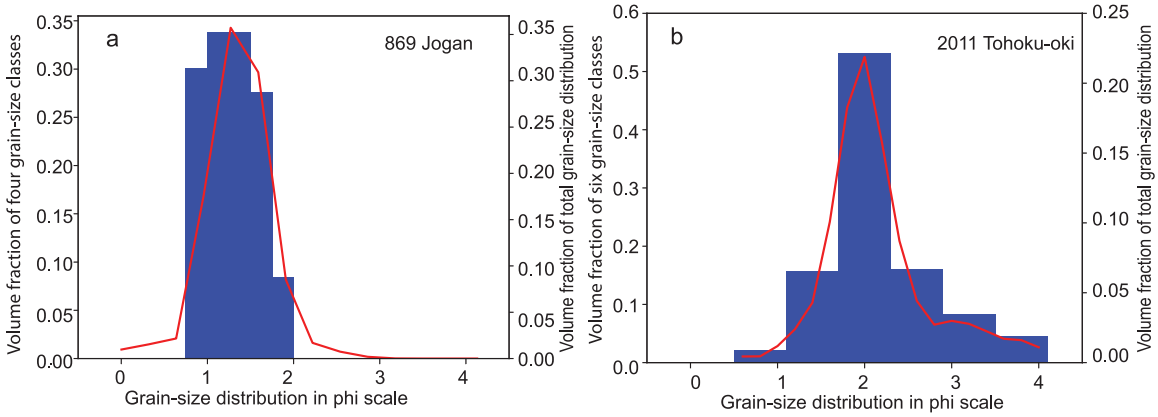

Figure 43: (a) Total grain-size distribution of the deposits of the 869 Jogan and the discretized fraction of the sediments in the four grain-size classes. (b) Total grain-size distribution of the deposits of the 2011 tohoku-oki tsunami in the Sendai Plain and the discretized fraction of the sediments in the six grain-size classes.

The deposit contains significant amounts of fine and very fine sands. This can be explained by difference in the sediment source areas. Although Goto et al. (2011) interpreted that the sediment sources of both events probably took place in the similar sedimentary environment and sedimentary processes, artificial structures or other obstacles can affect the depositional process in the case of the 2011 Tohoku-oki tsunami. Also, geomorphic settings of Sendai Plain in present should be different from those of 869 (Sugawara et al., 2012) because the presence of lagoon near the sampling location may have affected the tsunami flow condition at the depositional area. In addition, rice padding fields filled with mud were widely distributed in Sendai Plain at the 2011 event whereas the agricultural conditions of this region in 869 is uncertain. Hence, even though there is a possibility that the magnitude of both tsunamis can differ because of uncertainty of the inverse analysis, it is more likely that difference in the sediment sources resulted in variation of grain-size distribution of tsunami deposits. Further research is necessary to clarify this problem.

5.6 Conclusions

This chapter aims in reconstructing the tsunami characteristics such as flow velocity, maximum flow depth, sediment concentration from the 869 Jogan tsunami deposits and the results were compared with the DNN results of Sendai Plain. However, these are the preliminary result from the 869 Jogan tsunami deposits and first attempt to reconstruct the flow conditions from the ancient tsunami deposits using DNN inverse model. The predicted values for maximum inundation distance was 5,645 ± 287 m, flow velocity was 5.3 ± 1.5 m/s, maximum flow depth was 3.9 ± 1.0 m, for total sediment concentration was 3.6%. The results could be refined in the future improvements of the with DNN model and the forward model, which have potential to contribute more on the paleo-tsunami research.

Further investigations of the inundation area and depositional process of the Jogan tsunami may provide in-depth clarification about the tsunami characteristics of the 869 event. The number of available sampling locations were only 8 in this study. If more sampling locations are discovered in the same area, the accuracy and precision of the reconstruction must be improved largely.

6 Conclusions

The novel method of inverse model using deep neural network was proposed in this study as an efficient tool to estimate tsunami characteristics from their deposits with uncertainty analysis using jackknife method. The tsunami characteristics such as the maximum inundation distance, flow velocity, the maximum flow depth and sediment concentration are important for the mitigation strategies for tsunami disaster prevention at coastal areas. The estimated values of large-scale tsunamis in different regions, are the 2011 Tohoku-oki tsunami and the 2004 Indian Ocean tsunami, were compared with the in-situ observations. The results exhibited that the predicted values were significantly close with the reported values. Finally, the method was applied to the ancient deposit of the 869 Jogan tsunami. Although this analysis is in the preliminary stage, the reconstruction implied that 869 Jogan tsunami was almost the same scale as the 2011 Tohoku-oki tsunami, confirming the hypothesis that earthquakes of the similar magnitude are repeated every 1000 years in the subduction zone of the Japan Trench. Judging from the fact that reasonable reconstructions were obtained in various areas, the newly developed method in this study can be expected to be widely used for deposits of tsunamis that inundated a wide and gently sloping coastal plain.

6.1 Chapter summaries

This thesis proposed the DNN inversion method for tsunami deposits in Chapter 2. In this method, FITTNUSS forward model calculations were repeated for random initial flow conditions (e.g., maximum inundation distance, flow velocity, maximum flow depth and sediment concentration) to produce artificial training data sets of depositional characteristics, such as thickness and grain-size distribution. The DNN was then trained to establish a general inverse model based on artificial data sets derived from the forward model. Tests using independent artificial data sets indicated that the trained DNN can reconstruct the original flow conditions from the characteristics of deposits. Finally, the model was applied to a data set of the 2011 Tohoku-oki tsunami deposits. The predicted results of flow conditions were verified by the observational records at Sendai Plain. Jackknife resampling was applied to estimate the precision of the result. The estimated results of the flow velocity and maximum flow depth were approximately 5.4 ± 0.1 m/s and 4.1 ± 0.2 m, respectively, after the uncertainty analysis. The DNN showed promise for reconstruction of tsunami

characteristics from its deposits, which would help in estimating the hydraulic conditions of paleotsunamis.

In Chapter 3, a case study on the Phra Thong Island (Ko-Phra Thong) in Thailand, which was affected by the 2004 Indian Ocean tsunami, was conducted using DNN inverse modeling. The DNN inverse analysis reconstructed the values of flow conditions, such as maximum inundation distance, flow velocity and maximum flow depth, sediment concentration of five grain-size classes using the thickness and grain-size distribution of the tsunami deposit from the post-tsunami survey around Phra Thong Island. The quantification of uncertainty was also reported using the jackknife method. The predicted flow conditions were compared with the reported values of observations as well as results of another type of the inversion. The qualitative and quantitative comparisons demonstrated that the DNN inverse model is capable of estimating the physical characteristics of the large-scale tsunami in Thailand as well.

In Chapter 4, another region Odaka in Joban Coast, Fukushima, where the 2011 Tohoku-oki tsunami affected severely, was considered. In this study, the flow characteristics of tsunami were reconstructed from deposits using the DNN inverse model, suggesting that the tsunami inundation occurred in the Froude-supercritical condition. Despite having a few topographical instabilities that caused the flow height fluctuation to a great extent, the re-constructed maximum flow depth and flow velocity were reasonable and close to the values reported in the field observations. The reconstruction around the Odaka region was characterized by very high velocity (12.1 m/s). This study suggests that the large fluctuation of flow depths at Joban Coast comparing with stable flow depths at Sendai Plain can be explained by the inundation in supercritical flow condition. This thesis contributes a new dimension towards the hybrid approach of numerical modeling in tsunami deposit research and provide in-depth understanding of tsunami flow characteristics and flow regime for any large-scale tsunamis at any region consisting of flat coastal plains.

In Chapter 5, the 869 Jogan tsunami deposits from the Sendai Plain was considered and a preliminary results of tsunami characteristics were obtained using the DNN inverse model. It was the first attempt to reconstruct flow conditions from the ancient tsunami deposits using the inverse model. The DNN inverse model predicted the values of the maximum inundation distance, flow velocity, flow depth and the sediment concentration and the values were compared with the the results using the existing numerical models on the 869 Jogan

deposits. The comparision showed that the reconstructed values by the DNN inverse model is within the range of other reported values by different models. The reconstructed values by DNN inverse model were also comapared with the DNN predicted values of the 2011 Tohoku-oki tsunami at Sendai Plain to find the similarities of the magintude and size for the correlation of the events. However, the present results could be improved more in the future research by updating the DNN inverse model and this study can contribute to the tsunami hazard mitigation around Sendai Plain and advanced paleo-tsunami research.

6.2 Future Research Directions

The following three directions can be considered for the future research on DNN inverse modeling of tsunami deposits.

First, the internal algorithm of DNN can be improved in the future studies to obtain more accurate results without any additional bias generated during training of the model. For example, the application of convolutional neural networks to data containing multiple particle size classes may greatly improve the inverse analysis results. Also, when applying inverse analysis to actual deposits, it is necessary to convert the discontinuous data obtained in the field into continuous data by an interpolation method. Selection of the interpolation methods can improve to reduce the bias and precision which are caused by effect of irregularities in the sampling locations.

Second, the FITTNUSS forward model can be upgraded to fully hydrodynamic 1D or 2D forward model that deals with multiple grain-size classes. The inverse framework presented in this thesis permits free choice of the forward model. The role of the forward model is to provide training data to the neural network, and the generation of the data is not sequential, but can be fully parallelized. Thus, DNN inversions can potentially employ forward models that are more computationally demanding than in the past methodologies. At present, the forward model based on 1D and quasi-steady assumption is used in this study, and its application is limited to the flat coastal plain. However, if the forward model is developed to 2D hydrodynamic model, the DNN inversion method will be able to deal with complex topography, such as estuaries.

Finally, as this DNN inverse model has reasonable potential to predict the tsunami characteristics from the ancient deposits, the similar framework could be also used for the mitigation strategies of other coastal hazards such as flood or storms. Huge tsunamis and floods

that recur on geological time scales have similar impacts. This applicability of the model could be diversified to flood or storm deposits at different places if a suitable forward model is employed to produce depositional characteristics of tempestites or flood deposits.

Acknowledgments

I would like to express my heartfelt gratitude to my supervisor, Dr. Hajime Naruse, Kyoto University, Department of Earth and Planetary Sciences, for his continuous support and encouragement of my Ph.D. study. His patience, positivity, motivation, enthusiasm, and immense knowledge highly motivated me during the research and writing of this thesis.

I would like to express my deep sense of gratitude to Prof. Takao Ubukata for his enormous support, insightful comments and guidance throughout my my Ph.D. studies.

I would like to thank my collaborators Dr. Tomoya Abe, researcher in AIST, Japan, Dr. Shigehiro Fujino, University of Tsukuba, Dr. Daisuke Sugawara, Tohoku University, for their contibution towards the data set and grain-size analysis of tsunami deposits and my lab-mate Dr. Kazuki Kikuchi, post-doctoral fellow of Kyoto University, for performing the grain-size analysis of the sediments from the tsunami deposits at Odaka region. I would like to thank my labmates and all members of the Biosphere study group, especially Zhirong Cai, Haruna Furui and Koji Ohata for their continuous support throughout my Ph.D. studies.

I am thankful to the Sediment Dynamics Research Consortium (sponsored by INPEX, JOGMEC, JX Nippon Oil and Gas Exploration Corporation, JAPEX), Department of Geology and Mineralogy, Kyoto University, Japan and the Ministry of Education, Culture, Sports, Science and Technology, Japan, for providing the permission and scholarship for conducting this collaborative research in Japan.

Finally, I am grateful to my parents, loving sister and my husband Avishek Rudra, for their moral support, encouragement and inspiration to complete my Ph.D. studies.

7 Notations

The symbols L, M and T denote dimensions of length, mass and time respectively. The symbol [1] denotes that the value is dimensionless.

C : Total layer-averaged sediment concentration [1]
C_i : Layer-averaged sediment concentration of the ith grain-size class [1]
C_f : Bed friction coefficient [1]
E_{si} : Sediment entrainment coefficient [1]
F_i : Volumetric fraction of the ith grain-size class in the active layer [1]
H : Maximum flow depth of the tsunami at the seaward (upstream) boundary of the transect [L]
L_a : Thickness of the active layer [L]
R_w : maximum inundation distance [L]
S : Bed slope [1]
U : Run-up velocity of the tsunami [LT^{-1}]
g : Acceleration of gravity [LT^{-2}]
h : Flow depth of the tsunami [L]
r_{0i} : Ratio of near-bed sediment concentration of the ith grain-size class to layer-averaged concentration [1]
t : Time [T]
u_* : Friction velocity [LT^{-1}]
w_{si} : Settling velocity of sediment of the ith grain-size class [LT^{-1}]
x : Bed-attached streamwise coordinate [L]
η_i : Volume per unit area of sediment of the ith grain-size class [L]
λ_p : Porosity of the tsunami deposit [1]
μ : Dimensionless settling velocity of sediment of the ith grain-size class [LT^{-1}]
τ_{*m} : Shields dimensionless shear stress using the mean grain-size in the active layer [1]
ψ_i : Coefficient in the relation of turbulent suppression due to density stratification [1]
X_{norm} : Normalized values of input data [1]
X_{raw} : Original values of the input data respectively [1]
$\min(X_{raw})$: Minimum values of the raw input data [1]

$\max(X_{raw})$: Maximum values of the raw input data [1]

Y_{norm} : Normalized values of teaching data [1]

Y_{raw} : Original values of the teaching data respectively [1]

$\min(Y_{raw})$: Minimum values of raw teaching data [1]

I_k^{fm} Teaching data that are the initial parameters used for producing in the training data

I_k^{NN} : Predicted parameters using Neural networks

J : Loss function for the inverse model

8 Appendix

8.1 Uncertainty analysis of inversion results

The jackknife method was used for the error assessment of the results of the inverse model. This method estimates the standard error of the predicted value of the model using a resampled population. Quenouille (1949) first introduced this resampling method (Nisbet et al., 2009).

A jackknife test is similar to the bootstrap method, but instead of a random sampling of a data set, the inversion model works on each separate set of samples by omitting a single set of observations per iterations from a total of N observations. Inversions were carried out N times and the resulting ensemble of solutions were interrogated to a single estimate for each parameter. In short, it involves a leave-one-out strategy in a data set of N observations and the model works on the rest of the samples and gives results accordingly. Preferably, $N-1$ observations were built on the data set as resampled data for the model. Farrell and Singh (2010) discussed the importance of the jackknife method in survey sampling.

I briefly describe the jackknife uncertainty analysis. Sample and jackknife estimates are denoted as S and S^*, respectively. The number of observations in the sample is N and the set of observations is denoted as $\{X_1, ..., X_n, ..., X_N\}$. The sample estimate of the parameter is a function of the observations in the sample (Abdi and Williams, 2010). The equation is given as follows:

$$S = f(X_1, ..., X_n, ..., X_N) \tag{11}$$

Let S_{-n} be the $n-$th partial prediction of the parameter, which is produced by the inverse model without the nth observation. The equation for the prediction S_{-n} is given as follows:

$$S_{-n} = f(X_1, ..., X_{n-1}, X_{n+1}..., X_N) \tag{12}$$

S_n^* represents a pseudo value estimation of the nth observation. This parameter is defined as the difference between the estimates S obtained from the entire sample and the estimates S_{-n} obtained without the nth observation as follows:

$$S_n^* = NS - (N-1)S_{-n} \tag{13}$$

The mean of the pseudo values are regarded as the jackknife estimate S^*. The equation for the jackknife estimate is given as follows:

$$S^* = S_{mean}^* = \frac{1}{N}\sum_{n}^{N} S_n^* \tag{14}$$

where S_{mean}^* is also the mean of the pseudo values. The variance of the pseudo values is denoted as σ_{JK}^{var} and the formula for the variance is given as follows:

$$\sigma_{JK}^{var} = \frac{\sum(S_n^* - S_{mean}^*)^2}{N-1} \tag{15}$$

Finally, the jackknife standard error of the parameter estimate is denoted as σ_{JK}^{SE}, The formula for the jackknife standard error is

$$\sigma_{JK}^{SE} = \sqrt{\frac{\sigma_{JK}^{var}}{N}} = \sqrt{\frac{\sum(S_n^* - S_{mean}^*)^2}{N(N-1)}} \tag{16}$$

The confidence interval for this study has been computed using this jackknife standard error formula.

8.2 Supplementary material for chapter 4 and chapter 5

In chapter 4 and 5, after training the model, the deviation of the predicted values from the original values were plotted on a histogram to check the model performance. There was no large bias except the maximum flow depth, which showed that the predicted values for this parameter were approximately 0.4 m lower than the input values (Figure 44) and in chapter 4, and the value of the parameter was approximately 0.6 m lower than the input values in chapter 5 (Figure 45).

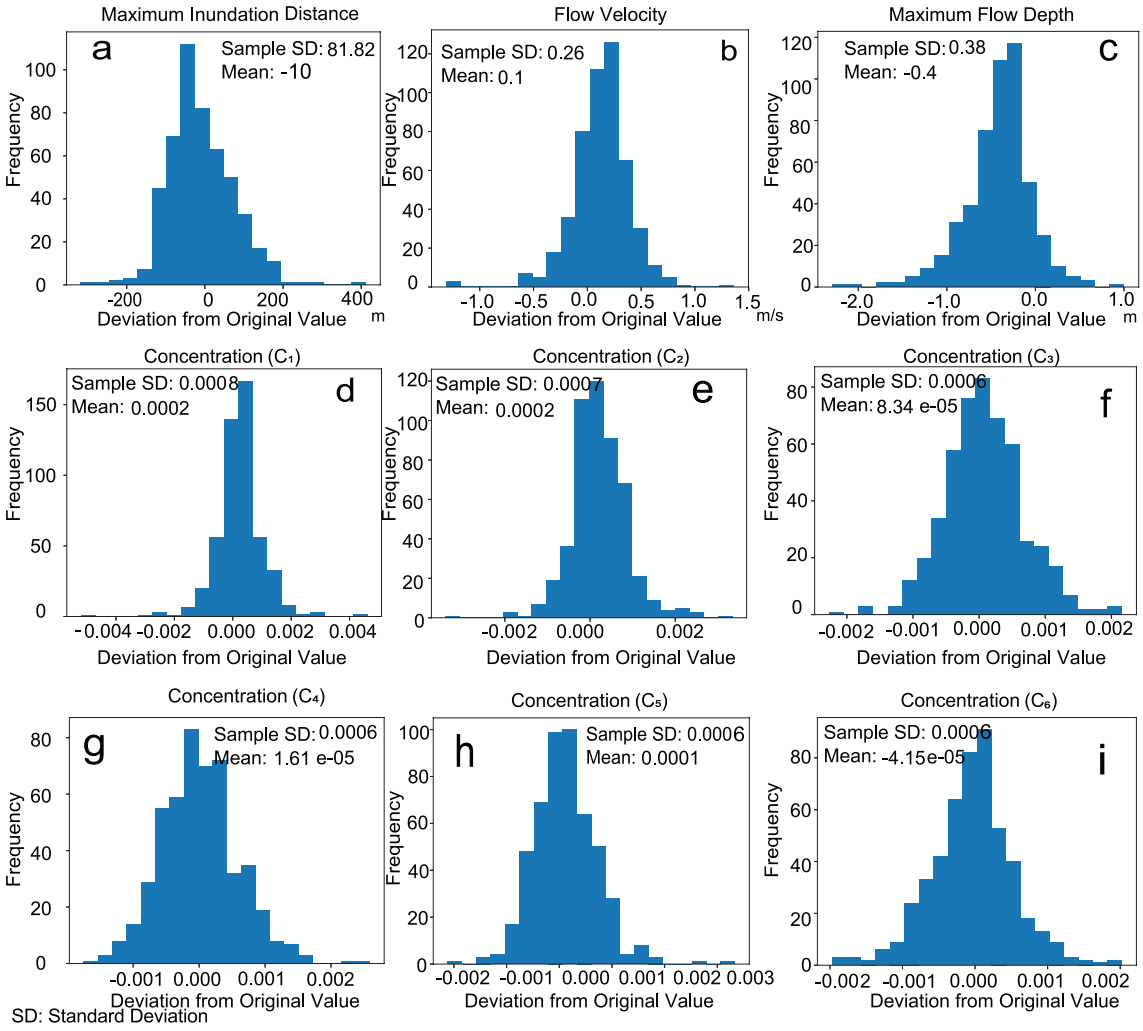

Figure 44: Histograms showing the deviation of the predicted results from the original values of the artificial test data sets. (a) Maximum inundation distance, (b) Flow velocity (c) Maximum flow depth, (d)–(i) Concentration of six grain-size classes.

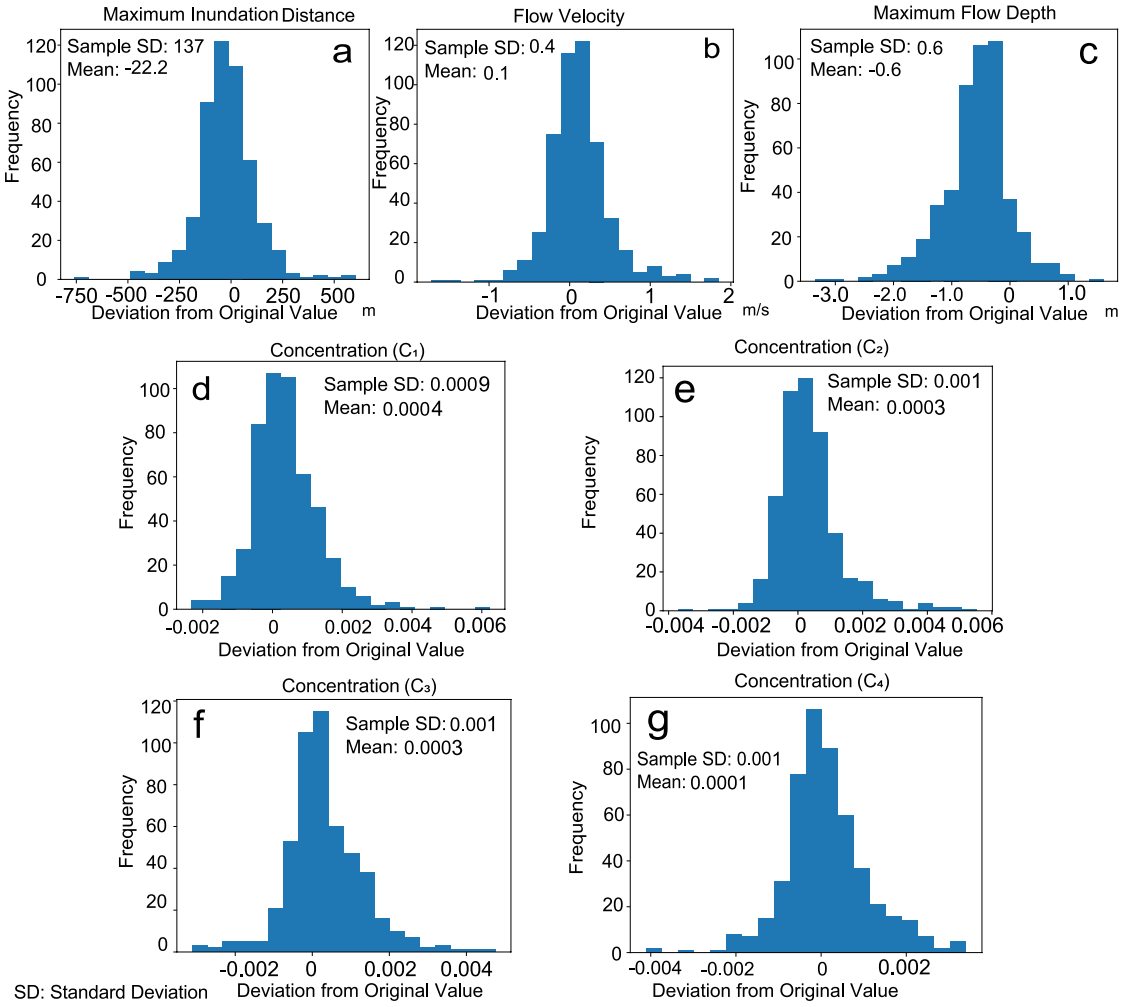

Figure 45: Histograms showing the deviation of the predicted results from the original values of the artificial test data sets. (a) Maximum inundation distance, (b) Flow velocity, (c) Maximum flow depth, (d)–(g) Concentrations of the four grain-size classes.

References

Abdi, H. and Williams, L. J.: Jackknife, Encyclopedia of research design, 2, 2010.

Abe, H.: Estimation of the height of the Sanriku Jogan 11 earthquake-tsunami (AD 869) in the Sendai Plain, Zisin (Journal of Seismological Society of Japan), 43, 513–525, 1990.

Abe, T., Goto, K., and Sugawara, D.: Relationship between the maximum extent of tsunami sand and the inundation limit of the 2011 Tohoku-oki tsunami on the Sendai Plain, Japan, Sedimentary Geology, 282, 142–150, 2012.

Abe, T., Goto, K., and Sugawara, D.: Spatial distribution and sources of tsunami deposits in a narrow valley setting-insight from 2011 Tohoku-oki tsunami deposits in northeastern Japan, Progress in Earth and Planetary Science, 7, 1–21, 2020.

Ali Hasan Muhammad, R. and Tanaka, N.: Energy reduction of a tsunami current through a hybrid defense system comprising a sea embankment followed by a coastal forest, Geosciences, 9, 247, 2019.

Andrade, V., Rajendran, K., and Rajendran, C.: Sheltered coastal environments as archives of paleo-tsunami deposits: Observations from the 2004 Indian Ocean tsunami, J Asian Earth Sci, 95, 331–341, 2014.

Apotsos, A., Buckley, M., Gelfenbaum, G., Jaffe, B., and Vatvani, D.: Nearshore tsunami inundation model validation: toward sediment transport applications, Pure and applied geophysics, 168, 2097–2119, 2011.

Arai, K., Naruse, H., Miura, R., Kawamura, K., Hino, R., Ito, Y., Inazu, D., Yokokawa, M., Izumi, N., Murayama, M., et al.: Tsunami-generated turbidity current of the 2011 Tohoku-Oki earthquake, Geology, 41, 1195–1198, 2013.

Atwater, B. F.: Evidence for great Holocene earthquakes along the outer coast of Washington State, Science, 236, 942–944, 1987.

Bishop, C. M.: Neural networks for pattern recognition, Oxford university press, 1995.

Board, O. S., Council, N. R., et al.: Tsunami warning and preparedness: an assessment of the us tsunami program and the nation's preparedness efforts, National Academies Press, 2011.

Bourgeois, J., Bernard, E., and Robinson, A.: Geologic effects and records of tsunamis, The Sea, 15, 53–91, 2009.

Bourke, P.: Interpolation methods, URL http://paulbourke.net/miscellaneous/interpolation/, 1999.

Braaten, D., Shaw, R., et al.: Particle resuspension in a turbulent boundary layer-observed and modeled, Journal of Aerosol Science, 21, 613–628, 1990.

Brill, D.: The Tsunami History of Southwest Thailand: Recurrence, Magnitude and Impact of Palaeo-tsunamis Inferred from Onshore Deposits, Ph.D. thesis, Universitäts-und Stadtbibliothek Köln, 2012.

Brill, D., Klasen, N., Brückner, H., Jankaew, K., Scheffers, A., Kelletat, D., and Scheffers, S.: OSL dating of tsunami deposits from Phra Thong Island, Thailand, Quat Geochronol, 10, 224–229, 2012a.

Brill, D., Klasen, N., Jankaew, K., Brückner, H., Kelletat, D., Scheffers, A., and Scheffers, S.: Local inundation distances and regional tsunami recurrence in the Indian Ocean inferred from luminescence dating of sandy deposits in Thailand, Nat. Hazards Earth Syst. Sci., 12, 2177–2192, 2012b.

Brill, D., Pint, A., Jankaew, K., Frenzel, P., Schwarzer, K., Vött, A., and Brückner, H.: Sediment transport and hydrodynamic parameters of tsunami waves recorded in onshore geoarchives, J. Coastal Res., 30, 922–941, 2014.

Brune, S., Ladage, S., Babeyko, A. Y., Müller, C., Kopp, H., and Sobolev, S. V.: Submarine landslides at the eastern Sunda margin: observations and tsunami impact assessment, Natural Hazards, 54, 547–562, 2010.

Chagué-Goff, C., Andrew, A., Szczuciński, W., Goff, J., and Nishimura, Y.: Geochemical signatures up to the maximum inundation of the 2011 Tohoku-oki tsunami—implications

for the 869 AD Jogan and other palaeotsunamis, Sedimentary Geology, 282, 65–77, 2012.

Charvet, I., Macabuag, J., and Rossetto, T.: Estimating tsunami-induced building damage through fragility functions: critical review and research needs, Frontiers in built environment, 3, 36, 2017.

Choi, B. H., Hong, S. J., and Pelinovsky, E.: Distribution of runup heights of the December 26, 2004 tsunami in the Indian Ocean, Geophysical Research Letters, 33, 2006.

Choowong, M., Murakoshi, N., Hisada, K., Charoentitirat, T., Charusiri, P., Phantuwongraj, S., Wongkok, P., Choowong, A., Subsayjun, R., Chutakositkanon, V., , Jankaew, K., and Kanjanapayont, P.: Flow conditions of the 2004 Indian Ocean tsunami in Thailand, inferred from capping bedforms and sedimentary structures, Terra Nova, 20, 141–149, 2008a.

Choowong, M., Murakoshi, N., Hisada, K.-i., Charusiri, P., Charoentitirat, T., Chutakositkanon, V., Jankaew, K., Kanjanapayont, P., and Phantuwongraj, S.: 2004 Indian Ocean tsunami inflow and outflow at Phuket, Thailand, Marine Geology, 248, 179–192, 2008b.

Costa, P. J., Andrade, C., Freitas, M. C., Oliveira, M. A., da Silva, C. M., Omira, R., Taborda, R., Baptista, M. A., and Dawson, A. G.: Boulder deposition during major tsunami events, Earth Surface Processes and Landforms, 36, 2054–2068, 2011.

Costa, P. J., Andrade, C., Cascalho, J., Dawson, A. G., Freitas, M. C., Paris, R., and Dawson, S.: Onshore tsunami sediment transport mechanisms inferred from heavy mineral assemblages, The Holocene, 25, 795–809, 2015.

Crank, J.: Free and moving boundary problems, Clarendon press Oxford, 1984.

Dawson, A.: Geomorphological effects of tsunami run-up and backwash, in: Geomorphology and natural hazards, pp. 83–94, Elsevier, 1994.

Dawson, A. G.: Linking tsunami deposits, submarine slides and offshore earthquakes, Quaternary International, 60, 119–126, 1999.

Dawson, A. G. and Shi, S.: Tsunami deposits, Pure Appl. Geophys., 157, 875–897, 2000.

Dawson, A. G., Long, D., and Smith, D.: The Storegga slides: evidence from eastern Scotland for a possible tsunami, Marine geology, 82, 271–276, 1988.

Dietrich, W. E.: Settling velocity of natural particles, Water Resources Research, 18, 1615–1626, 1982.

Eaton, J. P., Richter, D. H., and Ault, W. U.: The tsunami of May 23, 1960, on the Island of Hawaii, Bulletin of the Seismological Society of America, 51, 135–157, 1961.

Farrell, P. J. and Singh, S.: Some contributions to jackknifing two-phase sampling estimators, Survey Methodology, 36, 57–68, 2010.

Foytong, P., Ruangrassamee, A., Shoji, G., Hiraki, Y., and Ezura, Y.: Analysis of tsunami flow velocities during the March 2011 Tohoku, Japan, tsunami, Earthquake Spectra, 29, 161–181, 2013.

Francis, P.: The origin of the 1883 Krakatau tsunamis, Journal of volcanology and geothermal research, 25, 349–363, 1985.

Fritz, H. M., Borrero, J. C., Synolakis, C. E., and Yoo, J.: 2004 Indian Ocean tsunami flow velocity measurements from survivor videos, Geophysical Research Letters, 33, 2006.

Fritz, H. M., Petroff, C. M., Catalán, P. A., Cienfuegos, R., Winckler, P., Kalligeris, N., Weiss, R., Barrientos, S. E., Meneses, G., Valderas-Bermejo, C., et al.: Field survey of the 27 February 2010 Chile tsunami, Pure and Applied Geophysics, 168, 1989–2010, 2011.

Fujino, S., Naruse, H., Suphawajruksakul, A., Jarupongsakul, T., Murayama, M., and Ichihara, T.: Thickness and grain-size distribution of Indian Ocean tsunami deposits at Khao Lak and Phra Thong Island, south-western Thailand, in: Tsunamiites, edited by Shiki, T., Tsuji, Y., T, Y., and K, M., pp. 123–132, Elsevier, 2008.

Fujino, S., Naruse, H., Matsumoto, D., Jarupongsakul, T., Sphawajruksakul, A., and Sakakura, N.: Stratigraphic evidence for pre-2004 tsunamis in southwestern Thailand, Marine Geology, 262, 25–28, 2009.

Fujino, S., Naruse, H., Matsumoto, D., Sakakura, N., Suphawajruksakul, A., and Jarupongsakul, T.: Detailed measurements of thickness and grain size of a widespread onshore tsunami deposit in Phang-nga Province, southwestern Thailand, Isl. Arc, 19, 389–398, 2010.

Fujiwara, O. and Kamataki, T.: Identification of tsunami deposits considering the tsunami waveform: an example of subaqueous tsunami deposits in Holocene shallow bay on southern Boso Peninsula, Central Japan, Sedimentary Geology, 200, 295–313, 2007.

Furusato, E. and Tanaka, N.: Maximum sand sedimentation distance after backwash current of tsunami—Simple inverse model and laboratory experiments, Marine Geology, 353, 128–139, 2014.

Gelfenbaum, G., Vatvani, D., Jaffe, B., and Dekker, F.: Tsunami inundation and sediment transport in vicinity of coastal mangrove forest, in: Coastal Sediments' 07, pp. 1117–1128, 2007.

Ghobarah, A., Saatcioglu, M., and Nistor, I.: The impact of the 26 December 2004 earthquake and tsunami on structures and infrastructure, Engineering Structures, 28, 312–326, 2006.

Gianfreda, F., Mastronuzzi, G., and Sansò, P.: Impact of historical tsunamis on a sandy coastal barrier: an example from the northern Gargano coast, southern Italy, Natural Hazards and Earth System Sciences, 1, 213–219, 2001.

Goto, K., Imamura, F., Keerthi, N., Kunthasap, P., Matsui, T., Minoura, K., Ruangrassamee, A., Sugawara, D., and Supharatid, S.: Distribution and significance of the 2004 Indian Ocean tsunami deposits: initial results from Thailand and Sri Lanka, in: Tsunamiites, pp. 127–144, Elsevier, 2008.

Goto, K., Chagué-Goff, C., Fujino, S., Goff, J., Jaffe, B., Nishimura, Y., Richmond, B., Sugawara, D., Szczuciński, W., Tappin, D. R., et al.: New insights of tsunami hazard from the 2011 Tohoku-oki event, Marine Geology, 290, 46–50, 2011.

Goto, K., Chagué-Goff, C., Goff, J., and Jaffe, B.: The future of tsunami research following the 2011 Tohoku-oki event, Sedimentary Geology, 282, 1–13, 2012.

Goto, K., Hashimoto, K., Sugawara, D., Yanagisawa, H., and Abe, T.: Spatial thickness variability of the 2011 Tohoku-oki tsunami deposits along the coastline of Sendai Bay, Marine Geology, 358, 38–48, 2014.

Gouramanis, C., Switzer, A. D., Jankaew, K., Bristow, C. S., Pham, D. T., and Ildefonso, S. R.: High-frequency coastal overwash deposits from Phra Thong Island, Thailand, Sci. Rep., 7, 43 742, 2017.

Hayashi, S. and Koshimura, S.: The 2011 Tohoku tsunami flow velocity estimation by the aerial video analysis and numerical modeling, Journal of Disaster Research, 8, 561–572, 2013.

Hirano, M.: River bed degradation with armoring, Proceedings of Japan Society of Civil Engineers, 1971, 55–65, 1971.

Hirt, C. and Nichols, B.: Flow-3D User's manual, Flow Science Inc, 107, 1988.

Hoang, V. C., Tanaka, H., and Mitobe, Y.: Post-Tsunami Lagoon Morphology Restoration Sendai; Japan, in: Tsunamis and Earthquakes in Coastal Environments, pp. 153–166, Springer, 2016.

Ian, G. and Yoshua, B.: Deep learning (adaptive computation and machine learning), 2016.

Ikehara, K., Irino, T., Usami, K., Jenkins, R., Omura, A., and Ashi, J.: Possible submarine tsunami deposits on the outer shelf of Sendai Bay, Japan resulting from the 2011 earthquake and tsunami off the Pacific coast of Tohoku, Marine Geology, 358, 120–127, 2014.

Imamura, F., Boret, S. P., Suppasri, A., and Muhari, A.: Recent occurrences of serious tsunami damage and the future challenges of tsunami disaster risk reduction, Progress in Disaster Science, 1, 100 009, 2019a.

Imamura, F., Boret, S. P., Suppasri, A., and Muhari, A.: Recent occurrences of serious tsunami damage and the future challenges of tsunami disaster risk reduction, Progress in Disaster Science, 1, 100 009, 2019b.

Inoue, T., Goto, K., Nishimura, Y., Watanabe, M., Iijima, Y., and Sugawara, D.: Paleo-tsunami history along the northern Japan Trench: evidence from Noda Village, northern Sanriku coast, Japan, Progress in Earth and Planetary Science, 4, 1–15, 2017.

Ishimura, D. and Yamada, K.: Palaeo-tsunami inundation distances deduced from roundness of gravel particles in tsunami deposits, Scientific reports, 9, 1–8, 2019.

Ito, A.: Marine regression during the historical time in Sendai Coastal Plain, Northeastern Japan, Bulletin of the Faculty of Education, Kagoshima University, Studies in Education, 57, 1–8, 2006.

Jaffe, B., Goto, K., Sugawara, D., Richmond, B., Fujino, S., and Nishimura, Y.: Flow speed estimated by inverse modeling of sandy tsunami deposits: results from the 11 March 2011 tsunami on the coastal plain near the Sendai airport, Honshu, Japan, Sedimentary Geology, 282, 90–109, 2012.

Jaffe, B., Goto, K., Sugawara, D., Gelfenbaum, G., and La Selle, S.: Uncertainty in tsunami sediment transport modeling, Journal of Disaster Research, 11, 647–661, 2016.

Jaffe, B. E. and Gelfenbaum, G.: Using tsunami deposits to improve assessment of tsunami risk, in: Solutions to Coastal Disasters' 02, pp. 836–847, 2002.

Jaffe, B. E. and Gelfenbuam, G.: A simple model for calculating tsunami flow speed from tsunami deposits, Sedimentary Geology, 200, 347–361, 2007.

Jankaew, K., Atwater, B. F., Sawai, Y., Choowong, M., Charoentitirat, T., Martin, M. E., and Prendergast, A.: Medieval forewarning of the 2004 Indian Ocean tsunami in Thailand, Nature, 455, 1228–1231, 2008.

Jankaew, K., Martin, M. E., Sawai, Y., and Prendergast, A. L.: Sand sheets on a beach-ridge plain in Thailand: identification and dating of tsunami deposits in a far-field tropical setting, The Tsunami Threat–Research and Technology, edited by: Mörner, NA, pp. 299–324, 2011.

Jayasuriya, S. and McCawley, P.: Reconstruction after a major disaster: lessons from the post-tsunami experience in Indonesia, Sri Lanka, and Thailand, Tech. rep., ADBI Working Paper, 2008.

Jayasuriya, S. K. and McCawley, P.: The Asian tsunami: aid and reconstruction after a disaster, Edward Elgar Publishing, 2010.

Johnson, J. P., Delbecq, K., Kim, W., and Mohrig, D.: Experimental tsunami deposits: Linking hydrodynamics to sediment entrainment, advection lengths and downstream fining, Geomorphology, 253, 478–490, 2016.

Jordan, M. I. and Rumelhart, D. E.: Forward models: Supervised learning with a distal teacher, Cognitive Science, 16, 307–354, 1992.

Karlsson, M, J., Skelton, A., Sanden, M., Ioualalen, M., Kaewbanjak, N., Pophet, N., Asavanant, J., and von Matern, A.: Reconstructions of the coastal impact of the 2004 Indian Ocean tsunami in the Khao Lak area, Thailand, Journal of Geophysical Research: Oceans, 114, 2009.

Kennedy, J. F.: The mechanics of dunes and antidunes in erodible-bed channels, Journal of Fluid mechanics, 16, 521–544, 1963.

Kihara, N. and Matsuyama, M.: Numerical simulations of sediment transport induced by the 2004 Indian Ocean tsunami near Kirinda port in Sri Lanka, in: Proceedings of 32th International Conference on Coastal Engineering, 2010.

Koff, G., Borsukova, O., Popova, O., and Sidorin, A. Y.: On the causes of the great damage from the tsunami of March 11, 2011 on the northeast coast of Honshu Island, Seismic Instruments, 48, 105–123, 2012.

Koiwa, N., Takahashi, M., Sugisawa, S., Ito, A., Matsumoto, H., Tanavud, C., and Goto, K.: Barrier spit recovery following the 2004 Indian Ocean tsunami at Pakarang Cape, southwest Thailand, Geomorphology, 306, 314–324, 2018.

Konno, E.: Geological observations of the Sanriku coastal region damaged by tsunami due to the Chile earthquake in 1960, Contributions to the Institute of Geology and Paleontology, Tohoku University, 52, 1–40, 1961.

Kusumoto, S., Imai, K., Gusman, A. R., and Satake, K.: Reduction effect of tsunami sediment transport by a coastal forest: Numerical simulation of the 2011 Tohoku tsunami on the Sendai Plain, Japan, Sedimentary Geology, 407, 105 740, 2020.

Lacy, J. R., Rubin, D. M., and Buscombe, D.: Currents, drag, and sediment transport induced by a tsunami, Journal of Geophysical Research: Oceans, 117, 2012.

Larsen, B. E. and Fuhrman, D. R.: Full-scale CFD simulation of tsunamis. Part 2: Boundary layers and bed shear stresses, Coastal engineering, 151, 42–57, 2019.

Le, T. A., Baydin, A. G., Zinkov, R., and Wood, F.: Using synthetic data to train neural networks is model-based reasoning, in: 2017 International Joint Conference on Neural Networks (IJCNN), pp. 3514–3521, IEEE, 2017.

Li, L., Qiu, Q., and Huang, Z.: Numerical modeling of the morphological change in Lhok Nga, west Banda Aceh, during the 2004 Indian Ocean tsunami: understanding tsunami deposits using a forward modeling method, Natural Hazards, 64, 1549–1574, 2012.

Lin, A., Ikuta, R., and Rao, G.: Tsunami run-up associated with co-seismic thrust slip produced by the 2011 Mw 9.0 Off Pacific Coast of Tohoku earthquake, Japan, Earth Planetary Science Letters, 337, 121–132, 2012.

Maemunah, I., Suparka, E., Puspito, N. T., and Hidayati, S.: Sedimentary deposits study of the 2006 Java tsunami, in Pangandaran, West Java (preliminary result), in: AIP Conference Proceedings, vol. 1658, p. 050005, AIP Publishing LLC, 2015.

Masaya, R., Suppasri, A., Yamashita, K., Imamura, F., Gouramanis, C., and Leelawat, N.: Investigating beach erosion related with its recovery at Phra Thong Island, Thailand caused by the 2004 Indian Ocean tsunami, Nat. Hazards Earth Syst. Sci. Discuss., pp. 1–22, 2019.

Massel, S. R.: Tsunami in coastal zone due to meteorite impact, Coastal engineering, 66, 40–49, 2012.

Matsutomi, H. and Okamoto, K.: Inundation flow velocity of tsunami on land, Island Arc, 19, 443–457, 2010.

Matsutomi, H., Shuto, N., Imamura, F., and Takahashi, T.: Field survey of the 1996 Irian Jaya earthquake tsunami in Biak Island, Natural Hazards, 24, 199–212, 2001.

Matsutomi, H., Sakakiyama, T., Tsuji, Y., Tanioka, Y., Nishimura, Y., Kamataki, T., Murakami, Y., Matsuyama, M., and Kurizuka, K.: Challenges from the perspective of the

2004 Indian Ocean tsunami and damage estimates in and around Banda Aceh, Coastal Engineering Treatises, 52, 1366–1370, 2005.

May, S. M., Vött, A., Brückner, H., and Smedile, A.: The Gyra washover fan in the Lefkada Lagoon, NW Greece—possible evidence of the 365 AD Crete earthquake and tsunami, Earth, planets and space, 64, 859–874, 2012.

McArthur, A., Kane, I., Bozetti, G., Hansen, L., and Kneller, B. C.: Supercritical flows overspilling from bypass-dominated submarine channels and the development of overbank bedforms, The Depositional Record, 6, 21–40, 2020.

McSaveney, M., Goff, J., Darby, D., Goldsmith, P., Barnett, A., Elliott, S., and Nongkas, M.: The 17 July 1998 tsunami, Papua New Guinea: evidence and initial interpretation, Marine Geology, 170, 81–92, 2000.

Middleton, G. V. and Hampton, M. A.: Part I. Sediment gravity flows: mechanics of flow and deposition, Turbidites and Deep-Water Sedimentation, 1973.

Mimura, N., Yasuhara, K., Kawagoe, S., Yokoki, H., and Kazama, S.: Damage from the Great East Japan Earthquake and Tsunami-a quick report, Mitigation and adaptation strategies for global change, 16, 803–818, 2011.

Minoura, K.: Trances of tsunamis recorded in lake deposits-An example from Jusan, Shiura-mura, Aomori, Journal of Seismological Society of Japan, 40, 183–196, 1987.

Minoura, K. and Nakaya, S.: Traces of tsunami preserved in inter-tidal lacustrine and marsh deposits: some examples from northeast Japan, The Journal of Geology, 99, 265–287, 1991.

Minoura, K., Imamura, F., Sugawara, D., Kono, Y., and Iwashita, T.: The 869 Jogan tsunami deposit and recurrence interval of large-scale tsunami on the Pacific coast of northeast Japan, Journal of Natural Disaster Science, 23, 83–88, 2001.

Mitra, R., Naruse, H., and Abe, T.: Estimation of Tsunami Characteristics from Deposits: Inverse Modeling using a Deep-Learning Neural Network, Journal of Geophysical Research: Earth Surface, 125, e2020JF005 583, https://doi.org/10.1029/2020JF005583, 2020.

Mitra, R., Naruse, H., and Fujino, S.: Reconstruction of flow conditions from 2004 Indian Ocean tsunami deposits at the Phra Thong island using a deep neural network inverse model, Natural Hazards and Earth System Sciences, 21, 1667–1683, https://doi.org/10.5194/nhess-21-1667-2021, 2021.

Moore, A., McAdoo, B. G., and Ruffman, A.: Landward fining from multiple sources in a sand sheet deposited by the 1929 Grand Banks tsunami, Newfoundland, Sedimentary Geology, 200, 336–346, 2007.

Moore, A., Goff, J., McAdoo, B. G., Fritz, H. M., Gusman, A., Kalligeris, N., Kalsum, K., Susanto, A., Suteja, D., and Synolakis, C. E.: Sedimentary deposits from the 17 July 2006 Western Java Tsunami, Indonesia: use of grain size analyses to assess tsunami flow depth, speed, and traction carpet characteristics, Pure and Applied Geophysics, 168, 1951–1961, 2011.

Moore, A. L.: Landward fining in onshore gravel as evidence for a late Pleistocene tsunami on Molokai, Hawaii, Geology, 28, 247–250, 2000.

Moreira, S., Costa, P. J., Andrade, C., Lira, C. P., Freitas, M. C., Oliveira, M. A., and Reichart, G.-J.: High resolution geochemical and grain-size analysis of the AD 1755 tsunami deposit: Insights into the inland extent and inundation phases, Marine Geology, 390, 94–105, 2017.

Mori, N. and Takahashi, T.: Nationwide post event survey and analysis of the 2011 Tohoku earthquake tsunami, Coastal Engineering Journal, 54, 1–27, 2012.

Mori, N., Takahashi, T., Yasuda, T., and Yanagisawa, H.: Survey of 2011 Tohoku earthquake tsunami inundation and run-up, Geophysical Research Letters, 38, https://doi.org/https://doi.org/10.1029/2011GL049210, 2011a.

Mori, N., Takahashi, T., Yasuda, T., and Yanagisawa, H.: Survey of 2011 Tohoku earthquake tsunami inundation and run-up, Geophysical research letters, 38, 2011b.

Morton, R. A., Gelfenbaum, G., and Jaffe, B. E.: Physical criteria for distinguishing sandy tsunami and storm deposits using modern examples, Sedimentary Geology, 200, 184–207, 2007.

Morton, R. A., Buckley, M. L., Gelfenbaum, G., Richmond, B. M., Cecioni, A., Artal, O., Hoffman, C., and Perez, F.: Geological impacts and sedimentary record of the February 27, 2010, Chile tsunami—La Trinchera to Concepcion, US Geological Survey Open-File Report, 1116, 28, 2010.

Muste, M. and Hoitink, T.: Measuring flood discharge, in: Oxford research encyclopedia of natural hazard science, 2017.

Mutaqin, B., Lavigne, F., Hadmoko, D., and Ngalawani, M.: Volcanic Eruption-Induced Tsunami in Indonesia: A Review, in: IOP Conference Series: Earth and Environmental Science, vol. 256, p. 012023, IOP Publishing, 2019.

Nakajima, H. and Koarai, M.: Assessment of tsunami flood situation from the Great East Japan Earthquake, Bull Geospatial Info Authority Japan, 59, 55–66, 2011.

Nakata, T. and Kawana, T.: Historical and prehistorical large tsunamis in the southern Ryukyus, Japan, in: Tsunami: progress in prediction, disaster prevention and warning, pp. 211–221, Springer, 1995.

Namegaya, Y.: Numerical simulation of the AD 869 Jogan tsunami in Ishinomaki and Sendai plains and Ukedo river-mouth lowland, Ann. Rep. Active Fault Paleoearthq. Res., 10, 71–89, 2010.

Namegaya, Y. and Satake, K.: Reexamination of the AD 869 Jogan earthquake size from tsunami deposit distribution, simulated flow depth, and velocity, Geophysical Research Letters, 41, 2297–2303, 2014.

Nanayama, F. and Shigeno, K.: Inflow and outflow facies from the 1993 tsunami in south-west Hokkaido, Sedimentary Geology, 187, 139–158, 2006.

Nandasena, N., Sasaki, Y., and Tanaka, N.: Modeling field observations of the 2011 Great East Japan tsunami: Efficacy of artificial and natural structures on tsunami mitigation, Coastal Engineering, 67, 1–13, 2012.

Naruse, H.: Usage and advantages of an application program “STube” for settling tube grain-size analysis, Journal of the Sedimentological Society of Japan, 62, 55–61, 2005.

Naruse, H. and Abe, T.: Inverse Tsunami Flow Modeling Including Nonequilibrium Sediment Transport, With Application to Deposits From the 2011 Tohoku-Oki Tsunami, Journal of Geophysical Research: Earth Surface, 122, 2159–2182, 2017.

Naruse, H., Arai, K., Matsumoto, D., Takahashi, H., Yamashita, S., Tanaka, G., and Murayama, M.: Sedimentary features observed in the tsunami deposits at Rikuzentakata City, Sedimentary Geology, 282, 199–215, https://doi.org/10.1016/j.sedgeo.2012.08.012, 2012.

Nisbet, R., Elder, J., and Miner, G.: Handbook of statistical analysis and data mining applications, Academic Press, 2009.

Oota, K., Ishizawa, T., and Hoyanagi, K.: Formation processes of tsunami deposits following the 2011 Tohoku-oki earthquake in the estuary of Odaka District, Minamisoma City, Fukushima Prefecture, Northeast Japan, Journal of the Sedimentological Society of Japan, 76, 3–16, 2017.

Ota, Y., Kawana, T., and Moriwaki, H.: Late Holocene coastal morphology and sea-level records on three small islands, the South Ryukyus, Japan, Geographical review of Japan, Series B., 58, 185–194, 1985.

Paola, C., Wiele, S. M., and Reinhart, M. A.: Upper-regime parallel lamination as the result of turbulent sediment transport and low-amplitude bed forms, Sedimentology, 36, 47–59, 1989.

Pari, Y., Murthy, M. R., Kumar, J. S., Subramanian, B., and Ramachandran, S.: Morphological changes at Vellar estuary, India—Impact of the December 2004 tsunami, J. Environ. Manage., 89, 45–57, 2008.

Paris, R., Wassmer, P., Sartohadi, J., Lavigne, F., Barthomeuf, B., Desgages, E., Grancher, D., Baumert, P., Vautier, F., Brunstein, D., and G, C.: Tsunamis as geomorphic crises: lessons from the December 26, 2004 tsunami in Lhok Nga, west Banda Aceh (Sumatra, Indonesia), Geomorphology, 104, 59–72, 2009.

Patterson, J. and Gibson, A.: Deep learning: A practitioner's approach, O'Reilly Media, Inc., 2017.

Pham, D. T., Gouramanis, C., Switzer, A. D., Rubin, C. M., Jones, B. G., Jankaew, K., and Carr, P. F.: Elemental and mineralogical analysis of marine and coastal sediments from Phra Thong Island, Thailand: Insights into the provenance of coastal hazard deposits, Marine Geology, 385, 274–292, 2017.

Phantuwongraj, S. and Choowong, M.: Tsunamis versus storm deposits from Thailand, Natural Hazards, 63, 31–50, 2012.

Philibosian, B., Sieh, K., Avouac, J.-P., Natawidjaja, D. H., Chiang, H.-W., Wu, C.-C., Shen, C.-C., Daryono, M. R., Perfettini, H., Suwargadi, B. W., et al.: Earthquake supercycles on the Mentawai segment of the Sunda megathrust in the seventeenth century and earlier, Journal of Geophysical Research: Solid Earth, 122, 642–676, 2017.

Pignatelli, C., Sansò, P., and Mastronuzzi, G.: Evaluation of tsunami flooding using geomorphologic evidence, Marine Geology, 260, 6–18, 2009.

Qi, Z., Eames, I., and Johnson, E. R.: Force acting on a square cylinder fixed in a free-surface channel flow, Journal of Fluid Mechanics, 756, 716–727, 2014.

Quenouille, M.: Approximate Tests of Correlation in Time-Series, Journal of the Royal Statistical Society B, 11, 68–84, 1949.

Ramalanjaona, G.: Impact of 2004 tsunami in the islands of Indian ocean: Lessons learned, Emergency medicine international, 2011, 2011.

Ramirez, M. C. V., de Campos Velho, H. F., and Ferreira, N. J.: Artificial neural network technique for rainfall forecasting applied to the Sao Paulo region, Journal of Hydrology, 301, 146–162, 2005.

Reicherter, K.: Tsunamis as Paleoseismic Indicators, Encyclopedia of Earthquake Engineering, pp. 1–12, 2014.

Retsinis, E. and Papanicolaou, P.: Numerical and Experimental Study of Classical Hydraulic Jump, Water, 12, 1766, 2020.

Richmond, B., Szczuciński, W., Chagué-Goff, C., Goto, K., Sugawara, D., Witter, R., Tappin, D. R., Jaffe, B., Fujino, S., Nishimura, Y., et al.: Erosion, deposition and landscape

change on the Sendai coastal plain, Japan, resulting from the March 11, 2011 Tohoku-oki tsunami, Sedimentary Geology, 282, 27–39, 2012.

Röbke, B. and Vött, A.: The tsunami phenomenon, Progress in Oceanography, 159, 296–322, 2017.

Rodolfo, K. S.: Sediments of the Andaman basin, northeastern Indian Ocean, Marine Geology, 7, 371–402, 1969.

Romano, M., Liong, S.-Y., Vu, M. T., Zemskyy, P., Doan, C. D., Dao, M. H., and Tkalich, P.: Artificial neural network for tsunami forecasting, Journal of Asian Earth Sciences, 36, 29–37, 2009.

Rossetto, T., Peiris, N., Pomonis, A., Wilkinson, S., Del Re, D., Koo, R., and Gallocher, S.: The Indian Ocean tsunami of December 26, 2004: observations in Sri Lanka and Thailand, Natural Hazards, 42, 105–124, 2007.

Rubin, C. M., Horton, B. P., Sieh, K., Pilarczyk, J. E., Daly, P., Ismail, N., and Parnell, A. C.: Highly variable recurrence of tsunamis in the 7,400 years before the 2004 Indian Ocean tsunami, Nature communications, 8, 1–12, 2017.

Saatcioglu, M., Ghobarah, A., and Nistor, I.: Effects of the December 26, 2004 Sumatra earthquake and tsunami on physical infrastructure, ISET Journal of Earthquake Technology, 42, 79–94, 2005.

Sakakiyama, T.: Tsunami pressure on structures due to tsunami inundation flow, Coastal Engineering Proceedings, pp. 42–42, 2014.

Sakuna, D., Szczuciński, W., Feldens, P., Schwarzer, K., and Khokiattiwong, S.: Sedimentary deposits left by the 2004 Indian Ocean tsunami on the inner continental shelf offshore of Khao Lak, Andaman Sea (Thailand), Earth, planets and space, 64, 11, 2012.

Sanuki, H., Takemori, R., Tajima, Y., and Sato, S.: Study on tsunami flooding in river based on video images and numerical simulation, in: Proceedings of Coastal Engineering, JSCE, vol. 69, pp. 196–200, 2013.

Satake, K.: Advances in earthquake and tsunami sciences and disaster risk reduction since the 2004 Indian ocean tsunami, Geoscience Letters, 1, 15, 2014.

Satake, K., Aung, T. T., Sawai, Y., Okamura, Y., Win, K. S., Swe, W., Swe, C., Swe, T. L., Tun, S. T., Soe, M. M., O, T. Z., and Z, S. H.: Tsunami heights and damage along the Myanmar coast from the December 2004 Sumatra-Andaman earthquake, Earth, planets and space, 58, 243–252, 2006.

Sato, S., Liu, H., Takewaka, S., Nobuoka, H., and Aoki, S.-i.: Tsunami damages of Nakoso Coast due to the 2011 Tohoku Tsunami, Coastal Engineering Proceedings, pp. 2–2, 2012a.

Sato, S., Mizuhashi, K., Yeh, H., Isobe, M., Aizawa, H., and Ashino, H.: Coastal and nearshore behaviors of the 2011 Tohoku Tsunami along the central Fukushima Coast, Doboku Gakkai Ronbunshu B2. Kaigan Kogaku (Online), 68, 1–346, 2012b.

Sato, S., Okayasu, A., Yeh, H., Fritz, H. M., Tajima, Y., and Shimozono, T.: Delayed survey of the 2011 Tohoku Tsunami in the former exclusion zone in Minami-Soma, Fukushima Prefecture, Pure and Applied Geophysics, 171, 3229–3240, 2014.

Sawai, Y., Jankaew, K., Martin, M. E., Prendergast, A., Choowong, M., and Charoentitirat, T.: Diatom assemblages in tsunami deposits associated with the 2004 Indian Ocean tsunami at Phra Thong Island, Thailand, Mar. Micropaleontol, 73, 70–79, 2009.

Sawai, Y., Namegaya, Y., Okamura, Y., Satake, K., and Shishikura, M.: Challenges of anticipating the 2011 Tohoku earthquake and tsunami using coastal geology, Geophysical Research Letters, 39, 2012.

Scheffers, A.: Tsunami boulder deposits, in: Tsunamiites, pp. 299–317, Elsevier, 2008.

Scheffers, A. and Kelletat, D.: Sedimentologic and geomorphologic tsunami imprints worldwide—a review, Earth-Science Reviews, 63, 83–92, 2003.

Shephard, F., Macdonald, G., and Cox, D.: The tsunami of April, 1946, Bulletin of the Scripps Institution of Oceanography, 5, 391–528, 1950.

Shiki, T. and Yamazaki, T.: The term “tsunamiite”, in: Tsunamiites, pp. 5–7, Elsevier, 2008.

Shinozaki, T., Yamaguchi, N., and Sekiguchi, T.: Flume experiments test grain-size distribution of onshore tsunami deposits, Sedimentary Geology, 407, 105 750, 2020.

Shishikura, M., Sawai, Y., and Namegaya, Y.: Reconstruction of the 869 Jogan Earthquake, the predecessor of the 2011 Tohoku earthquake, by geological evidence combined with tsunami simulation, in: Proceeding of TC302 Symposium Osaka 2011: International Symposium on Backwards Problem in Geotechnical Engineering and Monitoring of Geo-Construction, pp. 25–28, 2011.

Shuto, N.: Tsunami hazard mitigation, Proceedings of the Japan Academy, Series B, 95, 151–164, 2019.

Simons, D. B., Rlchardson, E., and Nordin Jr, C.: Sedimentary structures generated by flow in alluvial channels, 1960.

Sinadinovski, C.: The event of 26th of December 2004–the biggest earthquake in the world in the last 40 years, Bulletin of Earthquake Engineering, 4, 131–139, 2006.

Smith, D., Foster, I. D., Long, D., and Shi, S.: Reconstructing the pattern and depth of flow onshore in a palaeotsunami from associated deposits, Sedimentary Geology, 200, 362–371, 2007.

Smith, J. and Eli, R. N.: Neural-network models of rainfall-runoff process, Journal of Water Resources Planning and Management, 121, 499–508, 1995.

Smith, S.: Digital signal processing: a practical guide for engineers and scientists, Elsevier, 2013.

Soulsby, R.: Dynamics of Marine Sands, T. Telford London, 1997.

Soulsby, R., Smith, D., and Ruffman, A.: Reconstructing tsunami run-up from sedimentary characteristics - a simple mathematical model, Coastal Sediments, 7, 1075–1088, 2007.

Srinivasalu, S., Thangadurai, N., Switzer, A. D., Mohan, V. R., and Ayyamperumal, T.: Erosion and sedimentation in Kalpakkam (N Tamil Nadu, India) from the 26th December 2004 tsunami, Marine Geology, 240, 65–75, 2007.

Srivastava, N., Hinton, G., Krizhevsky, A., Sutskever, I., and Salakhutdinov, R.: Dropout: a simple way to prevent neural networks from overfitting, Journal of Machine Learning Research, 15, 1929–1958, 2014.

Sugawara, D.: Extracting magnitude information from tsunami deposits, Joutnal of Geography-Chigaku Zassi, 123, 797–812, 2014.

Sugawara, D.: Chapter 4 - Trigger mechanisms and hydrodynamics of tsunamis, in: Geological Records of Tsunamis and Other Extreme Waves, edited by Engel, M., Pilarczyk, J., May, S. M., Brill, D., and Garrett, E., pp. 47–73, Elsevier, 2020.

Sugawara, D.: Lessons from the 2011 Tohoku-oki tsunami: implications for Paleotsunami research, in: Tsunamiites, pp. 155–181, Elsevier, 2021.

Sugawara, D. and Goto, K.: Numerical modeling of the 2011 Tohoku-oki tsunami in the offshore and onshore of Sendai Plain, Japan, Sedimentary Geology, 282, 110–123, 2012.

Sugawara, D., Minoura, K., and Imamura, F.: Tsunamis and tsunami sedimentology, in: Tsunamiites, pp. 9–49, Elsevier, 2008.

Sugawara, D., Imamura, F., Matsumoto, H., Goto, K., and Minoura, K.: Quantitative reconstruction of a paleo-tsunami: field survey of Jogan tsunami and paleotopography, DCRC Tsunami Engineering, 27, 103–132, 2010.

Sugawara, D., Imamura, F., Matsumoto, H., Goto, K., and Minoura, K.: Reconstruction of the 869 Jogan earthquake and tsunami using geological data, Natural Disaster Science, 29, 501–516, 2011.

Sugawara, D., Goto, K., Imamura, F., Matsumoto, H., and Minoura, K.: Assessing the magnitude of the 869 Jogan tsunami using sedimentary deposits: Prediction and consequence of the 2011 Tohoku-oki tsunami, Sedimentary Geology, 282, 14–26, 2012.

Sugawara, D., Imamura, F., Goto, K., Matsumoto, H., and Minoura, K.: The 2011 Tohoku-oki earthquake tsunami: similarities and differences to the 869 Jogan tsunami on the Sendai plain, Pure and Applied Geophysics, 170, 831–843, 2013.

Sugawara, D., Goto, K., and Jaffe, B. E.: Numerical models of tsunami sediment transport—Current understanding and future directions, Marine Geology, 352, 295–320, 2014.

Sugawara, D., Jaffe, B., Goto, K., Gelfenbaum, G., and La Selle, S.: Exploring hybrid modeling of tsunami flow and deposit characteristics, in: The Proceedings of the Coastal Sediments 2015, World Scientific, 2015.

Suppasri, A., Muhari, A., Ranasinghe, P., Mas, E., Shuto, N., Imamura, F., and Koshimura, S.: Damage and reconstruction after the 2004 Indian Ocean tsunami and the 2011 Great East Japan tsunami, Journal of Natural Disaster Science, 34, 19–39, 2012.

Suppasri, A., Goto, K., Muhari, A., Ranasinghe, P., Riyaz, M., Affan, M., Mas, E., Yasuda, M., and Imamura, F.: A decade after the 2004 Indian Ocean tsunami: the progress in disaster preparedness and future challenges in Indonesia, Sri Lanka, Thailand and the Maldives, Pure Appl. Geophys., 172, 3313–3341, 2015.

Sutskever, I., Martens, J., Dahl, G., and Hinton, G.: On the importance of initialization and momentum in deep learning, in: International Conference on Machine Learning, pp. 1139–1147, 2013.

Suzuki, H., Imaizumi, T., Ishiyama, T., Miyauchi, T., Kagohara, K., Haraguchi, T., Marushima, N., and Omachi, T.: Holocene tsunami deposits associated with earthquakes along Pacific coast, northeast Japan, in: AGU Fall Meeting Abstracts, vol. 2009, pp. T33B–1884, 2009.

Switzer, A. D. and Jones, B. G.: Large-scale washover sedimentation in a freshwater lagoon from the southeast Australian coast: sea-level change, tsunami or exceptionally large storm?, The Holocene, 18, 787–803, 2008.

Szczuciński, W., Kokociński, M., Rzeszewski, M., Chagué-Goff, C., Cachão, M., Goto, K., and Sugawara, D.: Sediment sources and sedimentation processes of 2011 Tohoku-oki tsunami deposits on the Sendai Plain, Japan—insights from diatoms, nannoliths and grain size distribution, Sedimentary Geology, 282, 40–56, 2012a.

Szczuciński, W., Rachlewicz, G., Chaimanee, N., Saisuttichai, D., Tepsuwan, T., and Lorenc, S.: 26 December 2004 tsunami deposits left in areas of various tsunami run up in coastal zone of Thailand, Earth, planets and space, 64, 5, 2012b.

Tang, H.: Forward and inverse modeling of tsunami sediment transport, Ph.D. thesis, Virginia Tech, 2017.

Tang, H. and Weiss, R.: A model for tsunami flow inversion from deposits (TSUFLIND), Marine Geology, 370, 55–62, 2015.

Tang, H., Wang, J., Weiss, R., and Xiao, H.: TSUFLIND-EnKF: Inversion of tsunami flow depth and flow speed from deposits with quantified uncertainties, Marine Geology, 396, 16–25, 2018.

Tanigawa, K., Sawai, Y., Shishikura, M., Namegaya, Y., and Matsumoto, D.: Geological evidence for an unusually large tsunami on the Pacific coast of Aomori, northern Japan, Journal of Quaternary Science, 29, 200–208, 2014.

Tobin, J., Fong, R., Ray, A., Schneider, J., Zaremba, W., and Abbeel, P.: Domain randomization for transferring deep neural networks from simulation to the real world, in: 2017 IEEE/RSJ International Conference on Intelligent Robots and Systems (IROS), pp. 23–30, IEEE, 2017.

Tremblay, J., Prakash, A., Acuna, D., Brophy, M., Jampani, V., Anil, C., To, T., Cameracci, E., Boochoon, S., and Birchfield, S.: Training deep networks with synthetic data: Bridging the reality gap by domain randomization, in: Proceedings of the IEEE Conference on Computer Vision and Pattern Recognition Workshops, pp. 969–977, 2018.

Tsuji, Y.: Combined investigation of tradition archives and sedimentary relics of tsunami hazards–with reference to the Great 1700 Cascadia tsunami and other examples, in: Tsunamiites, pp. 193–205, Elsevier, 2021.

Tsuji, Y., Namegaya, Y., Matsumoto, H., Iwasaki, S.-I., Kanbua, W., S, M., and Meesuk, V.: The 2004 Indian tsunami in Thailand: Surveyed runup heights and tide gauge records, Earth, planets and space, 58, 223–232, 2006.

Tsuruta, T., Harada, H., Misonou, T., Matsuoka, T., and Hodotsuka, Y.: Horizontal and vertical distributions of 137 Cs in seabed sediments around the river mouth near Fukushima Daiichi Nuclear Power Plant, Journal of Oceanography, 73, 547–558, 2017.

Tsushima, H., Hino, R., Tanioka, Y., Imamura, F., and Fujimoto, H.: Tsunami waveform inversion incorporating permanent seafloor deformation and its application to tsunami forecasting, Journal of Geophysical Research: Solid Earth, 117, 2012.

Udo, K., Takeda, Y., and Tanaka, H.: Coastal morphology change before and after 2011 off the Pacific coast of Tohoku earthquake tsunami at Rikuzen-Takata coast, Coastal Engineering Journal, 58, 1640 016–1, 2016.

Usami, T.: Descriptive catalogue of disaster earthquakes in Japan, 1975.

Van Rijn, L. C.: Sediment transport, part II: suspended load transport, Journal of Hydraulic Engineering, 110, 1613–1641, 1984.

Watanabe, H.: Is it possible to clarify the real state of past earthquakes and tsunamis on the basis of legends, As an example of the 869 Jogan earthquake and tsunami, Histor. Earthq (Rekishi-jishin), 17, 130–146, 2001.

Wijetunge, J. J.: Tsunami on 26 December 2004: spatial distribution of tsunami height and the extent of inundation in Sri Lanka, Science of tsunami hazards, 24, 225–239, 2006.

Williams, I. A. and Fuhrman, D. R.: Numerical simulation of tsunami-scale wave boundary layers, Coastal engineering, 110, 17–31, 2016.

Wright, C. and Mella, A.: Modifications to the soil pattern of South-Central Chile resulting from seismic and associated phenomenona during the period May to August 1960, Bulletin of the Seismological Society of America, 53, 1367–1402, 1963.

Wu, L., Tian, F., Xia, Y., Fan, Y., Qin, T., Jian-Huang, L., and Liu, T.-Y.: Learning to teach with dynamic loss functions, in: Advances in Neural Information Processing Systems, pp. 6466–6477, 2018.

Wünnemann, K. and Weiss, R.: The meteorite impact-induced tsunami hazard, Philosophical Transactions of the Royal Society A: Mathematical, Physical and Engineering Sciences, 373, 20140 381, 2015.

Yamaguchi, N. and Sekiguchi, T.: Effects of tsunami magnitude and terrestrial topography on sedimentary processes and distribution of tsunami deposits in flume experiments, Sedimentary Geology, 328, 115–121, 2015.

Yokoyama, I.: A scenario of the 1883 Krakatau tsunami, Journal of Volcanology and Geothermal Research, 34, 123–132, 1987.

Yoshii, T., Tanaka, S., and Matsuyama, M.: Tsunami inundation, sediment transport, and deposition process of tsunami deposits on coastal lowland inferred from the Tsunami Sand Transport Laboratory Experiment (TSTLE), Marine Geology, 400, 107–118, 2018.

Yoshikawa, Y. and Watanabe, Y.: Examine of Manning's coefficient and the Bed-load layer for One-dimensional Calculation of Bed Variation, Monthly Report of Civil Engineering Research Institute for Cold Region, 662, 11–20, 2008.